

THE UNIVERSITY OF CALGARY

WATER CALORIMETRY
FOR RADIATION DOSIMETRY

BY

ROBIN BRUCE BARNETT

A THESIS

SUBMITTED TO THE FACULTY OF GRADUATE STUDIES
IN PARTIAL FULFILLMENT OF THE REQUIREMENTS FOR THE
DEGREE OF DOCTOR OF PHILOSOPHY

DEPARTMENT OF MEDICAL SCIENCE

CALGARY, ALBERTA

JANUARY, 1986

© ROBIN BRUCE BARNETT 1986

UNIVERSITY OF CALGARY
FACULTY OF GRADUATE STUDIES

The undersigned certify that they have read, and recommend to the Faculty of Graduate Studies for acceptance, a thesis entitled, "Water Calorimetry for Radiation Dosimetry" submitted by Robin Bruce Barnett in partial fulfillment of the requirements for the degree of Doctor of Philosophy.



Dr. D. V. Cormack, Supervisor,
Department of Radiology



Dr. K. Arthur, Department of Radiology

Dr. H. Morrish, Department of
Radiology

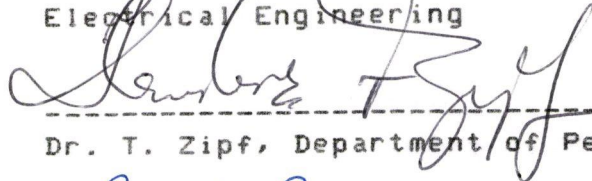


Dr. D. Armstrong, Department of
Chemistry





Dr. F. Trofimenkoff, Department of
Electrical Engineering



Dr. T. Zipf, Department of Pediatrics



Dr. D. W. O. Rogers, Ionizing
Radiation Standards, National Research
Council, Ottawa

86 01 31

Date

ABSTRACT

A calorimeter has been constructed, calibrated and used to measure the absorbed dose in water from several radiotherapy beams. The absorbed dose was determined from the product of the heat capacity of water and the temperature rise measured with the calorimeter. The temperature detector of the calorimeter contained two bead thermistors which were supported and insulated between thin polyethylene films. Temperature measurements were made in once-distilled water for a preset time or a preset number of monitor units. The calorimeter dose was designated D_c/U where U was either monitor units or time. To determine the consistency of D_c/U , temperature measurements were recorded as a function of accumulated dose. For irradiation with 15 MV x-rays, a steady state value of D_c/U was observed for accumulated doses greater than about 80 Gy. The standard error of the mean of the steady state value from several experiments was 0.6% (95% confidence). For accumulated doses less than 20 Gy, D_c/U was more variable and as much as 5% greater than the steady state value. For thermistor powers between 8.5 and 60 microwatts, no power dependence of D_c/U was observed. A dose comparison was made between the steady state values of D_c/U and ion chamber measurements (D_i/U) using the AAPM

TG-21 protocol. For beams of cobalt-60, 15 MV x-rays, and electrons with energies of 10, 12, 15, and 18 MeV D_c/D_i was $1.02 \pm 0.7\%$, $1.00 \pm 0.7\%$, $1.01 \pm 1.0\%$, $1.02 \pm 1.1\%$, $1.02 \pm 1.6\%$, and $1.04 \pm 1.2\%$ respectively (95% confidence). A similar comparison was made between D_c/U and Fricke (NRC) dose values (D_f/U). For 15 MV x-rays and electron beams with energies of 10, 12, 15, and 18 MeV D_c/D_f was $0.99 \pm 0.7\%$, $0.98 \pm 1.0\%$, $0.99 \pm 1.1\%$, $0.99 \pm 1.6\%$ and $1.00 \pm 1.2\%$ respectively. For cobalt-60 irradiation D_c/D_i was 1-2% lower than previously published data from three other studies. For 15 MV x-ray irradiation, D_c/D_i was 2-3% lower than published data for 10 and 25 MV x-ray beams. The implication from these data is that the constancy of water calorimeter temperature (dose) measurements must be determined by irradiating the water to a large accumulated dose. Previously published measurements of D_c/U may not have been steady state values. An alternate calorimeter temperature detector was constructed using directly immersible thermistors. Temperature measurements in a cobalt-60 beam with this detector were hampered by convection. For 15 MV x-rays no convection was observed and D_c/U was in good agreement with the value obtained from a polyethylene insulated detector.

ACKNOWLEDGEMENTS

The water calorimetry described in this thesis could not have evolved without the help and support of many friends and colleagues.

I would like to thank my supervisor, Dr. D.V. Cormack, for providing the opportunity to investigate water calorimetry. His extensive experience in radiation dosimetry has been an invaluable resource in the pursuit of this work.

I am indebted to the staff of the Tom Baker Cancer Centre for their encouragement and assistance throughout the project. I would especially like to thank Cliff Walls and Leo Moriarity for their suggestions and many hours of shop time. I would also like to thank Helen Boese for her assistance on many occasions with ion chamber measurements.

I am sincerely grateful to Dr. S. Domen of the National Bureau of Standards for demonstrating the NBS water calorimeter and for testing a thermistor detector during the initial development. Dr. Domen's suggestions have been very useful during this project.

I would like to acknowledge the collaboration of Dr. N. Klassen of the National Research Council in Ottawa. Discussions with Dr. Klassen have provided an essential perspective for this work.

I would like to thank Dr D. Armstrong of the University of Calgary (Department of Chemistry), for his advice and for suggesting the visit of Dr. Klassen.

I am grateful to Dr. F. Trofimenkoff of the University of Calgary (Dept of Electrical Engineering) for his assistance during the project and for providing essential lab facilities.

I would like to thank Dr. G. Schultz of the University of Calgary (Dept of Medical Science) for securing interim funding at the very end of this work.

Finally, I would like to thank Ursala and Linda for typing the tables in this thesis.

This work was supported by Grant H-155 of the Alberta Heritage Savings Trust Fund: Applied Research (Cancer).

DEDICATION

I would like to dedicate this thesis to Janice, Steven and Erinne for their patience and support throughout the project. No family could have given more.

TABLE OF CONTENTS

	Page
ABSTRACT	iii
ACKNOWLEDGEMENTS	v
DEDICATION	vii
TABLE OF CONTENTS	viii
LIST OF TABLES	xi
LIST OF FIGURES	xii
1.0 INTRODUCTION AND RESEARCH OBJECTIVES	1
1.1 Radiation Oncology and Radiation Dosimetry	1
1.1.1 Absorbed Dose in Water	1
1.1.2 Dose Accuracy	3
1.1.3 Ion Chamber Dosimetry	5
1.1.4 Chemical Dosimetry	11
1.1.5 Absorbed Dose Calorimetry	16
1.2 Water Calorimetry	20
1.2.1 NBS Water Calorimeter	20
1.2.2 Water Calorimeter Dose Measurements	21
1.2.3 Heats of Reaction During the Radiolysis of Water	24
1.2.4 Dependence of Water Calorimeter Dose on Thermistor Power	30
1.3 Research Objectives	31
2.0 CALORIMETER DESIGN AND CONSTRUCTION	33
2.1 Basic Principles	33
2.2 Conductive Heat Loss	34
2.3 Temperature Detection	38
2.4 Thermistor Detector	39
2.4.1 Basic Design Features	39
2.4.2 Excess Temperature of Polyethylene Films due to Irradiation	41
2.4.3 Excess Thermistor Temperature due to Irradiation	48
2.4.4 Total Excess Temperature due to Irradiation	50
2.5 Detector Construction	51
2.6 Calorimeter Tank	59
2.7 Wheatstone Bridge	65
2.8 Voltage Detection	72
2.9 Calorimetric Dose Determination	74
2.10 Signal to Noise Ratio Considerations	75
2.10.1 Thermal Noise	75
2.10.2 Detector Noise Bandwidth	78
2.10.3 Detector Signal to Noise Ratio	79
2.10.4 Additional Temperature Effects	80
2.10.4.1 Thermal Emfs	80
2.10.4.2 Temperature Drift Control	83
2.10.4.3 Thermistor Temperature and Power Increase During Irradiation	86
2.11 Convective Heat Loss	88

Table of Contents cont'd

Chapter		Page
2.11.1	Rayleigh Number	88
2.11.2	Threshold Temperature Gradient	90
3.0	INSTRUMENT AND THERMISTOR CALIBRATION	94
3.1	Calibration Requirements	94
3.2	Temperature Calibration	95
3.3	Thermistor Calibration	96
3.3.1	Material Constant	96
3.3.2	Excess Thermistor Temperature	99
3.3.3	Experimental Determination of the Thermistor Material Constant	100
3.3.4	Calibration Data	105
3.3.4.1	Material Constant Variation with Temperature	105
3.3.4.2	Effect of Polyethylene Films	106
3.3.4.3	Thermistor Calibration in a Cobalt-60 Beam . .	118
3.4	Nanovoltmeter Calibration	118
4.0	ABSORBED DOSE MEASUREMENTS	124
4.1	Experimental Procedure	124
4.1.1	Experimental Parameters for Calorimeter Dose Measurements	124
4.1.1.1	Calorimeter Water	124
4.1.1.2	Operating Temperature	124
4.1.1.3	Thermistor Detector Equilibration	125
4.1.1.4	Calorimeter Transport and Initial Setup . . .	127
4.1.1.5	Field Size	129
4.1.1.6	Depth of Measurement	129
4.1.2	Calorimeter Operation	130
4.1.3	Water Calorimeter Data Analysis	134
4.1.4	Ion Chamber Measurements	137
4.1.5	Correction Factors for Variation in Machine Dosimetry	139
4.1.6	Practical Absorbed Dose Quantities	143
4.2	Effect of Accumulated Dose on Calorimetric Dose	143
4.3	Effect of Thermistor Power on Absorbed Dose	152
4.4	Absorbed Dose Comparison	159
4.4.1	Dosimetry Intercomparison	159
4.4.1.1	Experimental Uncertainties	161
4.4.2	Comparison with Published Data	164
5.0	SUMMARY AND CONCLUSIONS	167
5.1	Calorimeter Design and Calibration	167

Table of Contents cont'd

Appendix		Page
5.2	Temperature Drift and Operational Control . . .	171
5.3	Experimental Precision	172
5.4	Absorbed Dose Measurements	172
6.0	REFERENCES	177
A	HEAT CONDUCTION AND EXCESS THERMISTOR TEMPERATURE	185
A.1	Goldenberg Equations	185
A.2	Steady State Thermistor Temperature	188
A.3	Excess Thermistor Temperature from Power Dissipation	190
A.4	Excess Thermistor Temperature During Irradiation	192
A.5	Temperature Gradient in Water Produced by a Thermistor	196
A.6	Thermal Conductivity of a Thermistor	199
B	TEMPERATURE DEPENDENCE OF THERMAL PROPERTIES OF WATER	202
B.1	Thermal Properties of Water	202
C	HEAT CONDUCTION IN WATER	205
C.1	Heat Conduction	205
C.2	Axial Temperature Profiles	206
C.3	Conductive Heat Loss in Water	207
D	DOSE MEASUREMENTS WITH IMMERSIBLE THERMISTORS	221
D.1	Immersible Thermistors	221
D.2	Modified Detector Construction	225
D.3	Investigation of Convection	225
D.4	Explanation of Convection	230
D.5	Dose Measurements with 15 MV X-rays	234

LIST OF TABLES

Table	Page
3.1	Thermistor Detector Calibration Data: Polyethylene Film Insulated 107
3.2	Thermistor Calibration Data: Comparison of Immersible and Poly Insulated Thermistors . . 111
4.1	Parameters For AAPM TG-21 Ion Chamber Dosimetry Protocol 140
4.2	Water Calorimeter Absorbed Dose Values: Effect of Accumulated Dose 150
4.3	Water Calorimeter Absorbed Dose Values: Effect of Thermistor Power 156
4.4	Absorbed Dose Comparison 160
B.1	Thermal Properties of Water 203

LIST OF FIGURES

Figure	Page
2.1 Percent Excess Temperature of Non Water Materials During Irradiation	46
2.2 Polyethylene Film Insulated Thermistor Detector	52
2.3 Construction Details of the Water Calorimeter	60
2.4 Wheatstone Bridge and Thevenin Equivalent Circuit	66
2.5 Circuit Diagram for the Water Calorimeter . .	70
3.1 Thermistor Detector Calibration Circuit . . .	101
3.2 Variation of the Thermistor Material Constant with Temperature	108
3.3 Variation of Excess Thermistor Temperature per Unit Power with Water Temperature (I) . .	112
3.4 Variation of Excess Thermistor Temperature per Unit Power with Water Temperature (II) . .	115
3.5 Nanovoltmeter and Recorder Calibration	121
4.1 Sample Chart Tracing from a Calorimeter Temperature Measurement (15 MV X-rays)	132
4.2 Variation of Calorimeter Absorbed Dose with Accumulated Dose (15 MV X-rays)	147
4.3 Variation of Calorimeter Absorbed Dose with Thermistor Power (15 MV X-rays)	154
A.1 Variation of Excess Thermistor Temperature per Unit Power with Thermistor Diameter . . .	193
A.2 Variation of the Temperature Gradient in Water with Thermistor Size and Power	197

List of Figures cont'd

Figure		Page
C.1	Variation of Conductive Heat Loss in Water with Position and Time (Cobalt-60)	209
C.2	Variation of Conductive Heat Loss in Water with Position and Time (15 MV X-rays)	211
C.3	Variation of Conductive Heat Loss in Water with Position and Time (10 MeV Electrons)	213
C.4	Variation of Conductive Heat Loss in Water with Position and Time (12 MeV Electrons)	215
C.5	Variation of Conductive Heat Loss in Water with Position and Time (15 MeV Electrons)	217
C.6	Variation of Conductive Heat Loss in Water with Position and Time (18 MeV Electrons)	219
D.1	Effect of Thermistor Size and Trapped Air on the Excess Thermistor Temperature	223
D.2	Convection During Temperature Measurements in a Cobalt-60 Beam	226
D.3	Penumbral Temperature Gradient and Convective Circulation in a Water Calorimeter	231
D.4	Sample Chart Tracing for Temperature Measurements in a Beam of 15 MV x-rays	236

CHAPTER 1

INTRODUCTION AND RESEARCH OBJECTIVES

1.1 Radiation Oncology And Radiation Dosimetry

1.1.1 Absorbed Dose In Water -

Radiation oncology is the branch of medical science which utilises ionizing radiation to destroy cancerous tissue. A large number of malignant tumors lie several centimeters below the skin and require highly penetrating radiation to receive a uniform and lethal dose. For this reason, the source of radiation for external beam radiotherapy has shifted from cobalt-60 teletherapy to electron linear accelerators (Johns and Rawlinson, 1976). Many medical accelerators have the capability for producing electron beams in addition to high energy x-rays.

X-rays are absorbed by several different physical processes in which part (or all) of the incident photon energy is converted to kinetic energy of an electron. High energy electrons which are produced from primary interactions then undergo thousands of subsequent collisions with other electrons and atoms until the kinetic energy has been dissipated. A detailed description of x-ray absorption is available from several references (e.g. Evans, 1966; ICRU, 1978; Johns and Cunningham, 1983). The three most important absorption processes for x-rays within an energy range of 0.5 and 50 MeV are photoelectric absorption, Compton scattering, and pair production. Each of these processes has a separate functional dependence on the beam energy and on the density and atomic number of the absorbing material.

For the majority of x-ray beams currently used for external radiotherapy (cobalt-60 - 25 MV x-rays), the dominant absorption process is via Compton scattering. The probability of a Compton event depends mainly on the physical density of the absorbing material (more correctly the electron density) and is largely independent of the atomic number.

The human body is made up of tissues which range in density from 0.00121 g/cm^3 (air in lung) to 1.65 g/cm^3 (bone). Most of the body, however, is made up from soft tissue which has nearly the same density as water (1 g/cm^3). Because of the large amount of water in tissue, and due to its abundance, water has been accepted as a standard reference in which the absorbed dose is measured.

1.1.2 Dose Accuracy -

There are a number of factors which contribute to the prognosis of the radiotherapy patient. Of obvious importance is the accuracy to which the prescribed dose is delivered.

A limitation of conventional radiotherapy (due to the depth dose characteristics of x-rays and electrons) is that healthy tissue in the vicinity of an assessed tumor volume (or in the path of a beam but outside the tumor volume) will unavoidably receive some radiation. The use of fractionation (Goitien, 1976) and multifield and/or arc radiotherapy reduces this problem but does not eliminate it.

The probability for combined tumor control and minimum morbidity is considered to be a sensitive function of absorbed dose. On the basis of a number of clinical

observations in which systematic errors were detected in the dose delivered to patients, the ICRU (1976) have recommended that an accuracy of 5% (or better) may be necessary for optimum patient management.

To achieve a 5% dose accuracy for patients receiving external beam radiotherapy requires careful management of five separate phases of the overall process. These are;

- o the initial dose calibration of the output from a therapy unit and regular verification of the same
- o the measurement from each therapy unit of extensive beam data (percentage depth dose, tissue phantom ratios, tissue air ratios, beam profiles etc) for radiotherapy treatment planning
- o the provision of a diagnostic unit (simulator, CT scanner) for determining the site and extent of disease and for providing the necessary anatomical information for radiotherapy planning (e.g. body contour, internal tissue densities, tumor volume)
- o the provision of a system for radiotherapy planning (dose calculations indicating the dose distribution within the irradiated volume)

- o the provision of patient immobilization devices, accessories, and techniques for ensuring accurate and reproducible patient set up

Each of these functions plays an essential part in delivering a prescribed dose to the patient.

The subject material of this thesis is most relevant to the dose calibration of therapy units and in particular to the accuracy with which a calibration can be made. Accurate dosimetry is fundamental for safe and effective use of ionizing radiation.

1.1.3 Ion Chamber Dosimetry -

The most widely used instrument for the dosimetry of megavoltage x-ray and electron beams is an ionization chamber (or simply ion chamber). An ion chamber is an enclosure containing a gas and an electrode for collecting the ionization produced from the absorption of radiation. An electrometer is required to provide the collecting voltage across the chamber electrodes and to provide the circuitry for ionization measurement. The theory and design of ion chambers has been extensively reviewed by Boag (1966). Electrometer operation has been described by Keithley (1972) and Keithley et al (1984).

The determination of the absorbed dose in a medium using an ion chamber is based on the well known Bragg-Gray cavity theory. The basic theory and practical revisions have been reviewed by Burlin (1966). According to the Spencer-Attix formulation the dose in the medium (med) is given by

$$D_{\text{med}} = \frac{Q}{m} \frac{W}{e} \left(\frac{L}{\rho} \right)_{\text{air}} \quad (1.1)$$

where Q is the charge, m is the air mass in the chamber, W is the average energy required to produce an ion pair in air (see ICRU, 1979), e is the charge on the electron, and L/ρ is the restricted mass stopping power ratio of the medium to air (see ICRU, 1984b).

Q/m is defined as the specific ionization of the gas and has often been assigned the symbol "J". The product of the specific ionization and W/e defines the absorbed dose to the gas.

The concept of mass stopping power has been reviewed by Bichsel (1966) and the current definition is given by the ICRU (1980, 1984b). Whereas the mass stopping power is strongly dependent upon particle energy the ratio of

the mass stopping powers of two materials is much less energy dependent. The term "restricted" indicates that the computation of the mass stopping power is restricted to collisions in which the imparted energy (by an electron to the medium) is below a defined limit. Collisions which impart larger energies are assumed to produce a delta ray i.e. a high velocity electron which is not absorbed locally. Delta rays are accounted for, however, by appropriately modifying the electron fluence over which the stopping power is averaged. An important assumption of the Bragg-Gray theory is that the cavity has minimal influence on the charged particle fluence. In practice, equation 1.1 is usually multiplied by a factor (A) to correct for attenuation of the electron fluence when the cavity is replaced by the medium.

The mass of the gas in an ion chamber cannot be determined accurately because of the uncertainty in determining the chamber volume. However, for an ion chamber which has been calibrated in terms of exposure for cobalt-60 radiation, and for which the thickness and composition of the wall are known, the volume of its air cavity can be derived. The chamber can then be used (after applying appropriate factors to allow for the size of the cavity and the thickness and nature of the wall) as a Bragg-Gray cavity to measure absorbed dose not only for

cobalt-60 but also for high energy x-rays and electrons. This approach was first proposed by Greene and Massey (1966) for high energy x-rays and was adapted for electrons by Almond (1967). These methods allow for the calculation of conversion factors, designated C_{λ} , and C_E for x-rays and electrons respectively by which the absorbed dose, D , in a medium irradiated with a high energy beam can be obtained from the reading, M , of a chamber whose cobalt-60 exposure calibration factor is N_x . i.e.,

$$D = M N_x C_{\lambda} \quad (1.2)$$

for x-rays, and

$$D = M N_x C_E \quad (1.3)$$

for electrons.

The use of these methods was further discussed in Reports 14 and 21 of the ICRU (1969, 1972) who also gave tables of recommended values. These C_{λ} and C_E values were incorporated in a number of dosimetry protocols (e.g. HPA, 1969; AAPM SCRAD, 1971; NACP, 1972; NCRP, 1981) and have served as the basis for radiation dosimetry for over 10 years.

Radiation exposure standards are maintained in Canada through a section of the National Research Council (NRC) in Ottawa. A free air ionization chamber provides an exposure calibration for x-rays generated at potentials up to 400 KVp and a graphite cavity chamber is used for calibration with cobalt-60 radiation.

Since the generation of ICRU Reports 14 and 21 (1969, 1972), a number of authors have pointed out an inconsistency in the derivation of the C_{λ} and C_E (Nahum and Greening, 1976; Nahum and Greening, 1978; Shiragai, 1978; Williams, 1977; and Holt and Kessaris, 1977). Part of the inconsistency involves the origin of electrons which contribute to the ionization in the chamber. In practice, the relative number of electrons originating from the medium, buildup cap or wall depends on the chamber composition and geometry and on both the calibration and measurement energies (Almond and Svensson, 1977; Lempert et al, 1983).

The inconsistency in the derivation can be resolved by using an empirical approach suggested by Almond and Svensson (1977). An alternate approach has been proposed by Shiragai (1978). Chamber-wall corrections, revised stopping power ratios (Berger and Seltzer, 1982), and other refinements (Hubbell, 1977; ICRU, 1979) have been incorporated in a number of recent dosimetry protocols

(NACP, 1980; HPA, 1983; AAPM TG-21, 1983).

Ion chambers are calibrated in terms of exposure or air kerma because there are currently no dose standards for x-ray beams with an accelerating potential greater than 4 MV (equivalent to cobalt-60). The available absorbed dose standard for cobalt-60 is based on a graphite calorimeter measurement transferred to water with the use of a thick walled graphite ion chamber. The transfer process involves uncertainties which are comparable to those encountered with a normal ion chamber measurement. There are no absorbed dose standards for electron beams.

The equations for converting an ionization measurement to absorbed dose involve a number of parameters and theoretical assumptions. Quantities such as the restricted stopping power, the mass energy absorption coefficient, and the average energy required to produce an ion pair are subject to periodic revision and the user must be aware of the most current data. While these data and some of the correction factors are found tabulated in various protocols, the user must correctly measure the appropriate beam parameters for which the data apply. Quantities such as the ion collection efficiency must be measured for each quality of radiation from which the dose is measured.

It is unfortunate that there are currently so many protocols in use (NACP, 1980; HPA, 1983; AAPM, 1983; HPA, 1985) for the dosimetry of megavoltage x-ray and electron beams. This makes it extremely difficult to intercompare dose measurements not to mention small differences between international exposure standards. Clearly, improvement must be made in this area.

1.1.4 Chemical Dosimetry -

A chemical dosimeter is a chemical system in which the formation (or degradation) of a component is proportional to the absorbed dose. The most widely used chemical system for radiation dosimetry is the ferrous sulphate or Fricke dosimeter. During irradiation of a Fricke system, ferrous ions (Fe^{++}) are oxidized to ferric ions (Fe^{+++}). The concentration of ferric ion is determined from the absorption of ultraviolet light in a spectrophotometer. The radiation chemistry of the Fricke dosimeter and other technical aspects are described by Allen (1961), Fricke and Hart (1966), and Spinks and Woods (1964).

The equation which describes the absorbed dose as measured by a Fricke system is (e.g. ICRU, 1969);

$$D = \frac{dA \cdot N}{\rho \cdot l \cdot \epsilon \cdot G} \cdot k \quad (1.3)$$

where dA is the increase in optical absorbance due to the production of Fe^{+++} , N is Avogadro's number, ρ is the density of the solution, l is the path length of the cell in which the absorbance is measured, ϵ is the molar linear absorption coefficient for ferric ions, and G is the chemical yield of ferric ion (Fe^{+++}) in molecules per 100 eV. The constant k is required to obtain the dose in Gy.

In general, dA and ϵ are functions of temperature and apply to the temperature of the sample compartment of the spectrophotometer. G is also a function of temperature and applies to the temperature at which the sample was irradiated.

The overall stoichiometry (mass-energy balance) for a Fricke system using aerated water is given by (Spinks and Woods, 1964) as:

$$G(Fe^{+++}) = 2 G(H_2O_2) + 3 G(H_2) + G(OH) \quad (1.4)$$

It has long been recognized that the chemical yield for ferric ion is a function of the linear energy transfer,

LET; (see ICRU, 1980; Fricke and Hart, 1966) of the incident beam.

From a number of experimental determinations, ICRU (1969) recommended $G(\text{Fe}^{+++})$ values (in number per 100 eV) of 15.3 for Cs-137 x-rays, 15.4 for 2MV x-rays, 15.5 for Co-60 and 4MV x-rays, 15.6 for x-rays in the range 5 -10 MV x-rays, and 15.7 for x-rays in the range 11-30 MV. For electron beams, ICRU (1972) recommended a $G(\text{Fe}^{+++})$ value of 15.7 for energies between 1 and 30 MeV. These values apply to Fricke solutions in which the acid concentration is 400 mol/m³.

Since the publication of ICRU Reports 14 and 21 (1969, 1974), some of the $G(\text{Fe}^{+++})$ values determined from experiments using ion chambers have been reevaluated using more recent dosimetry protocols. As indicated by Nahum and Greening (1978) who reworked the data of Law and Naylor (1972), the revised $G(\text{Fe}^{+++})$ values for 8, 15 and 33 MV x-rays were almost the same as the revised values determined from electron beams between 3 and 35 MeV. Their conclusion was that a constant $G(\text{Fe}^{+++})$ value of 15.5 should be used for both megavoltage x-ray and electron beams.

By examining previous calorimetric determinations of $G(\text{Fe}^{+++})$, and applying scattering corrections for the presence of the Fricke cell (where previously neglected) Svensson and Brahme (1979) demonstrated that within experimental error, $\epsilon G(\text{Fe}^{+++})$ was constant for electron energies between 1 and 30 MeV and that the corresponding $G(\text{Fe}^{+++})$ value (15.4) was about 2% lower than that previously recommended by ICRU (1972).

Using a Monte Carlo simulation of photon and electron transport, Nahum et al (1981) have revised a semi-empirical relationship between $G(\text{Fe}^{+++})$ and LET100 originally proposed by Burch (1959). The revised calculations predicted that for x-ray beams with an energy range between cobalt-60 and 31 MV, and for electron beams with energies between 5 - 30 MeV, $G(\text{Fe}^{+++})$ was about 15.5 and was independent of energy.

From measurements with a graphite calorimeter, Cottens (1978) demonstrated that $\epsilon G(\text{Fe}^{+++})$ for electron beams with energies between 3.5 and 14.5 MeV was constant within an experimental error of 0.6%.

On the basis of recent experimental data and reevaluation of previous data, ICRU (1984a) has recently recommended an $\epsilon G(\text{Fe}^{+++})$ product of $352 \times 10^{-6} \text{ m}^2 \text{ kg}^{-1} \text{ Gy}^{-1}$ for electrons with an energy range of 1 -

30 MeV.

The sensitivity of a Fricke dosimeter is less than ideal and about 10 Gy are required to achieve an experimental precision of 1%. Chemical impurities arising in the water can significantly affect $G(\text{Fe}^{+++})$ (Spinks and Woods, 1964). In sealed vessels, the available oxygen can be used up during irradiation (extremely high dosage) and this has been reported to lower $G(\text{Fe}^{+++})$ (ICRU, 1984a). By lowering the concentration of sulphuric acid from 400 mol/m³ to 50 mol/m³ $G(\text{Fe}^{+++})$ has been reported to decrease by 1-3%. (ICRU, 1984a). The acid concentration dependence of $G(\text{Fe}^{+++})$ has been discussed by Fricke and Hart (1966).

The dosimetry section of the NRC offer a Fricke service in which vials are prepared under well controlled conditions and then sent out into the field for irradiation. The samples are then returned for spectrophotometer analysis in the NRC laboratory. While this is the most practical way to offer such a service, the number of available vials must be necessarily restricted. This is a significant limitation where a large number of measurements are required.

1.1.5 Absorbed Dose Calorimetry -

A radiation calorimeter is a device which measures the temperature increase produced by the absorption of radiation. Calorimeters have been used for many years to determine the absorbed dose and/or total energy fluence from radiation beams and for calibrating radioisotopes.

Calorimetry is considered to be the most direct method for determining the absorbed dose. A review of the fundamentals of radiation calorimetry and a summary of various calorimeter designs and applications is provided by Gunn (1964, 1970, 1976). A review of absorbed dose calorimetry is given by Laughlin and Genna (1956, 1966).

For most solids, the thermal diffusivity is sufficiently large that conductive heat loss (resulting from the axial temperature gradient produced by beam absorption) would be too large to attempt a temperature measurement at a point within a continuous medium. Thus, the design of most solid calorimeters requires that a small mass (core) of a suitable material be thermally isolated inside a larger mass (jacket) of the same material.

The core of the calorimeter must be carefully suspended using a minimum of supporting material (thin quartz fibres have been used by a number of investigators). The gap between the core and jacket(s) must be as small as possible so that the perturbation in a radiation field is minimal. In addition, the gap volume must be evacuated so that conductive heat loss is negligible.

For a radiation calorimeter, the absorbed dose is given by

$$D = E/m = c \quad dT \quad (1.5)$$

where E is the absorbed energy, m is the mass of the core, c is the heat capacity of the core, and where dT is the measured temperature rise. A calorimeter is often calibrated by introducing a known quantity of energy (E) into the core and determining the associated rise in temperature. An integral part of the calibration procedure is to determine a small correction for heat loss from the core to the environment. The measured temperature increase produced from the absorption of radiation is then used to determine the absorbed dose via equation 1.4.

McDonald et al (1976) built a portable calorimeter from A-150 (tissue equivalent) plastic. In their design, four independent thermally floating shields surround the core. The calorimeter was calibrated using a quasi-adiabatic technique (the core and first surrounding jacket are both heated with the same power density to minimize heat loss between the core and jacket). A heat defect has been reported for A-150 plastic of about 4% (McDonald and Goodman, 1982). A positive heat defect implies that not all of the absorbed energy is converted to heat and that the measured dose is low. Heat defects for solids must be determined experimentally.

Domen and Lamperti (1974) constructed a graphite calorimeter in which the core was surrounded by a single jacket and a thermally floating shield. The graphite calorimeter was operated in a "heat loss compensated mode"; i.e. the calorimeter was calibrated by heating the core only and measuring the sum of the temperature rises in the jacket and the core. This technique is simpler than a quasi-adiabatic calibration (e.g Laughlin and Genna, 1966) and permits direct evaluation of the effects of temperature gradients.

Based on the NBS design (Domen and Lamperti, 1974), a number of graphite calorimeters have been constructed and tested internationally (e.g. Cottens et al, 1978; Ross et al, 1982). In general, the reported performance of these calorimeters has been excellent. An experimental precision of 0.5 % has been reported by several investigators.

There are, however, a number of difficulties using solid calorimeters as the basis for an absorbed dose standard. The quantity of interest for the purpose of radiation oncology is the absorbed dose in water. In order to derive this quantity from the absorbed dose measured e.g. with a graphite calorimeter, a thick walled ion chamber is usually required as a transfer instrument. A thick wall is necessary to provide charged particle equilibrium at the point of measurement and therefore this technique is limited to cobalt-60 and lower energy beams. This procedure has been described by ICRU (1969) and implemented by Pruitt et al (1981) for cobalt-60. The uncertainty in the overall determination is then comparable to that from using an ion chamber alone.

Another problem with solid calorimeters arises from the gap between the core and jacket. For electron beams (especially low energy), the presence of a gap in a medium can significantly alter the measured dose. The extent of

this effect will depend on the dimensions of the gap, the position of measurement, and on the energy spectrum of the incident electrons. This problem has been referred to by Domen (1982b).

1.2 Water Calorimetry

1.2.1 NBS Water Calorimeter -

To avoid the dose conversion and vacuum gap problems associated with solid calorimeters, Domen (1980, 1982b) designed and constructed a water calorimeter. The temperature detector of the calorimeter consisted of two bead thermistors (0.25 mm diameter) which were connected in opposite sides of a Wheatstone bridge. The thermistors were electrically insulated and supported between two thin polyethylene films which were stretched and held watertight with a set of polystyrene rings (20.3 cm diameter). The entire thermistor detector was immersed directly in a large water bath.

The design of the water calorimeter was based on the assumptions that;

- o conductive heat loss in water (due to temperature gradients produced by the beam profile) is negligible during a dose measurement of a few minutes.

- o convection does not occur in the water

As discussed by Domen (1982b), conductive heat loss in water is very small because of its low thermal diffusivity. While this effect also depends on the shape of the axial temperature profile, the absorbed dose from most x-ray and electron beams can be measured directly in a continuous water bath without requiring corrections for heat loss. This feature greatly simplifies calorimeter design.

Using a liquid as an absorber introduces the potential for convection. For Domen's water calorimeter, temperature gradients were kept sufficiently low that convection was not observed. All dose measurements were made in a cobalt-60 beam at a depth of 5 cm in water and thermistor powers of 10 microwatts were employed.

1.2.2 Water Calorimeter Dose Measurements -

Compared to the NBS absorbed dose standard for cobalt-60 radiation (Pruitt et al, 1981), Domen's water calorimeter measurements were 3.5% high. The exact nature of this effect was not resolved although it was postulated (Domen, 1982b) that radiation induced chemical reactions could be a source of the apparent exothermicity. This topic is discussed in Section 1.3.2.

Using copies of Domen's calorimeter, a number of investigators have reported nearly identical discrepancies (de Marles, 1981, Kubo, 1983, Mattsson, 1984) for cobalt-60 measurements. Compared to their respective ionometric values, Kubo's water calorimeter measurements were 3.5% higher, de Marles were 3.8% higher and Mattsson's were 3.3% higher.

In an attempt to resolve the reported discrepancy between water calorimeter measurements, Domen constructed a polystyrene-water calorimeter in which the dose was measured in a 2 cm thick polystyrene disk immersed in a large water tank (Domen, 1983). To obtain the temperature rise in the polystyrene, two thermistors were embedded between 1 cm thick layers. The dose in water was determined by multiplying the calorimeter measurements by the ratio of mass energy absorption coefficients (polystyrene/water) and then by a replacement factor to allow for an altered photon fluence produced by the polystyrene. From the polystyrene-water calorimeter and a cobalt-60 beam, Domen determined an absorbed dose in water which was in excellent agreement with the NBS standard (i.e. about 3.4% lower than for the water calorimeter). Using a copy of the polystyrene-water calorimeter, Kubo (1985b) has reported similar findings.

The problem with a polystyrene-water calorimeter is that the dose is determined in polystyrene. Thus, conversion constants for ionometric protocols must be used which introduce additional uncertainty in a dose measurement. This is particularly significant for measurements with high energy x-ray beams because of a wider spectrum of photon energies. A further disadvantage of this dosimeter is that conductive heat loss may be significant during dose measurements. This problem has been discussed by Kubo (1985b).

De Marles (1981) reported that for x-ray beams of 6, 18 and 25 MV the absorbed dose from a water calorimeter was about 3.8% higher than the dose derived from an exposure calibrated ion chamber using a protocol recommended by NACP (1980). The calorimeter dose from electron beams with nominal energies of 13, 17, and 20 MeV was determined to be 1% lower than the dose determined with an ion chamber.

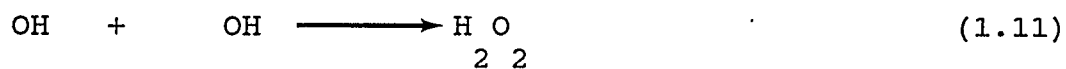
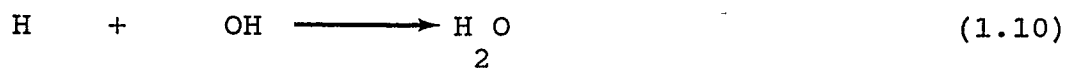
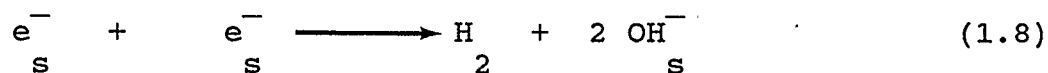
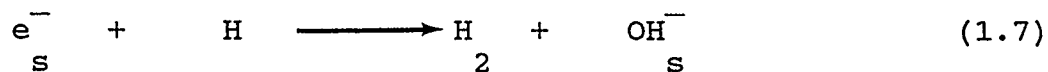
Water calorimeter measurements have been made by Kubo (1984) for 10 and 25 MV x-rays were reported to be 3 and 2% higher respectively than the dose determined with an exposure calibrated ion chamber using the protocol recommended by AAPM TG-21 (1983). The calorimeter dose for electron beams with nominal energies of 18 and 23 MeV were 3.6% and 3.4% higher respectively than the dose

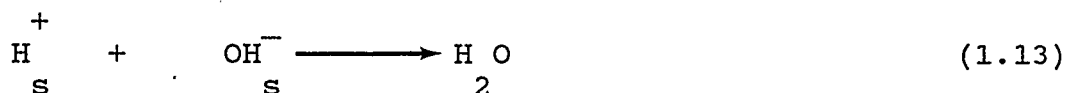
determined with an ion chamber. Mattsson (1984) has reported similar data for a range of electron beams between 2 and 20 MeV.

1.2.3 Heats Of Reaction During The Radiolysis Of Water -

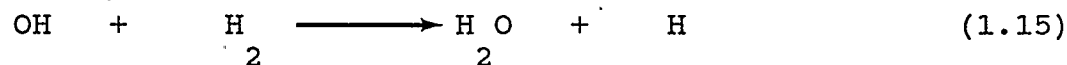
During the radiolysis of pure water, free radicals and solvated electrons are formed which react to form molecular hydrogen and hydrogen peroxide (e.g. Allen, 1961; Spinks and Woods, 1964). The important chemical reactions are;

(The subscript s indicates solvated)





As the concentration of H_2 and H_2O_2 increases (with continued low LET irradiation), the following back reactions occur;



which result in the formation of water. When the rate of decomposition of water (during radiolysis) is equal to the rate of formation from the back reactions, a steady state is established in which there is no net heat of formation. This would be the ideal system for a water calorimeter because the measured temperature increase would be truly indicative of the physical dose to water. The described steady state has been reported by a number of authors (Allen, 1961; Schwartz, 1962; Fletcher, 1982).

The radiolysis of impure (e.g. aerated) water, however, can induce chemical reactions which are either exo- or endothermic. To determine the net heat per unit absorbed dose which is produced during radiolysis the

overall stoichiometry must be known along with the heats of formation of the various end products. For convenience in the discussion to follow, the net heat produced per unit absorbed dose will be designated H/U.

Boyd, Carver and Dixon (1980) developed a computer program for investigating reactant and product concentrations during the radiolysis of aqueous solutions. The basis of the program is a system of differential equations describing the reaction kinetics resulting from 41 known chemical reactions. The input to the program are the measured rate constants for the various reactions along with the initial concentrations of reactants. The available reactants included hydrogen, oxygen and hydrogen peroxide. The chemical yields were based on low LET radiation and the dose rate in the program is variable.

Using the Boyd-Carver-Dixon model, Fletcher (1984) simulated the radiolysis of various aqueous solutions with solutes of hydrogen, oxygen, hydrogen/oxygen mixtures, and hydrogen peroxide. The radiolysis of pure water was also simulated for comparison.

As mentioned previously, a steady state is produced from the radiolysis of pure water in which the reactant and product concentrations do not change with further accumulated dose and for which H/U is zero. For the

radiolysis of aerated water, however, a true steady state is not obtained with respect to reactant and product concentrations but the value of H/U becomes constant as a function of accumulated dose. For convenience in this study the term "steady state" will be used to refer to the value of H/U as opposed to chemical concentrations. Unless otherwise stated, the independent variable associated with the steady state will be the accumulated dose.

From the calculations of Fletcher (1984) for the irradiation of pure water, a steady state value of H/U was obtained for an accumulated dose of about 150 Gy. For accumulated doses less than 150 Gy, H/U was endothermic and decreased from a maximum of 4.9% at zero accumulated dose to the steady state value of zero at 150 Gy.

For the irradiation of aerated water in Fletcher's report, a steady state value for H/U was again obtained for an accumulated dose of about 150 Gy. In this case, however, the steady state value of H/U was 2% endothermic with respect to the value for pure water. The endothermicity of H/U was attributed to the conversion of water and oxygen into hydrogen peroxide. For accumulated doses less than 150 Gy, H/U for aerated water was again endothermic and decreased from a maximum of 3.4% at zero dose to the steady state value at 150 Gy.

Ross et al (1984) constructed a calorimeter to measure H/U for aqueous solutions containing various dissolved gasses. The calorimeter was a small gold flashed vessel in which the contents were continually stirred. A single thermistor was used to measure the temperature changes and was immersed directly in the solution. The thermistor leads were insulated with very fine tubing and an enamel coating. These authors reported relative measurements and H/U was described in terms of temperature increase per unit dose.

Using a beam of 20 MV x-rays Ross et al (1984) measured H/U for aqueous solutions containing nitrogen, oxygen, air, hydrogen, and hydrogen/oxygen (50/50 partial pressure). A comparison was then made between the measured data and the values for H/U predicted by the Boyd-Carver-Dixon model. Because the measurements were not absolute, the data was normalized to the hydrogen/oxygen system (i.e. the value for H/U for the hydrogen/oxygen solution was equated with the predicted steady state value for the same system). For large accumulated doses, excellent agreement was observed between the measured values of H/U (steady state) and the model for nitrogen, air, and oxygen saturated water.

The data of Ross et al (1984) are particularly relevant to water calorimetry for a number of reasons. For aerated water which had been irradiated to an accumulated dose of about 100 Gy, a steady state value of H/U was measured. The zero-dose value of H/U for the same system, however, was found to be a few percent higher (i.e. exothermic) than the steady state value and decreased steadily with accumulated dose.

The initially high values of H/U for aerated water were postulated by Ross et al (1984) to be due to the presence of organic impurities. According to their model, organic impurities are preferred scavengers of OH radicals and react to produce the observed exothermicity. As the organics are consumed, H/U decreases until reaching a constant value for aerated water. The initial exothermicity for low accumulated doses observed by Ross et al (1984) is the opposite to that predicted in Fletcher's report (1982).

The data of Ross et al (1984) suggests that the first objective with the water calorimeter should be to establish the existence of a steady state temperature measurement (i.e a temperature measurement which is not influenced by a variation of H/U with accumulated dose) The inference from the previous data is that a steady state temperature measurement in water is obtainable by

irradiating the water to a large accumulated dose. Studying the calorimeter dose as a function of accumulated dose would be a necessary prerequisite to determining a steady state dose value.

1.2.4 Dependence Of Water Calorimeter Dose On Thermistor Power -

Domen's original water calorimeter dose measurements (Domen, 1980) were taken using thermistor powers of 200 microwatts. While this power ensured an excellent signal to noise ratio, Domen (1982b) found that the measured dose rate from a cobalt-60 beam was a function of thermistor power. By decreasing the thermistor power from 200 to 10 microwatts a 4% increase was observed in the apparent absorbed dose rate. Subsequent to this finding, the dose measurements were reported by using thermistor powers of about 10 microwatts and all the previous data was extrapolated to "zero power". Domen was unable to explain the power dependence of the measured dose rate and this was an obvious area for further study.

Kubo (1983), de Marles (1981), and Mattsson (1984) have reported dose measurements using thermistor powers less than 10 microwatts. These authors, however, did not investigate the effect of thermistor power on their measurements. It is therefore not clear whether a low

power measurement is really a maximum as was indicated from Domen's data. Low thermistor power necessarily limits the signal to noise ratio of the calorimeter and can only be compensated for by measuring extremely large absorbed doses (e.g. 10 Gy).

1.3 Research Objectives

In light of the previous discussion, the objectives of this study were:

- o to construct a water calorimeter after the design of Domen (1982b)
- o to implement satisfactory temperature control and establish stable calorimeter operation in a hospital environment
- o to calibrate the calorimeter; i.e. to determine the material constants of the thermistors in the temperature detector and to calibrate the detecting circuitry using temperature and resistance standards

- o to investigate the water calorimeter dose dependence on accumulated dose; i.e. to irradiate the calorimeter to large doses (200 Gy) to determine the existence of a steady state dose condition and to study any transient endo- or exdothermic chemical reactions

- o to investigate the water calorimeter dose dependence on thermistor power

- o to measure the absorbed dose (the steady state water calorimeter dose) from cobalt-60 and 15 MV x-ray beams and electron beams with nominal energies of 18, 15, 12, and 10 MeV.

- o to compare the absorbed dose measurements in a cobalt-60 beam with ion chamber measurements traceable to national standards

- o to compare the absorbed dose measurements using 15 MV x-ray or electron beams with exposure calibrated ion chamber measurements converted to absorbed dose using published protocols (e.g. AAPM TG-21, 1983)

CHAPTER 2

WATER CALORIMETER DESIGN AND CONSTRUCTION

2.1 Basic Principles

For radiation calorimetry, the absorbed dose D is related to the heat capacity c and the rise in temperature dT by

$$D = c \, dT \quad (2.1)$$

It is assumed in equation 2.1 that all of the absorbed energy is converted to heat and that no additional chemical changes within the medium contribute to dT . It is also assumed that there is no heat loss (or gain) at the point of temperature measurement due to conduction, convection or radiation. In situations where these assumptions are invalid, appropriate corrections to dT must be applied. To minimize temperature gradients within a calorimeter which contribute to heat transfer

both the thermal and radiation absorption properties of the construction materials must be carefully considered.

2.2 Conductive Heat Loss

Conductive heat transfer is described by the well known Fourier equation. For heat conduction in one dimension and constant thermal diffusivity (α), the Fourier equation is given by

$$\alpha \frac{d^2 T(x,t)}{dx^2} + g_0/(\rho c) = \frac{dT(x,t)}{dt} \quad (2.2)$$

In equation 2.2, g_0 is a heat source and α is the thermal diffusivity defined by;

$$\alpha = \frac{K}{\rho c} \quad (2.3)$$

where K is the thermal conductivity, ρ is the physical density, and c is the heat capacity.

A number of solid calorimeters have been constructed to measure the absorbed dose (locally absorbed) from a beam of ionizing radiation (Domen and Lamperti, 1974; McDonald, 1976). For this type of calorimeter the temperature measurement is obtained from a small,

thermally isolated "core" which is suspended in a larger body of identical composition. This design is necessary because most solid materials have a sufficiently high thermal diffusivity that a significant fraction of the heat produced by radiation absorption will be conducted away during the measurement.

The thermal diffusivity of water, however, is low enough that it is feasible to make calorimetric measurements directly in a continuous water phantom. This is one of the most important design features of the water calorimeter proposed by Domen (1980).

Using a numerical solution to equation 2.2 (finite differences; Schmidt, 1949), Domen (1982b) has studied the decay of temperature distributions in water as a function of time. The relative temperature distributions in his analysis were assumed to be the same as the percentage depth dose distributions produced after a short pulse of radiation.

Using a radial temperature profile produced from the absorption of cobalt-60, Domen (1982b) calculated a temperature decrease of 0.24% for a point in the beam penumbra and a decay time of 10 minutes. From the initial central axis temperature profile produced by the absorption of 11 MeV electrons, the decrease in

temperature near the peak of the curve was 0.8% after 60 seconds.

These calculations showed that for the temperature profiles produced from typical radiotherapy beams, conductive heat loss in water was generally small. This is primarily due to the low thermal diffusivity of water. However, in cases where the temperature gradient is changing rapidly (for example electron beam central axis temperature profiles) a small temperature correction may be necessary. A correction may also be necessary for calorimeter measurements of long duration.

Using the same numerical technique as Domen (1982b), the central axis temperature decay (i.e. the decrease due to conductive heat loss) was calculated for the radiation beams used in this study. These included cobalt-60, 15 MV x-ray and electron beams with energies of 18, 15, 12, and 10 MeV. This analysis is summarized in Figures C.1-C.6 (Appendix C) where the initial temperature profiles for each beam are plotted with the percent differences for decay times of 55 and 222 seconds.

Because broad beams were used exclusively (beams with a cross sectional area completely encompassing the water phantom) only the central axis temperature profiles were considered. For narrow beams, heat conduction would be

influenced by the radial profile in addition to the axial profile.

According to equation 2.2, the decrease in temperature per unit time is directly proportional to the the second derivative of the temperature with respect to depth (i.e on the shape of the temperature profile along the central axis). As expected, therefore, the largest decrease per unit time was observed for the electron beams.

Because of the design of the water calorimeter (to be described) it was not feasible to change the depth of measurement once an experiment was started. To provide efficient useage, therefore, a fixed depth of measurement was selected for all beam qualities that were used from the linear accelerator. From central axis depth dose data (temperature profiles) and the calculations in Appendix C a depth of measurement of 2.5 cm was chosen. At a depth of 2.5 cm and for a decay time of 55 seconds, the decrease in the initial temperature produced from the absorption of 15 MV x-rays was 0.25%. For the same conditions, a decrease of 0.6% was predicted from the initial temperature produced by the absorption of 10 MeV electrons. The decrease in the central axis temperature at a depth of 2.5 cm and after 55 seconds for the remaining electron beams was less than 0.05%.

For 15 MV x-rays, a detector depth of 2.5 cm is not optimum as indicated by Figure C.2. However, for the electron beams it can be seen that the temperature decay for depths immediately beyond 2.5 cm is significant and would require correction for measurement times exceeding 60 seconds.

From Figure C.1, it can be seen that conductive heat loss for cobalt-60 irradiation is very small for all practical depths of measurement. Most of the cobalt-60 dose measurements (calorimetric) reported in this thesis were taken at a depth of 5 cm. For some measurements taken immediately after an experiment with linear accelerator beams, however, the depth of measurement was 2.5 cm. At this position, the decrease in temperature due to conduction is 0.03% for a decay time of 222 seconds.

For the detector depths and measurement times used in this study, no heat loss corrections were applied.

2.3 Temperature Detection

Thermistors are good temperature sensors for absorbed dose calorimetry because of their small size and high temperature coefficient of resistance. A thermistor is a mixture of semiconductive metallic oxides which is sintered onto platinum leads. The resistance of a

thermistor as a function of temperature is normally described by (e.g. VECO, 1966)

$$R(T) = R_0 e^{B(1/T - 1/T_0)} \quad (2.4)$$

where R_0 is the resistance at a reference temperature T_0 (usually taken as 298 K), and where B is a material constant determined from a separate calibration for each thermistor. A temperature coefficient of resistance can be derived from this equation and is given by

$$a = \frac{dR}{R dT} = - \frac{B}{T^2} \quad (2.5)$$

For a small bead thermistor (0.25 mm diameter) a typical B value is 3000 K and the temperature coefficient of resistance at 295 K is 3.5%.

2.4 Thermistor Detector

2.4.1 Basic Design Features -

The requirement for minimal perturbation of a water phantom dictates the use of a very small thermistor. Thermistors are commercially available in a wide range of sizes with the smallest being about 0.13 mm in diameter (e.g. VECO microbead). However, as the thermistor size

decreases, the practical problems associated with handling (mounting) increase and the excess thermistor temperature per unit electrical power increases. The latter property has an important bearing on potential variability in dose measurements (to be discussed in Section 2.4, Section 3.3.4.2 and Appendix D).

Commercial thermistors are fabricated by sintering the appropriate metal oxides onto very fine platinum wires (0.025 mm in diameter). The platinum lead lengths are variable but because of a high resistance per unit length (typically 3 ohms per cm) are usually kept as short as possible. Where long leads are required copper (or other) wire extensions can be attached. This process is quite difficult without the proper equipment and lead attachment can be requested from the manufacturer.

The bare platinum thermistor leads present a problem for placement in water because of their conductivity. Ross et al (1984) have overcome this difficulty by using fine tubing and enamel to insulate the thermistor and leads. In their calorimeter, the insulated thermistor is immersed directly in water. However, the immersion of a thermistor directly in water is not generally practical for temperature measurements in a stagnant water calorimeter because of the potential for convection (Schulz and Weinhaus, 1985; Appendix D).

The detector assembly of the water calorimeter built by Domen, (1982b) consists of two thermistors sandwiched between thin (0.025 mm) polyethylene films. The films are supported and kept watertight with a set of polystyrene rings and rubber gaskets. This design offers a number of desirable features including electrical insulation of the thermistors from the water, protection for the thermistors, a well defined plane of measurement, and a barrier for convective heat flow.

2.4.2 Excess Temperature Of Polyethylene Films Due To Irradiation -

An important concern with this detector format is the excess temperature that will be produced in the polyethylene films during irradiation. The absorbed dose in the polyethylene will be nearly the same as that in water because the films are thin and the mean mass stopping power ratio of polyethylene to water is approximately 1.05 for both cobalt-60 and 15 MV x-rays (estimated from data in ICRU 37). However, since the heat capacity of polyethylene is about half that of water, its temperature will rise twice as high for the same absorbed dose (in isolation).

To estimate the excess temperature of polyethylene and/or other non-water materials such as the thermistors and wire leads, equation 2.2 must be solved throughout the central region of the detector. To attempt a composite analytical solution would be extremely difficult and a more reasonable approach is to treat each non-water component separately and add their excess temperatures in superposition. Three-dimensional numerical solutions can be used (Ozisik, 1980; Thomas and MacRoberts, 1965) but these are difficult to implement and cannot be evaluated without an approximate analytical solution.

The calculation of the excess temperature due to the absorption of radiation can be simplified by treating the heat generation in non-water materials as the sum of two components; one which causes the material to rise in temperature at the same rate as the surrounding water, and the other which is an excess component.

As long as two materials are at the same temperature there will be no exchange of heat. This also applies when the water and non-water material are rising in temperature at the same rate. The excess temperature in a non-water material, therefore, will be produced entirely from the excess heating component. The excess temperature calculation reduces to solving the Fourier equation for conductive heat transfer between a non-water material in

which heat is generated with the excess component referred to above and an infinite water medium in which no heat is generated. A percent excess temperature can then be derived from the ratio of the excess temperature and the rise in temperature of the water in isolation.

The rate of temperature rise in water due to the absorption of radiation is given by

$$\frac{dv_w}{dt} = \frac{DR_w}{c_w} \quad (2.6)$$

where v is the temperature, DR is the absorbed dose rate and c is the heat capacity. The subscript w has been used to indicate that these quantities apply to water. A similar expression can be derived for non-water materials except that the value of the absorbed dose rate will depend on the material. For example, if a thin polyethylene film is immersed in water the dose rate from a cobalt-60 beam in the polyethylene is about 1.05 times as large as the dose rate in water (using a mass stopping power ratio of polyethylene to water of 1.05).

The rate of excess heat generation from the absorption of radiation in non-water materials is given by

$$A = \rho c \left(\frac{dv}{dt} - \frac{dv_w}{dt} \right) \quad (2.7)$$

where dv/dt and dv_w/dt are derived separately from equation 2.6 and where ρ and c apply to the non-water material. In equation 2.7, "A" is expressed in units of energy per unit volume per unit time.

The quantity "A" can be also be expressed as the product of an excess absorbed dose rate (DR_x) and the density (ρ) of the non-water material. For this situation the excess absorbed dose rate is given by

$$DR_x = c \left(\frac{dv}{dt} - \frac{dv_w}{dt} \right) \quad (2.8)$$

The excess temperature of polyethylene films produced from the absorption of radiation was estimated from an analytical solution to the Fourier equation derived by Carslaw and Jaeger (1959; Chapter 2, P76). The solution applies to the heating of an infinite medium by a film of thickness $2d$ in which heat is being generated at a

constant rate per unit volume. This procedure was employed by Domen (1982b).

For a polyethylene film of thickness $2d$ heating an infinite water medium at a rate "A" (energy per unit time per unit volume) the excess temperature at the centre of the film is given by;

$$v_{xr} = \frac{2 \alpha A t}{K} (1 - 4 \text{I2ERFC}(d/(2\sqrt{\alpha t}))) \quad (2.9)$$

where A is the excess heating component (equation 2.7), α is the thermal diffusivity, K is the thermal conductivity and t is the time of irradiation. I2ERFC() is an integral function derived from the error function and is tabulated in Carslaw and Jaeger (1959, Appendix 2). The subscript "xr" has been used to indicate that the temperature is an excess quantity ("x") and that the source of the excess temperature is the absorbed radiation ("r"). A limitation of this equation is that it applies strictly to a homogeneous medium; i.e. the film and water are assumed to have the same thermal properties.

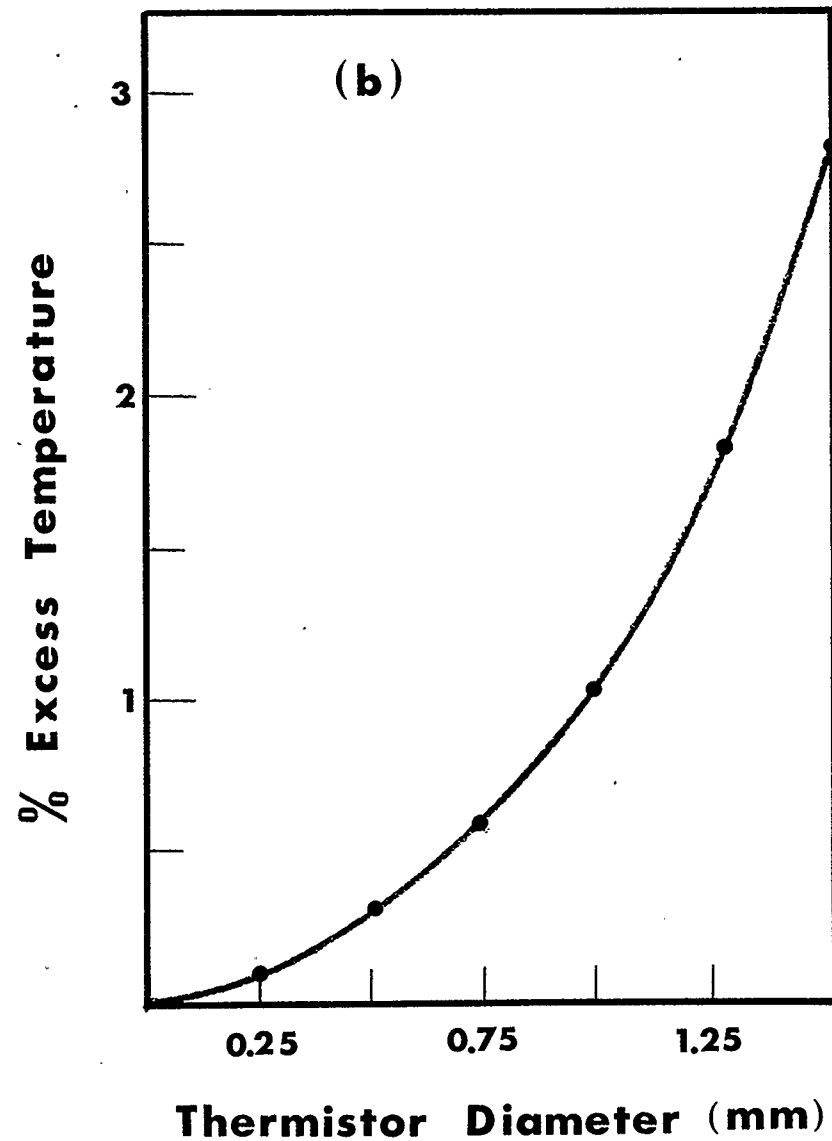
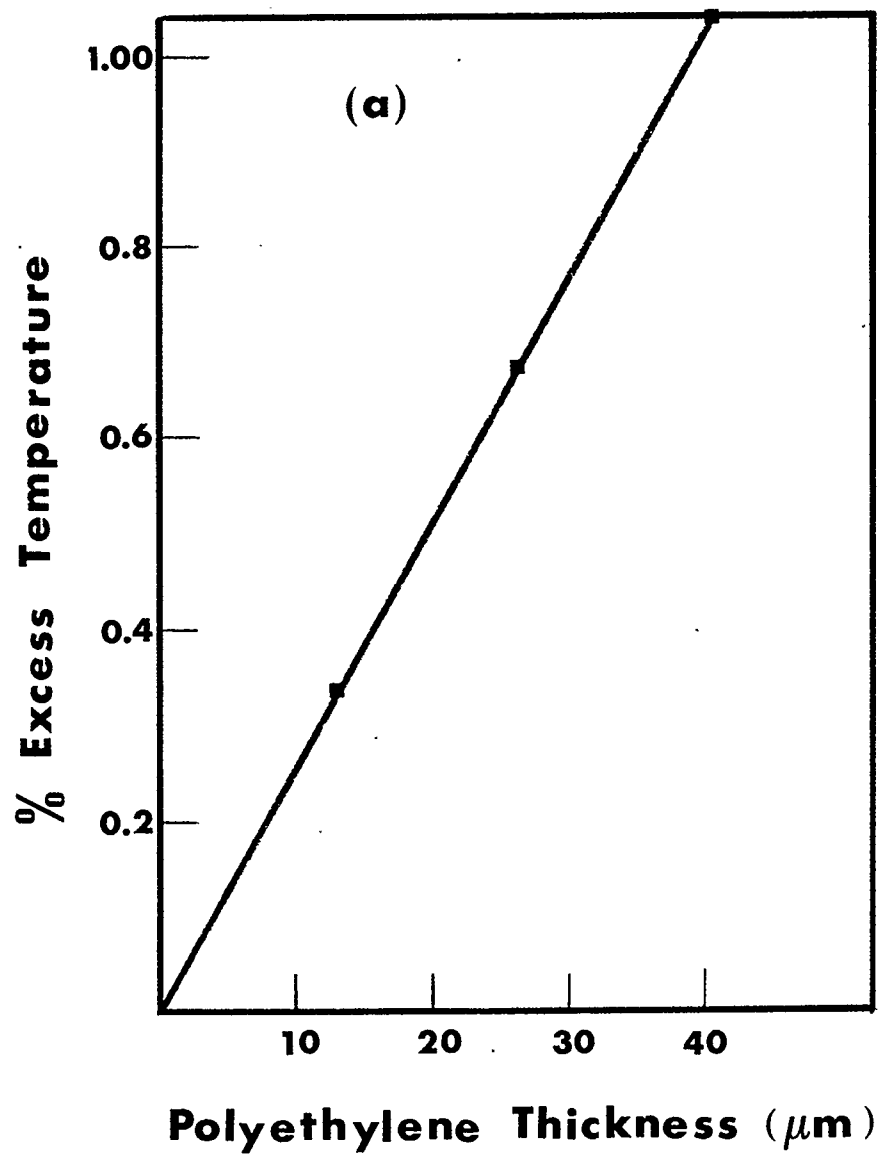
The percent excess temperature produced from the polyethylene films is shown as a function of film thickness in Figure 2.1. This graph was obtained by assuming a dose rate in water of 257 cGy/min and a total

Figure 2.1. Per Cent Excess Temperature of Non Water Materials During Irradiation

(a) Excess temperature at the centre of a polyethylene film due to irradiation.

(b) Excess temperature at the centre of a small thermistor due to irradiation.

Percent excess temperatures are relative to the temperature rise in pure water assuming a uniform dose rate of 257 cGy per minute and an irradiation time of 1 minute.



radiation time of 1 min. The excess temperature in the films was determined from equation 2.7 by averaging the excess temperatures calculated separately for water and polyethylene. For polyethylene thicknesses less than 0.025 mm the excess temperature should be no greater than 0.2%.

2.4.3 Excess Thermistor Temperature Due To Irradiation -

To calculate the excess thermistor temperature produced from the absorption of radiation an analytical solution derived by Goldenberg (Goldenberg, 1951; Goldenberg and Tranter, 1952) was used. Because of its importance in understanding the behavior of thermistors as applied to calorimetry the derivation of Goldenberg is described separately in Appendix A. For calculating the excess temperature in the thermistor produced from the absorption of radiation this is a better solution than that for the polyethylene films (see equation 2.9) because it takes into account both the thermal properties of the thermistor material and water.

For a small thermistor immersed in a large water bath, the excess temperature produced from the absorption of radiation quickly reaches a steady state (see Appendix A). The time required to reach the steady state is approximately given by

$$t_{ss} = \frac{100 \text{ rad}^2}{\alpha} \quad (2.10)$$

where rad is the radius of the thermistor, and α is the thermal diffusivity. For a 0.25 mm diameter thermistor placed in water, t_{ss} is about eleven seconds. Assuming that the steady state has been reached, the average excess temperature of the thermistor (averaged over the thermistor volume) is given by

$$\bar{v}_{xr} = \frac{A \text{ rad}^2}{3} \left(\frac{1}{K2} + \frac{1}{5 K1} \right) \quad (2.11)$$

where A is the excess heating component (equation 2.7), rad is the thermistor radius, K1 is the thermal conductivity of the thermistor, and K2 is the thermal conductivity of water. Equation 2.11 can also be written as (see equation A.14, Appendix A)

$$\bar{v}_{xr} = \frac{DR_x \rho \text{ rad}^2}{3} \left(\frac{1}{K2} + \frac{1}{5 K1} \right) \quad (A.14)$$

where DR_x is the excess absorbed dose rate and ρ is the density of the thermistor material.

The percent excess temperature is graphed as a function of thermistor radius in Figure 2.1 . For this graph, the average conductivity of the thermistor was assumed to be $2.1 \times 10^{-3} \text{ W cm}^{-1}\text{K}^{-1}$ (Appendix A). The excess heating component in the thermistor was calculated by assuming that the thermistor material was acrylic plastic (Ablestick epoxy insulated; Thermometrics, 1985) and that the dose rate in the thermistor was 0.97 times as large as the dose rate in water (the mass stopping power ratio of acrylic plastic to water for cobalt-60 and 15 MV x-rays is about 0.97; AAPM TG-21, 1983).

2.4.4 Total Excess Temperature Due To Irradiation -

The total excess temperature produced from irradiation of the films and thermistor can be obtained by summing the individual contributions in Figure 2.1. By keeping the thermistor diameter below 0.38 mm and using a polyethylene thickness of 0.013 mm, the total excess temperature for a 257 cGy dose (257 cGy/min dose rate and a 1 minute irradiation) is about 0.6%. These dimensions were considered to be an acceptable compromise.

A calculation of the excess thermistor temperature was compared with temperature measurements from a calorimeter detector with 1.27 mm diameter thermistors. A 3% excess temperature was observed for a 1 minute dose

measurement (dose rate of 257 cGy/min) with a 15 MV x-ray beam (see Appendix A and Figure D.4, Appendix D) and this value was in reasonable agreement with the 2% estimate shown in Figure 2.1.

The excess temperature of a thermistor is also influenced by the dissipation of electrical power. This topic is described in Appendix A and Chapter 3.

2.5 Detector Construction

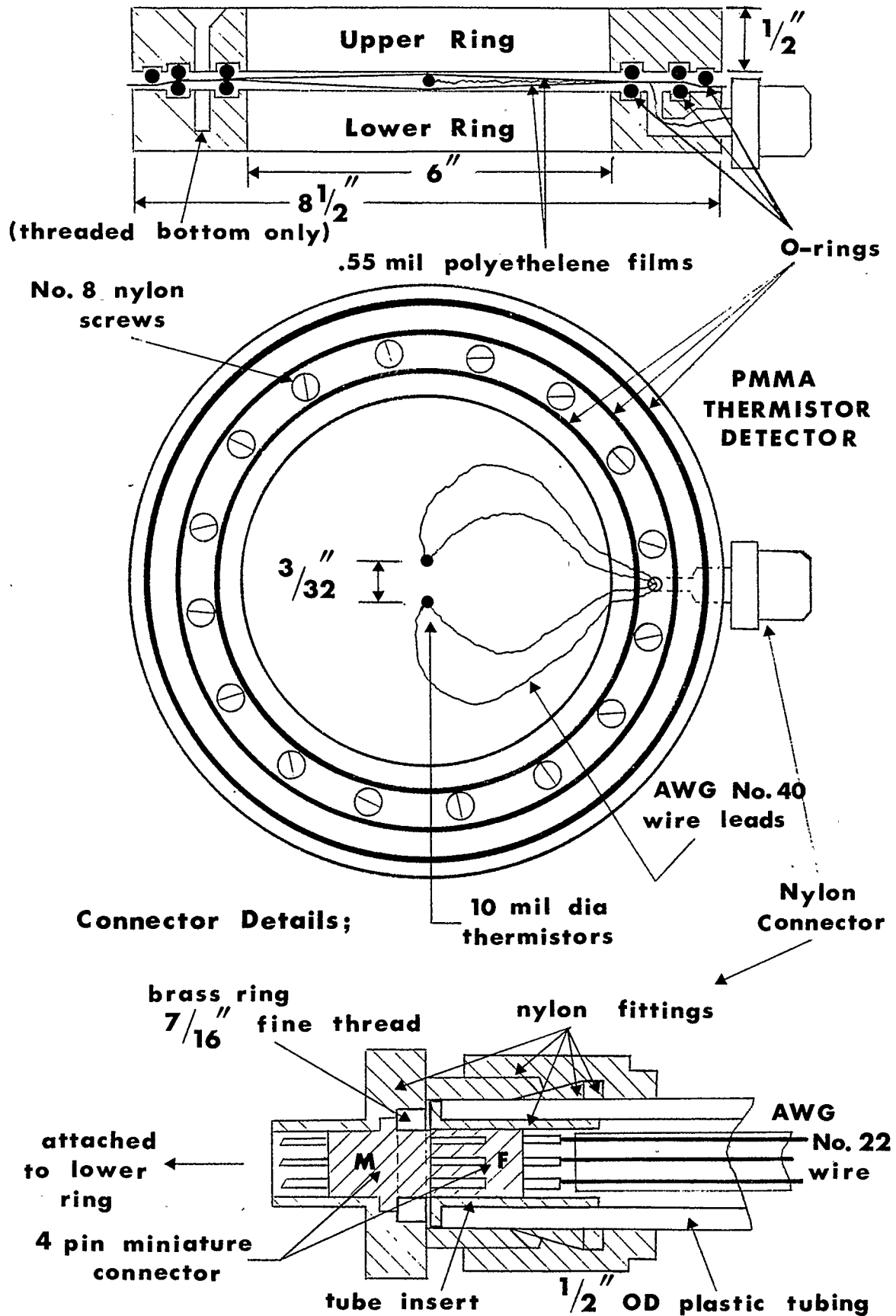
A diagram of the thermistor detector is shown in Figure 2.2. This is essentially a copy of Domen's detector with a few practical modifications.

The supporting rings were made from acrylic plastic (PMMA) as opposed to polystyrene. Acrylic plastic is slightly harder than polystyrene and was preferred for machining. Its thermal properties are very similar to those of polystyrene and no serious temperature effects (temperature gradients causing thermal drift) were observed even for large accumulated doses (see Chapter 4).

Among the more difficult construction problems was making the thermistor detector watertight. This is an obvious requirement for the water calorimeter but in practice was not easy to accomplish. The quality of a watertight seal is especially important where long term

Figure 2.2. Polyethylene Film Insulated Thermistor Detector

Dimensions are in SAE units to correspond with stock materials and machine tools actually used.



irradiations are required (see Chapter 4). The design features which are shown in Figure 2.2 are the result of many early disappointments.

To provide a reliable water seal, five large "o" rings were used between the acrylic rings. This is a departure from Domen's original design in which there were only two. The purpose of the four central "o" rings was to provide rubber on rubber contact as opposed to rubber on plastic. In this way, a lower tension was required to provide a watertight seal and improved contact was achieved where the thermistor leads cross the "o" rings. The fifth "o" ring prevented water from getting between the films from outside the rings. This was basically an insurance feature which negated the need for additional silicone sealant.

An essential provision with this design was the addition of thin spacers positioned on the "o" rings and adjacent to the thermistor leads. The spacers acted as channels for the wires and helped prevent air from being trapped between the films. Without adding this feature, the calorimeter measurements were found to be noisy as the result of intermittent contact between the film and thermistor.

Another important design objective was a waterproof connector so that the thermistor detectors could be easily exchanged. This was accomplished by modifying a commercial tube fitting to house a miniature four pin connector. The design features are shown in the bottom of Figure 2.2. The tube fitting was a nylon reducing union which was permanently attached to the lower ring assembly. The core of the fitting was bored out slightly to accommodate the male half of the miniature connector. The connector was designed to be stationary and was held in place by a small threaded brass ring. The core of the nylon fitting was threaded to accommodate the brass ring (see Figure 2.2).

The signal cable was housed in 12.7 mm (outside diameter) flexible plastic tubing. To fit comfortably into the reducing union, the female half of the miniature connector was machined and inserted into a commercial nylon fitting. This fixture acted to reinforce the flexible tubing at the point of connection.

The polyethylene film that was used for the thermistor detector was obtained from the produce section of a grocery store. The thickness was determined by weight to be 0.013 mm (assumed specific gravity = 0.91). Thicker samples of polyethylene were obtained from various packaging companies (0.019, 0.025, and 0.032 mm) but were

more prone to tearing at the point where the thermistor leads cross the "o" rings. To investigate the effect of film thicknesses greater than 0.013 mm, multiple layers of the thin plastic were used instead of a single thick layer (see Chapter 3).

All samples of the polyethylene film had small surface imperfections resulting in tiny patches of water leaking into the films. As long as the leaks did not appear near the thermistors this was not a problem. In some cases, however, the water leakage worsened to the point where it was necessary to dismantle the detector.

As the first part of the detector assembly, the polyethylene films were stretched and taped over an open rectangular brace (one each for top and bottom). These were made out of 6.4 mm aluminum and were designed to fit comfortably over the acrylic rings. In this way the plastic remained uniformly taut and conveniently supported throughout the assembly. A small tool was made out of 6.4 mm metal tubing (outside diameter) to cut a hole in the lower plastic layer. This was required to accommodate the thermistor leads.

During construction, the lower acrylic ring was secured with masking tape to a wooden base. An acrylic disk was placed in the center of the lower ring to support

the film while the thermistors were being attached.

Thermistors are extremely fragile and are very easily destroyed. To minimize the danger associated with their handling, the manufacturer was requested to ship the thermistors mounted to thin pieces of clear plastic. The plastic was cut from transparent sheets (normally used for photocopying) into squares measuring 2 cm on a side. The thermistor leads were secured to the plastic with small pieces of masking tape and protected with a cover plate of the same material.

Attaching the thermistors to the polyethylene required two separate operations. The first step was to guide the leads down through the hole in the lower acrylic ring and solder the leads to the miniature connector. The second step was to secure the connector in the reducing union and then attach the thermistors to the polyethylene film.

Thin strips of clear cellulose tape were used to mount the thermistors to the polyethylene films. These provided a good adhesive, were extremely thin, and were removable in case the detector was damaged and the thermistors had to be removed. The thermistors were positioned in the centre of the detector about 3 mm apart and secured with the strips of tape. The tape was

attached immediately below the plastic squares on which the thermistors were mounted. The strips of masking tape which held the thermistors to the plastic squares were removed by applying a small amount of flux remover. This procedure dissolved the adhesive on the tape and the plastic squares were then carefully pulled away.

Before applying the upper polyethylene film, thin strips of electrical tape were positioned on the inner "o" ring and on each side of the thermistor leads. These "channels" allowed air to escape from between the films and were essential for good detector performance. The upper layer of polyethylene was then positioned on top of the thermistors.

The final stage of the detector assembly was to screw down the upper acrylic ring. To provide a more homogenous detector (with respect to thermal properties), nylon screws were used instead of stainless steel. With this design, the only metal in the tank was the temperature probe (which was about 10 cm from the thermistors) and the thermistor leads. When the upper ring was secure, the polyethylene film was cut along the edges of the detector with a sharp knife. The detector was then leak tested before being placed in the calorimeter.

2.6 Calorimeter Tank

The main features of the calorimeter are shown in Figure 2.3 .

The water tank was assembled from 12.7 mm acrylic plastic (PMMA) with inside dimensions of 30 x 30 x 30 cm. This size permitted full phantom measurements to a maximum field size of 25 x 25 cm.

The tank was magnetically shielded with a 0.25 mm thick nickel foil (Co-Netic AA alloy, Perfection Mica). This material can be easily cut and soldered and is commercially available with an adhesive backing. The foil does not provide as good a shield as mu-metal of the same thickness but can be drilled and machined without affecting its shielding efficiency. The purpose of the foil was to shield against magnetic field effects produced from the bending magnet of the linear accelerator.

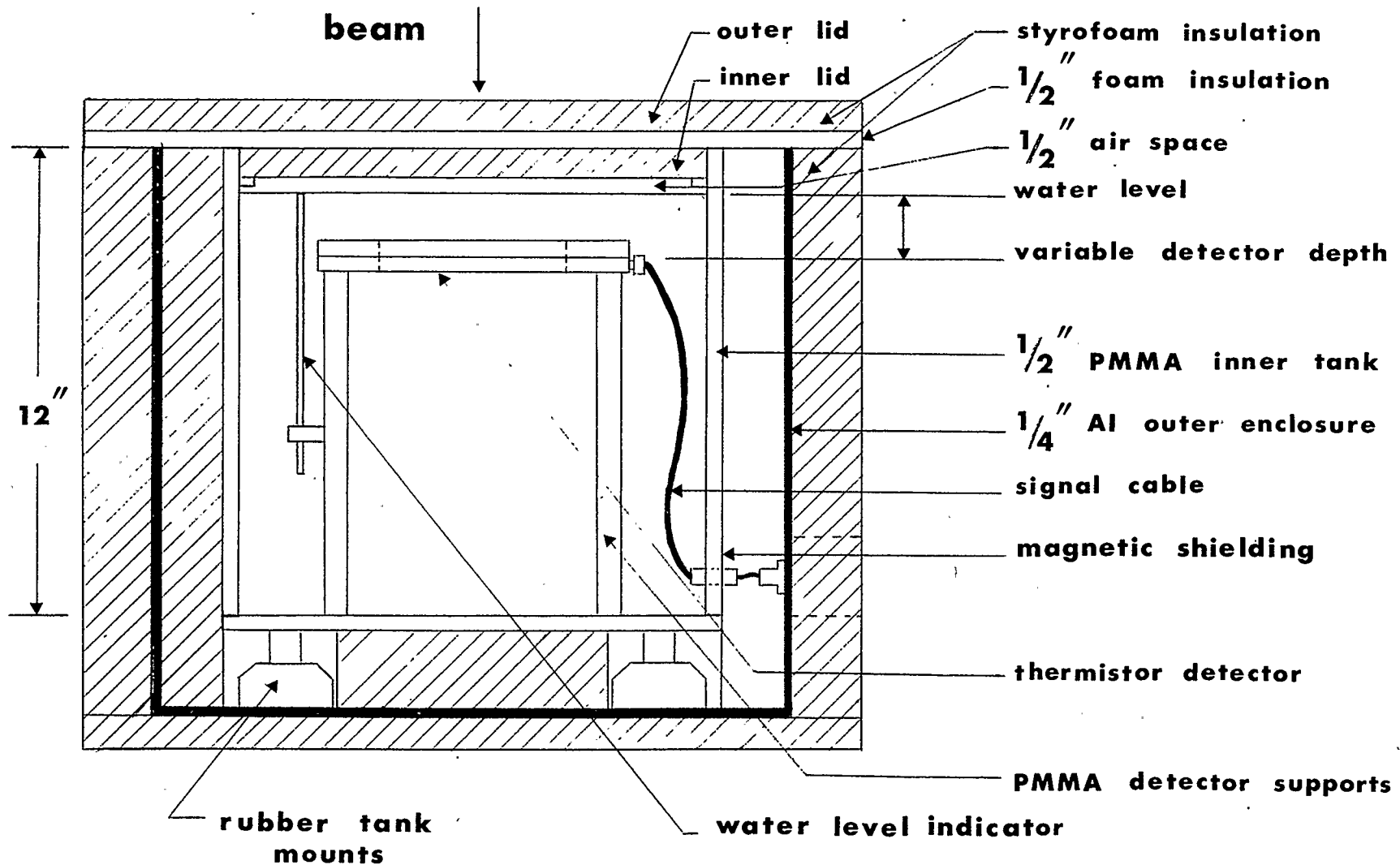
Several holes were drilled in one side of the tank to accommodate the required accessories. These included the detector cable, two immersion heaters, a temperature probe, and an assembly for gassing the tank.

Special acrylic fittings were constructed to facilitate interchanging the tank components and to provide a watertight seal. The basic design was a

Figure 2.3. Construction Details of the Water Calorimeter

Dimensions are in SAE units to correspond with stock materials and machine tools actually used.

WATER CALORIMETER



threaded cylindrical plug with a hole in the centre for the various devices. The central hole was partially drilled from the front to accommodate a rubber gasket and a threaded brass ring. The ring and gasket were slid onto the device which was then pressed into the acrylic fitting. The brass ring was tightened against the gasket to provide a seal..

The calorimeter detector was supported in the tank with three 19.1 mm diameter acrylic legs. These were secured to the bottom of the tank with stainless steel screws. A depth indicator was made from a small length of narrow acrylic rod and attached vertically to one of the legs. The height of the rod was made adjustable by means of a tightening screw on the holder. Holes were drilled in the top of the acrylic legs to accommodate the locating pins on the bottom of the thermistor detector. The locating pins were secured by means of tightening screws on the side of the legs.

The detector signal cable was housed in flexible plastic tubing (12.7 mm outside diameter) and attached to the front wall of the tank with a commercial nylon bulkhead. The signal cable was made from a shielded, four conductor (AWG #22) wire. The connection to the thermistor detector was described previously.

Two 400 watt immersion heaters were mounted from the front side of the tank. These were positioned on the outside of the detector legs and about half way up the tank from the bottom. The immersion heaters were only required for detector calibration and were removed for normal calorimeter operation.

A single probe was used to monitor the temperature of the tank. This was a dual thermistor sensor (YSI 700 series described in more detail in Chapter 3) encased in a stainless steel sheath. The temperature probe was positioned close to the calorimeter detector inside the tank.

A system for bubbling gas into the tank was assembled from plastic tubing and commercial nylon fittings. A hollow vertical column (19.1 mm acrylic tubing) was attached to the front of the tank and connected, via standard tube fittings, near the bottom. The top of the column was fitted with a pressure relief valve. A gas inlet on the exterior of the calorimeter was connected to the relief valve with a length of flexible tubing. A "tee" fitting on the inside of the tank was joined to the vertical column. From the "tee", two separate flexible lines were connected to rigid plastic tubes positioned along opposite sides of bottom of the tank. The system was designed to force the gas flow up from the bottom

corners of the tank and prevent gas pockets from forming beneath the thermistor detector. The gas fittings were used for circulating the water during calibration measurements and were removed from the tank for routine measurements.

The exterior of the calorimeter was made out of 6.4 mm aluminum. The water tank was mounted to the base of the exterior with rubber compressor mounts. These acted to dampen small vibrations which could cause thermal disturbances inside the tank.

The inner tank was thermally insulated from the exterior with 5.1 cm of styrofoam placed uniformly around the tank. In addition to the interior thermal insulation, a 5.1 cm thick styrofoam shell was constructed which fit snugly around the entire calorimeter. This was assembled in pieces before each experiment and was held in place with masking tape.

The lid of the calorimeter consisted of two layers. The first layer was a 2.5 cm thick piece of styrofoam which was cut to fit into the top part of the inner tank. Small acrylic supports were glued in the corners to hold this piece in place. The second layer was a larger piece of the same thickness which covered the entire top of the calorimeter. This system was not designed to be airtight

and a half inch foam backing was attached to the upper lid to ensure this property. The foam provided good thermal insulation and at the same time allowed the system to "breathe". The lid was held in place with masking tape during the experiments.

All of the electrical connectors were placed on one face of the aluminum exterior. The aluminum casing provided good electrical shielding and served as a convenient circuit ground. Rubber feet were attached to the bottom of the aluminum base and metal handles were bolted onto the sides for easy lifting and transporting.

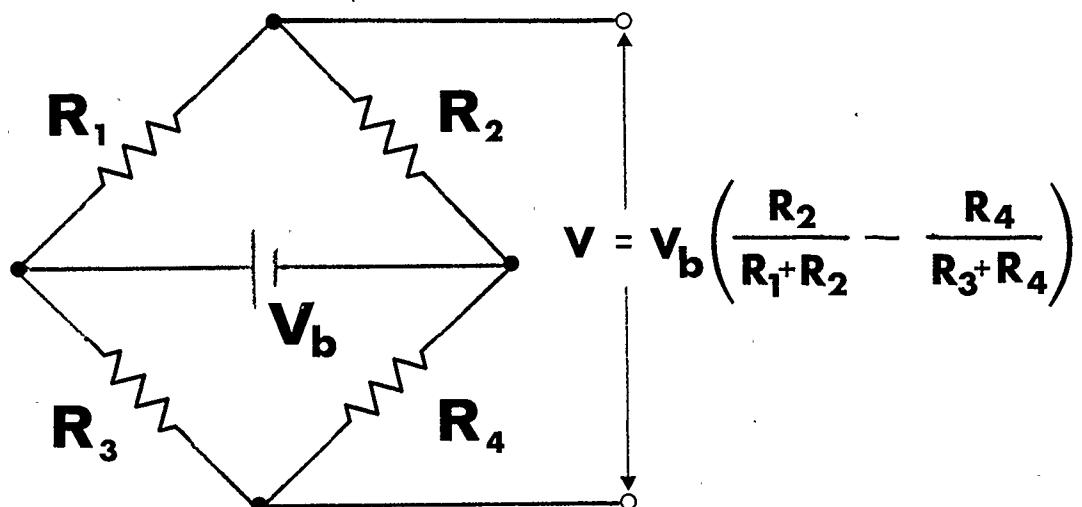
2.7 Wheatstone Bridge

The most accurate and widely used method for measuring resistance is with a Wheatstone bridge. A diagram of this circuit is shown in Figure 2.4. This circuit has been extensively used for calorimetry (Laughlin and Genna, 1966; Gunn, 1964).

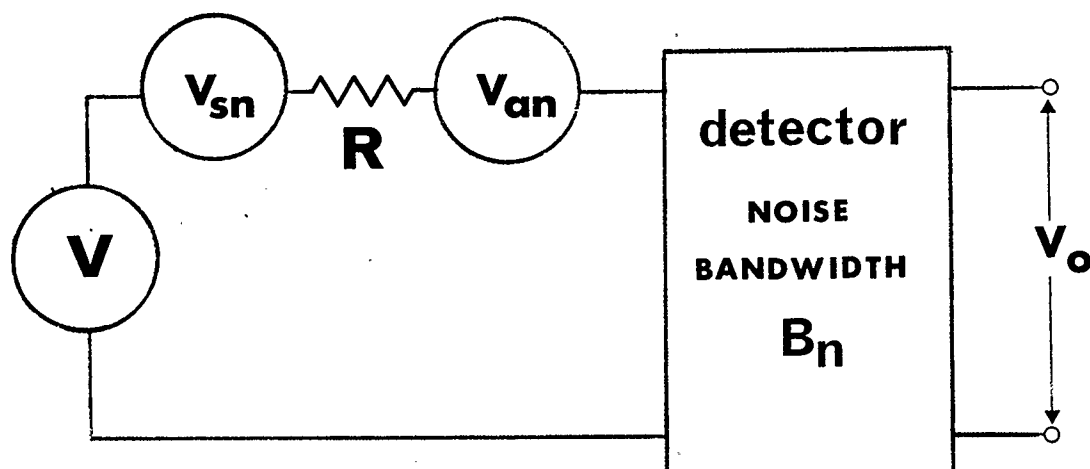
At least one of the resistances is variable so that the voltage across the output terminals can be zeroed. At this point the bridge is "balanced" and from basic circuit considerations (Kirchhoff's laws),

Figure 2.4. Wheatstone Bridge and Thevenin Equivalent Circuit

Wheatstone Bridge



Thevenin Equivalent



$$R = \frac{R_1 R_2}{R_1 + R_2} + \frac{R_3 R_4}{R_3 + R_4}$$

$$V_{sn} = \sqrt{4kTRB_n} \quad \text{THERMAL NOISE VOLTAGE}$$

$$V_{an} = \text{DETECTOR NOISE VOLTAGE}$$

$$\frac{R_1}{R_2} = \frac{R_3}{R_4} \quad \text{or} \quad \frac{R_1}{R_3} = \frac{R_2}{R_4} \quad (2.12)$$

where R_1 , R_2 , R_3 , and R_4 are as shown in Figure 2.4.

For use in calorimetry, one of the resistors in the bridge is replaced with a thermistor. As the thermistor temperature changes (e.g. in response to heating produced from the absorption of radiation), the resistance will change according to equation 2.4. The resulting thermistor resistance can be determined by rebalancing the bridge with a variable calibrated resistor and using equation 2.12. The change in temperature produced from the absorption of radiation can then be calculated from equation 2.5.

The temperature sensitivity (Laughlin and Genna, 1966) of a Wheatstone bridge can be doubled by placing a thermistor in each arm of the circuit. Suppose that R_1 and R_4 (Figure 2.4) are thermistors, R_3 is fixed, and R_2 is variable. Suppose further that R_1 and R_4 decrease by the amounts dR_1 and dR_4 and that the bridge is then rebalanced by lowering R_2 by dR_2 . From equation 2.12 ,

$$\frac{R1 - dR1}{R2 - dR2} = \frac{R3}{R4 - dR4} \quad (2.13)$$

and using equation 2.12 again to eliminate R3,

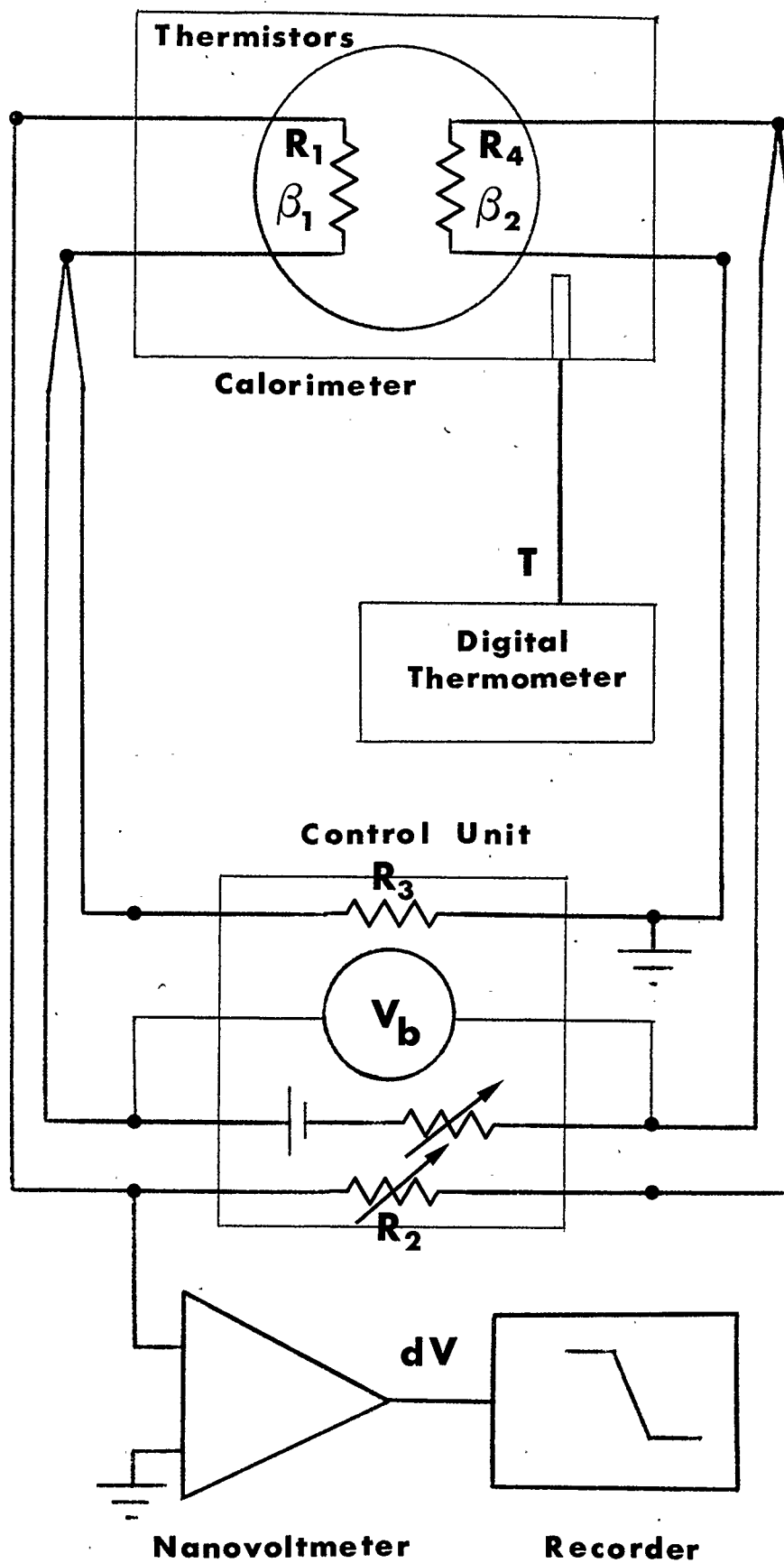
$$dR2/R2 = dR1/R1 + dR4/R4 - (dR1/R1 \cdot dR4/R4) \quad (2.14)$$

For situations where $dR1/R1$ and $dR4/R4$ are much less than one, the total fractional change in resistance $dR2/R2$ will be equal to the sum of the fractional changes from each thermistor ($dR1/R1 + dR4/R4$).

The Wheatstone Bridge circuit that was used for the calorimeter is shown in Figure 2.5. Precision resistors with very low temperature coefficients (less than 1 ppm/K) were used in the circuit along with high quality decade resistances (less than 10 ppm/K). The cable arrangement shown in Figure 2.5 was previously described by Domen (1982b). The circuit was powered with a "D" size 1.35 V mercury cell.

A possible improvement in this circuit would be to connect the power supply right at the calorimeter. In this way, small resistance changes in the leads connecting the dc voltage will have less influence on thermal drift. When this circuit was built and compared to the circuit

Figure 2.5. Circuit Diagram for the Water Calorimeter



shown in Figure 2.5 however, no improvement was observed. It is an obvious practical advantage to locate the power supply away from the calorimeter for power adjustment and switching. Further details concerning the Wheatstone bridge circuit are presented in Chapter 3.

2.8 Voltage Detection

In describing the Wheatstone bridge it was assumed that the initial and final balance conditions were stable. With this assumption, the circuit analysis of the bridge is simplified to a consideration of resistance alone.

Stable balance conditions rarely exist for calorimetry and temperature measurements are usually made in an environment whose temperature is changing slowly and linearly with time. Under these conditions, the change in thermistor resistance must be determined from the change in bridge voltage monitored over time.

From basic circuit (Figure 2.4) considerations, the bridge voltage for an arbitrary set of resistances is given by

$$V = V_b \left[\frac{R_2}{(R_1 + R_2)} - \frac{R_4}{(R_3 + R_4)} \right] \quad (2.15)$$

where V_b is the bridge power supply.

Assuming that R1 and R4 apply to the thermistors, V can be expanded in a series as a simultaneous function of R1 and R4 (e.g. Sokolnikoff and Redheffer, 1966; P336). To second order, the change in the bridge voltage is;

$$dV = V_b \left[\frac{R_2 dR_1}{(R_1 + R_2)^2} + \frac{R_3 dR_4}{(R_3 + R_4)^2} - \frac{R_2^2 dR_1^2}{(R_1 + R_2)^3} - \frac{R_3^2 dR_4^2}{(R_3 + R_4)^3} \right] \quad (2.16)$$

where dR1 and dR4 are the changes in the thermistor resistances and V_b is the bridge power supply.

By using decade resistances, R2 and R3 can be adjusted so that R1=R2 and R3=R4. For this situation equation 2.16 reduces to

$$dV = V_b \left[\frac{1}{4} (dR_1/R_1 + dR_4/R_4) - \frac{1}{8} ((dR_1/R_1)^2 + (dR_4/R_4)^2) \right] \quad (2.17)$$

For the absorbed dose measurements in this study, dR/R is of the order of 10^{-5} and therefore the second order terms

in equation 2.17 can be neglected. The change in bridge voltage reduces to

$$dV = \frac{1}{4} V_b (dR_1/R_1 + dR_4/R_4) \quad (2.18)$$

2.9 Calorimetric Dose Determination

The sum of the fractional changes in resistance produced by two thermistors undergoing the same temperature change is derived from equation 2.5 as

$$dR/R = dR_1/R_1 + dR_2/R_2 = dT \frac{(B_1 + B_2)}{T^2} \quad (2.19)$$

where dT is the change in temperature, and B_1 and B_2 are the thermistor material constants. In this equation it is assumed that the self heating of the thermistors is small and that their initial temperatures are equal. The validity of this assumption is shown in Chapter 3.

The absorbed dose in water is determined by combining equations 2.1 and 2.20). The absorbed dose is

$$D = \frac{c}{w} \frac{T^2}{(B_1 + B_2)} dR/R \quad (2.20)$$

or in terms of voltage,

$$D = \frac{4}{W} \frac{c}{W} \frac{1}{V_b} \frac{T^2}{(B_1 + B_2)} dV \quad (2.21)$$

To obtain the absorbed dose in Gy, the units of heat capacity should be $J \, kg^{-1} K^{-1}$. The heat capacity of water is $4186 \, J \, kg^{-1} K^{-1}$. Equations 2.20 and 2.21 are the design equations of the water calorimeter.

2.10 Signal To Noise Ratio Considerations

2.10.1 Thermal Noise -

The limiting noise level of an electrical circuit is the Johnson or thermal noise. The combination of thermal and additional circuit noise determines the experimental precision with which a voltage measurement can be made. A noise analysis was performed on the water calorimeter circuitry to determine this precision.

A Thevenin equivalent circuit was used to simplify the noise analysis and is shown in Figure 2.4. In general, the open circuit voltage is given by

$$V_s = \left(\frac{R_2}{R_1+R_2} - \frac{R_4}{R_3+R_4} \right) V_b \quad (2.22)$$

where V_b is the bridge power supply. For dose measurement with the calorimeter, the open circuit voltage is given by equation 2.16 .

Since the bridge resistances are much greater than the internal source resistance, the short circuit bridge resistance is given by,

$$R_s = \frac{R_1 R_2}{R_1+R_2} + \frac{R_3 R_4}{R_3+R_4} \quad (2.23)$$

and the thermal noise voltage associated with R_s is determined from (e.g. Simpson, 1974),

$$V_{sn} = \sqrt{4 kT R_s B_n} \quad (2.24)$$

where k is Boltzmann's constant, T is the absolute temperature and where B_n is the detector noise bandwidth.

For Figure 2.4 it was assumed that the current noise is much less than the voltage noise and the total amplifier noise was reduced to that of a single voltage generator. This assumption is justified on the basis that the total detector noise (calculated in the next section)

was approximately the same as the measured noise with the detector input shorted.

To short the input to the detector, a shielded connector was constructed in which the connecting pins were crimped to a short length of copper wire. This technique was suggested by the manufacturer to minimize thermal emfs.

For a detector noise v_n and an amplifier gain G , the signal to noise ratio at the output of the detector is given by

$$(S/N)_{\text{out}} = \frac{G V_s}{G \sqrt{B_n (4 kT R_s + v_{an}^2)}} \quad (2.25)$$

It is assumed in this equation that the noise sources are independent and uncorrelated. To use equations 2.24 and 2.25 it is necessary to calculate the noise equivalent bandwidth of the detector.

2.10.2 Detector Noise Bandwidth -

The detector for the bridge circuit was a Keithley 181 nanovoltmeter. This is a first order detector whose transfer function is given by

$$G(f) = \frac{G_0}{1 + (2 \pi f t_c)^2} \quad (2.26)$$

where f is the frequency of the input voltage, j is $\sqrt{-1}$, G_0 is the maximum gain, and t_c is the detector time constant. This is identical to the transfer function of a low pass RC filter with the same time constant.

The rise time is defined as the time required for a signal to rise from 0.1 to 0.9 of its final value. The rise time can be determined from the step function response of the detector given by

$$r(t) = G_0 (1 - e^{-t/t_c}) \quad (2.27)$$

Solving for t in equation 2.27 the detector rise time is $2.2 t_c$.

Finally, the noise equivalent bandwidth of the detector is defined by

$$B_n = \int_0^{\infty} [G(f)/G_0]^2 df = 1/(4tc) \quad (2.28)$$

or in terms of the rise time t_r

$$B_n = \frac{0.55}{t_r} \quad (2.29)$$

The rise time of the Keithley 181 depends on the selected voltage range. For the 20 mV range (all calorimeter measurements were taken in this range) the rise time is 1 second and therefore the noise bandwidth is 0.55 Hz.

2.10.3 Detector Signal To Noise Ratio -

Using a detector noise bandwidth of 0.55 Hz and a short circuit bridge resistance of 2200Ω in equation 2.24, the rms thermal noise voltage at 297 K is 4.45 nV. This corresponds to a peak to peak thermal noise voltage of 12.6 nV.

The detector noise voltage was observed at about 30 nV p-p for the 20 mV range. This is approximately three times the thermal noise from the bridge resistance. Combining these in quadrature, the total noise voltage at

the output of the detector is 32.5 nV p-p or 11.5 nV rms.

Combining equations 2.25 and 2.21 the overall signal-to-noise-ratio (SNR) is given by

$$SNR = \frac{D}{4} \frac{(B_1 + B_2)}{c_w T^2} \frac{V_b}{\sqrt{B_n (4kTR_s + \frac{V_{an}^2}{s})}} \quad (2.30)$$

For an absorbed dose of 100 cGy, equal B values of 3200 K, a water temperature of 297 K and a bridge voltage of 0.5 V, the signal to noise ratio is 185/1.

2.10.4 Additional Temperature Effects -

2.10.4.1 Thermal Emfs -

The previous analysis has considered the temperature rise from the absorption of radiation as an isolated event. In practice, the detector signal will include an additional background component which may be increasing or decreasing with respect to time. Unless the background is small compared to the voltage produced from the absorbed dose and linear as a function of time, the calorimeter will not provide an accurate measurement.

The background signal originates from two sources; the calorimeter, itself, and thermal effects on the Wheatstone bridge circuit.

If the calorimeter is not in complete thermal equilibrium with its surroundings, the temperature of the water will either be increasing or decreasing. This behavior is usually referred to as "temperature drift" and has often been the nemesis of calorimetry. Temperature drift is the most significant component of the background signal. Methods for controlling drift are discussed in the discussed in the next section.

The Wheatstone bridge was designed to minimize thermal effects. The resistors in the circuit have extremely low temperature coefficients and the connecting cables were built with low resistance wire. However, because the calorimeter signals are in the microvolt range, thermal effects on the Wheatstone bridge can be significant. Equation 2.18 is used to show this.

The fixed resistance in one arm of the bridge circuit is described by

$$R = R_1 + R_2 R_3 / (R_2 + R_3) \quad (2.31)$$

where R_1 and R_2 are precision resistors and R_3 is a variable decade. Assuming that all the resistors change

simultaneously, the differential in R is given by (first order)

$$dR = dR_1 + dR_2 \left(\frac{R_3}{(R_2+R_3)} \right)^2 + dR_3 \left(\frac{R_2}{(R_2+R_3)} \right)^2 \quad (2.32)$$

The temperature coefficient of resistance (manufacturer quoted) for the precision resistors is less than 1 ppm/K. For the decade resistance, this value is range dependent but is generally less than 10 ppm/K. Using these coefficients and component values of $R_1=500 \Omega$, $R_2=5000 \Omega$, and $R_3=4000 \Omega$, the change in resistance produced by a one degree change in temperature is 1.44×10^{-2} . By substituting this value in equation 2.18, the change in detector voltage for a one degree change in temperature and a bridge supply voltage of 0.5 V is $1.32 \mu V$. This is extremely large and is of the same order of magnitude as the absorbed dose signal voltage.

Fortunately, large isolated temperature changes do not occur in the circuit during calorimeter operation and the above behavior was not observed. Potential circuit effects were studied by replacing the thermistor detector with precision resistors and monitoring the bridge output with time. This was performed on a number of occasions to troubleshoot erratic calorimeter behavior. No significant

thermal effects from the bridge circuit were ever observed.

2.10.4.2 Temperature Drift Control -

Two techniques for controlling temperature drift have been reported by Domen (1982b; 1983). The first method was to apply a DC voltage across planar, stainless steel electrodes placed on opposite sides of the water tank. By varying the applied voltage, a level of ohmic heating (I^2R) was achieved to balance the temperature drift. This method is limited to controlling cooling drifts and complicates the interpretation of the heat of reaction from the radiolysis of water (see Chapter 4). Consistent water purity (as determined by electrical conductivity) is mandatory for this method to be practical.

The second method proposed by Domen was to apply a small voltage directly to the bridge output to exactly compensate for the drift. This technique requires the construction of an RC circuit (Domen, 1983) with a variable time constant. Using the circuit, a small (approximately linear) ramping voltage is applied directly to the output of the calorimeter bridge. The slope of the ramp is controlled by adjusting the RC time constant and the initial magnitude is preset with a potentiometer. This method can be used to compensate for either heating

or cooling drifts.

The RC circuit was preferred over the parallel electrode method and was built into the control unit. Four 1.35V mercury cells were used in series to power the circuit and time constants of 3, 7, 15, and 30 minutes were selectable. The large time constants were achieved with a 2.2 microfarad capacitor and high-megaohm metal oxide resistors obtained from Victoreen. The RC circuit was tested and found to perform very well.

Temperature drift, however, is not simply a minor technical problem that can be eliminated by using an RC circuit. Considerable effort must be expended to ensure that the calorimeter, water, and surrounding air temperature are very nearly equal. Failure to achieve these conditions will result in temperature drift which is well beyond the controlling capabilities of the RC circuit described previously.

The most important factor in controlling temperature drift is the regulation of the air temperature surrounding the calorimeter. This is a significant problem in a hospital environment where the room temperature may vary by a few degrees during a long series of dose measurements. To minimize this effect, a 5.1 cm layer of styrofoam insulation was added to the exterior of the

calorimeter (described previously).

The water calorimeter has an advantage for controlling temperature drift in that the water can be easily and quickly matched to the initial room temperature. However, because it is easily disturbed, air temperature is generally a poor reference and a preferred method was to monitor the wall temperature of the tank.

A narrow hole was drilled in the tank wall to accommodate a removable thermistor probe. The same probe was used to match the water temperature and was left undisturbed in the tank wall until required. Immediately prior to mixing the water, the wall temperature was monitored until a steady reading was obtained. Both the water and the empty calorimeter were stored in the room for several hours prior to measurement (typically 10 hours). The required volume of water was kept in a single Nalgene container.

To obtain the required temperature, warmer or cooler water was added to the water from the nalgene tank. The mixing process was performed in clean plastic pails and the water was then poured into the calorimeter and covered with styrofoam insulation.

This procedure was used routinely to provide from 6-8 hours of calorimeter operation. For the measurements in this study, no additional means for drift control were required. It is important to note, however, that the air conditioning system of the hospital was an integral part of the operation of the calorimeter.

2.10.4.3 Thermistor Temperature And Power Increase During Irradiation -

During a calorimeter measurement the thermistor resistance will decrease with increasing thermistor temperature and therefore the power level and self heating will increase.

Assuming that the voltage across the thermistor remains constant during a run, (this was a reasonable approximation to four significant figures i.e 10^{-4} V) an expression can be derived for the change in thermistor power as a function of resistance. Subtracting the thermistor powers before and after a small temperature increase dT ,

$$dP = \frac{V^2}{R} \left(\frac{1}{1 - a dT} - 1 \right) = \frac{V^2}{R} \frac{a dT}{(1 - a dT)} \quad (2.33)$$

where V is the thermistor voltage, R is the initial thermistor resistance, and α is the temperature coefficient of resistance (equation 2.5) of the thermistor. Since $\alpha \Delta T$ is much less than one, it follows from equation 2.33 that $dP/P = \alpha \Delta T$. This shows that the fractional change in thermistor power per degree K is approximately the same as the magnitude of the temperature coefficient of resistance. For an initial thermistor power of 30 microwatts and a temperature coefficient of resistance of 0.036/K, the power increase per degree K increase in temperature is given by 10^{-6} W/K. For a temperature change of 2.39×10^{-4} K (100 cGy) the corresponding change in thermistor power would be 2.39×10^{-10} W.

It can be shown theoretically (Appendix A) and is demonstrated experimentally (Chapter 3), that the excess thermistor temperature per unit power (for a 0.25 mm diameter thermistor insulated with polyethylene films) due to its power consumption is about 2.6×10^{-3} K per microwatt. Thus the expected temperature rise due to the small power change calculated above is 10^{-7} K. This represents a change in the signal voltage of a few nanovolts which is comparable to the thermal noise generated by the bridge resistance (i.e insignificant).

2.11 Convective Heat Loss

2.11.1 Rayleigh Number -

Heat transfer by convection is an important consideration in the design of a water calorimeter. If this process could not be eliminated then the calorimeter would have little practical value.

In a liquid, conduction and convection compete simultaneously and both of these processes are initiated by the presence a temperature gradient. In the higher temperature region, the molecules will expand with increased kinetic energy and will experience a buoyant force due to a lower density in the gravitational field. Counteracting the buoyant force, is the viscosity of the liquid and the continuous loss of heat due to conduction.

Convection will occur when the buoyant force overcomes viscous drag. This implies that convection is a threshold process and is controlled by both the temperature gradient and the properties of the liquid.

The onset of convection is characterized by the Rayleigh number (McLaughlin, 1965) which is the product of the Prandtl and Grashof numbers. These are characteristic parameters derived from basic conservation laws (Schmidt, 1949). Defining Ra as the Rayleigh number,

$$Ra = Pr \ Gr \quad (2.34)$$

where Pr and Gr are the Prandtl and Grasof numbers.

For a given geometry and liquid, there will be a critical Rayleigh number such that convection will occur for all values greater than or equal to that number.

The Prandtl number is defined by (Schmidt, 1949),

$$Pr = \nu/\alpha \quad (2.35)$$

and the Grasof number by

$$Gr = g \ \xi \ dT \ \frac{d^3}{\nu^2} \quad (2.36)$$

where dT is the temperature difference between horizontal planes, d is the separation of the planes, g is the acceleration due to gravity, ξ is the volumetric coefficient of expansion, ν is the kinematic viscosity, and α is the thermal diffusivity. Note that the definition of the Grasof number applies to a geometry in which the fluid in question is between two infinite parallel planes.

As described by McLaughlin (1965), the Grashof number is a measure of the relative importance of the buoyant and viscous forces while the Prandtl number is the ratio of the molecular diffusivity of momentum to the molecular diffusivity of energy.

Equation 2.35 and 2.36 show that the important functional dependence of the Rayleigh number is on the temperature difference. The d dependence in the Grashof number is misleading because it is built in to the equation in the same way as the viscosity (i.e. it is fixed for a given determination of a threshold for convection).

2.11.2 Threshold Temperature Gradient -

If the critical Rayleigh number is known, then it is possible to derive a threshold temperature gradient which is a more relevant parameter for the design of a calorimeter. Velarde and Normand (1980), reported that the critical Rayleigh number for a silicone oil system (parallel plane geometry), and for a depth of a few millimeters, is approximately 1700. This information can be used to derive the Rayleigh number for an equivalent water system.

From equation 2.35 , the ratio of critical Rayleigh numbers for different liquids in the same geometry is

$$\frac{Ra_1}{Ra_2} = \frac{\xi_1 \alpha_2 \nu_2}{\xi_2 \alpha_1 \nu_1} \quad (2.37)$$

where the constants are the same as defined previously. Substituting the appropriate values for water and the silicone oil at room temperature, the critical Rayleigh number for water is 489.

Using this Rayleigh number in equation 2.34 , the temperature gradient (vertical direction) in water required to cause convection is 0.5 K/mm. It should be stressed that this analysis applies strictly to a parallel plane geometry in which the temperature gradient across the planes is uniform and constant. In practice, the critical temperature gradient for the onset of convection may be substantially less than this value and depends on the exact geometry.

The concern about convection in the water calorimeter arises from a non-uniform temperature distribution produced from the absorption of a beam of radiation. As shown in Appendix D, convection in water may occur from the absorption of a beam of cobalt-60. By using the thermistor detector described in Section 2.4, however,

convection is prevented by the polyethylene films (Appendix D).

It is of interest to note that the largest temperature gradient occurring in the water tank is in the immediate vicinity of the thermistors. From Appendix A, the temperature gradient in water outside the thermistor is given by

$$\frac{dT}{dr} = - \frac{P}{4 \pi K} \frac{1}{r^2} \quad (A.16)$$

where P is the thermistor power, K is the thermal conductivity of water and r is the distance from the centre of the thermistor to the point at which the gradient is calculated (the maximum gradient occurs at the outer surface of the thermistor where r is equal to the radius). For a 0.25 mm diameter thermistor dissipating 20 microwatts of electrical power (see Figure A.2, Appendix A) the temperature gradient at the outside surface is approximately 0.2 K/mm. This is extremely close to the approximate threshold for convection calculated above.

Because of the large temperature gradients it is very likely that there is an ongoing convective circulation in the vicinity of the thermistors. This applies even to thermistor detectors using polyethylene films. As long as

these currents remain in equilibrium (undisturbed), however, this should have no influence on dose measurements. This supposition is supported experimentally in Section 4.3.3. It should be noted that the temperature gradient due to the thermistor can be reduced by using a larger thermistor or by reducing the thermistor power (equation A.16, Appendix A).

CHAPTER 3

INSTRUMENT AND THERMISTOR CALIBRATION

3.1 Calibration Requirements

The calibration requirements for the water calorimeter are evident from equation 2.21 which defines the absorbed dose. Introducing D_w as the dose in water and c_w as the heat capacity of water, the absorbed dose is given by

$$D_w = c_w dT \quad (3.1)$$

where dT is the temperature rise due to radiation absorption. Using a two thermistor detector and a Wheatstone bridge, the temperature rise is determined from

$$dT = \frac{V_b^4 T^2}{(B1 + B2)} dV \quad (3.2)$$

where B1 and B2 are the thermistor material constants, T is the initial temperature of the water, V_b is the bridge supply voltage, and dV is the change in signal voltage (bridge output) produced by radiation absorption.

A schematic of the calorimeter instrumentation is shown in Figure 2.5.

3.2 Temperature Calibration

The water temperature was measured with a commercial digital thermometer with a precision of 0.01 K. This instrument was designed for use with dual thermistor probes of the YSI format (Yellow Spring Instruments, 700 series). For 0.01 K accuracy, these probes are not suitable without a calibration against a temperature standard.

All the probes used in this study were calibrated against a Rosemount platinum resistance thermometer (model 162CE). The Rosemount probe had been previously calibrated using a triple point cell and the IPTS-68 temperature scale (CIPM, 1969; CIPM 1976).

The calibration of the thermistor probes was done in a temperature controlled bath (Guildline 9734) using a silicon liquid (Dow Corning 200 fluid). The bath temperature was varied between 286 and 305 K and regulated to ± 0.01 K. At each temperature, the readout from the digital thermometer was recorded with the resistance of the Rosemount probe. Resistance readings were determined from a precision ohmmeter (Guildline) and a four wire technique to eliminate lead resistance. A computer algorithm was written to fit the resistance of the Rosemount probe to a third order polynomial in temperature (Bevington, 1969). In this way, rapid and accurate temperature conversion was automatically incorporated into the calorimetric data analysis. The overall procedure provided a temperature measuring system with an accuracy of ± 0.01 K.

3.3 Thermistor Calibration

3.3.1 Material Constant -

As stated in Chapter 2 (equation 2.4), the resistance of a thermistor is related to its temperature by

$$R(T) = R_0 e^{B(1/T - 1/T_0)}$$

where T is the absolute temperature, R_0 is the resistance at T_0 (usually 298 K) and B is the material constant of the thermistor. The object of a calibration is to determine B for each thermistor.

Equation 2.4 is theoretically based on the conduction of a pure semiconductor. The conductivity for such materials is largely dependent on the energy gap between the valence and conduction electronic energy levels. These semiconductors are defined as "intrinsic" and are characterized by a linear relationship between $\ln R$ and $1/T$.

The thermistors used in this study were manufactured from metal oxides and these exhibit extrinsic conduction. The conductivity in these materials is determined by the number of lattice defects which control the excess of charge carriers in the valence band. Factors which affect the number of lattice defects include the relative concentration of the oxides, the absolute concentration of oxygen, the temperature, and the method of fabrication. For these materials B is a function of temperature and as

pointed out by Sapoff (1982) B increases slightly with increasing temperature.

The conventional method for determining B is from the slope of a linear graph of $\ln R$ and $1/T$. For temperature ranges exceeding 10 K, however, this method is limited because of the temperature variation of B.

A more satisfactory approach (Sapoff et al, 1982) is to fit $\ln R$ to a quadratic polynomial in $1/T$ and determine B from the derivative of the polynomial. Shown explicitly,

$$\ln(R) = a + b (1/T) + c (1/T)^2 \quad (3.3)$$

and the material constant is derived from

$$B = \frac{d(\ln R)}{d(1/T)} = b + \frac{2c}{T} \quad (3.4)$$

With this technique, B is evaluated as a continuous function of temperature.

3.3.2 Excess Thermistor Temperature -

The measurement of thermistor resistance requires finite power consumption and therefore the temperature of the thermistor is always slightly above that of its immediate environment. This problem limits the accuracy with which the material constant can be determined because of the uncertainty of the thermistor temperature.

To minimize this uncertainty, the resistance of a thermistor can be determined at several different power levels and graphically extrapolated to zero power. By definition, the zero power resistance corresponds to the same temperature as that of the environment.

Equation A.13 (Appendix A) states that the excess thermistor temperature due to electrical power dissipation is directly proportional to the thermistor power. Because the resistance of a thermistor is exponentially dependent on $1/T$ (equation 2.4, Chapter 2), the thermistor resistance should be exponentially dependent on $1/P$. For thermistor powers less than 100 microwatts, however (excess thermistor temperature less than 0.26 K), the thermistor resistance (to five significant figures) is directly proportional to the temperature. Thus, for thermistor powers less than 100 microwatts, equation A.13 predicts that thermistor resistance should be directly

proportional to the power.

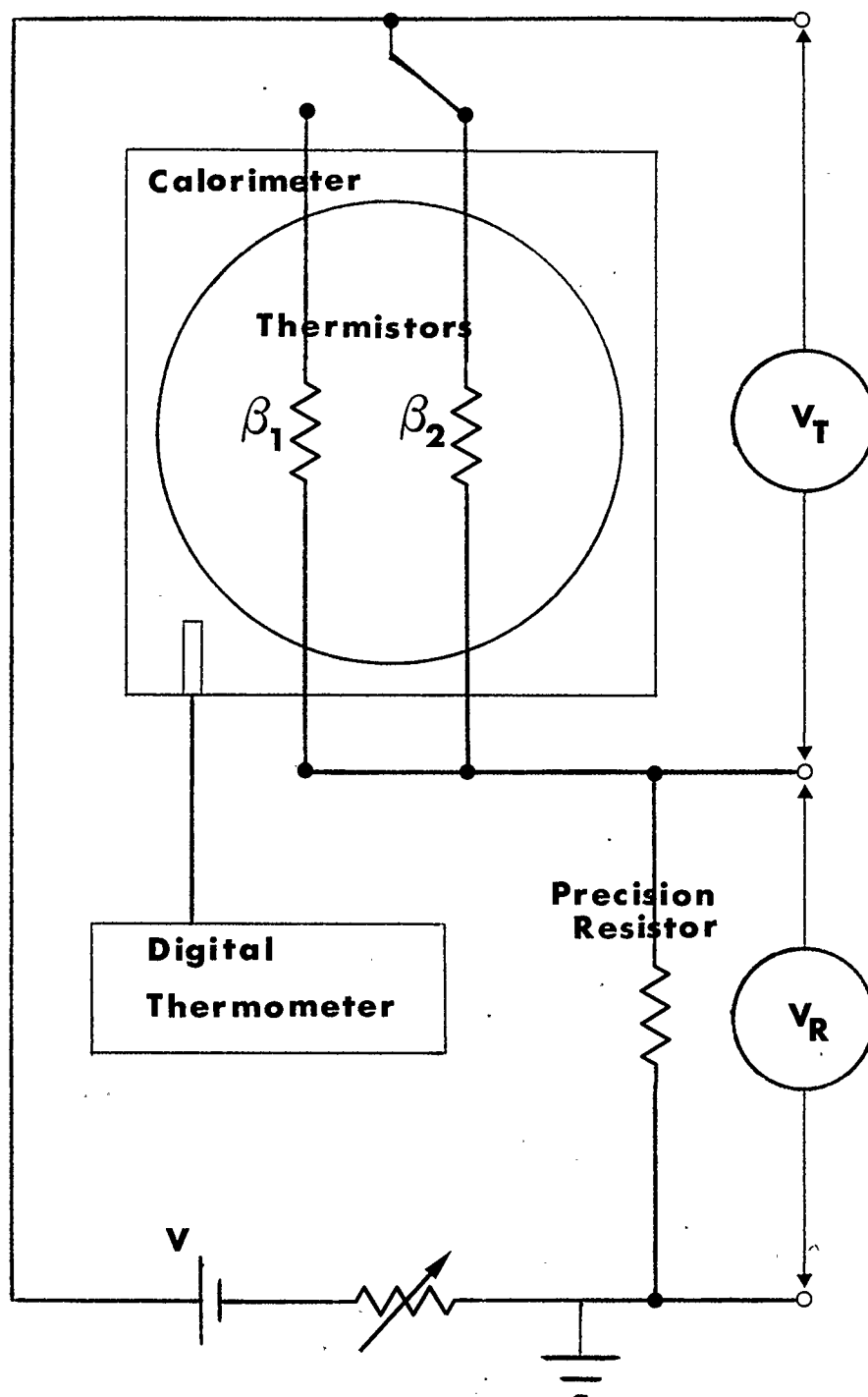
In practice, plots of thermistor resistance versus power were very linear and zero power resistances (y-intercept) were determined with typical uncertainties of 0.01% (95% confidence).

3.3.3 Experimental Determination Of The Thermistor Material Constant -

A separate circuit was constructed for the thermistor calibration and is shown in Figure 3.1. With this circuit, either thermistor in the detector could be switched in series with a DC voltage, a variable resistor and a fixed precision resistor. The voltages across the thermistor and precision resistor were monitored with a high impedance voltmeter.

The measured thermistor voltage included a small lead component which was subtracted from the total to obtain the actual "bead" voltage. The lead voltage could not be measured directly and was calculated from the product of the current and the lead resistance. Lead resistances were determined from the product of the length and resistance per unit length. The largest fraction of the lead resistance was from the 0.025 mm diameter Pt-Ir leads emerging from the thermistor. The resistance per unit

Figure 3.1. Thermistor Detector Calibration Circuit



length of the Pt-Ir wire leads was measured from segments which had inadvertently broken away from thermistors during detector construction (A four wire technique was used to eliminate meter lead resistance). The resistance per unit length of the longer (0.075 mm diameter) Cu wire leads (or for some thermistors Ni) was determined from the slope of a resistance versus length graph (Resistance measurements were made for lead lengths between 10 and 90 cm). The current in the calibration circuit was determined from the quotient of the voltage across the precision resistor and the and the measured resistance. The resistance of the thermistor bead was then calculated from the quotient of the bead voltage and the current.

The impedance of the voltmeter used in the calibration was of the order of 10^9 ohms and therefore no circuit correction was needed. The thermistor power was variable between 0-100 microwatts. This is approximately the same range as was available from the calorimeter circuit.

At the start of a calibration, the calorimeter was filled with water at about 288 K. Voltage readings were then taken across the precision resistor and each thermistor at ten different power levels. The temperature of the water was then raised with two immersion heaters and the water was circulated by bubbling nitrogen. This

procedure was repeated in one degree increments until a final temperature of 304 K was reached. Approximately 15 minutes were required for the calorimeter to equilibrate at each temperature. The calibration voltage readings were then stored in a data file (one file per thermistor) for subsequent analysis.

A computer program was written to process the calibration voltage data. In addition to calculating the material constants, the program also calculated the excess temperature per unit thermistor power. This parameter was used to correct the temperature in the calorimeter data analysis. The important steps in the program included;

- o a calculation of thermistor resistance and power from the voltage data
- o a correction of water temperature measurements to agree with temperature standard
- o a calculation of zero power thermistor resistance (at each water temperature) from a linear plot of resistance versus power
- o a regression fit of $\ln(\text{zero power resistance})$ to a quadratic polynomial in $1/T$

- o a determination of $B(T)$ from derivative of regression polynomial; i.e. $d \ln(R)/d(1/T)$
- o a calculation of excess thermistor temperatures at each power using equation 2.4
- o a determination of excess thermistor temperature per unit power (at each water temperature) from linear graph of temperature versus power
- o a regression fit of resistance versus power data to third order polynomial in water temperature
- o a regression fit of excess temperature per unit power data to third order polynomial in water temperature
- o a calculation of various statistics e.g. B at 296 K
- o storage of calibration data for use in processing calorimeter measurements

3.3.4 Calibration Data -

3.3.4.1 Material Constant Variation With Temperature -

Calibration was performed on sixteen separate detector assemblies with differing physical properties such as thermistor size, polyethylene thickness, lead material, and material constants. The important

calibration data is summarized in Table 3.1.

The material constant for all thermistors was found to increase with increasing temperature. However, the fractional change in B per unit temperature increase is very small and as indicated by the data in Table 3.1 was no larger than 0.11%. For an operating temperature range of 293-298 K, the maximum change in a material constant was 0.55%.

As indicated from the correlation coefficients, graphs of thermistor resistance versus power were highly linear and the maximum uncertainty (95% confidence interval) in the zero power resistance at any temperature was 0.04%. The graphs of $\ln(R)$ versus $1/T$ were also very linear with a typical correlation coefficient of 0.9995. Using the linear technique ($\ln R$ vs $1/T$) and temperature intervals of 10 K, the maximum uncertainty (95% confidence level) in B was found to be 0.15%. Typical calibration data are shown in Figure 3.2.

3.3.4.2 Effect Of Polyethylene Films -

To demonstrate the effect of the polyethylene films a calibration was done using thermistors which could be immersed directly in water. This type of thermistor is available commercially (Thermometrics, 1985). The object

TABLE 3.1

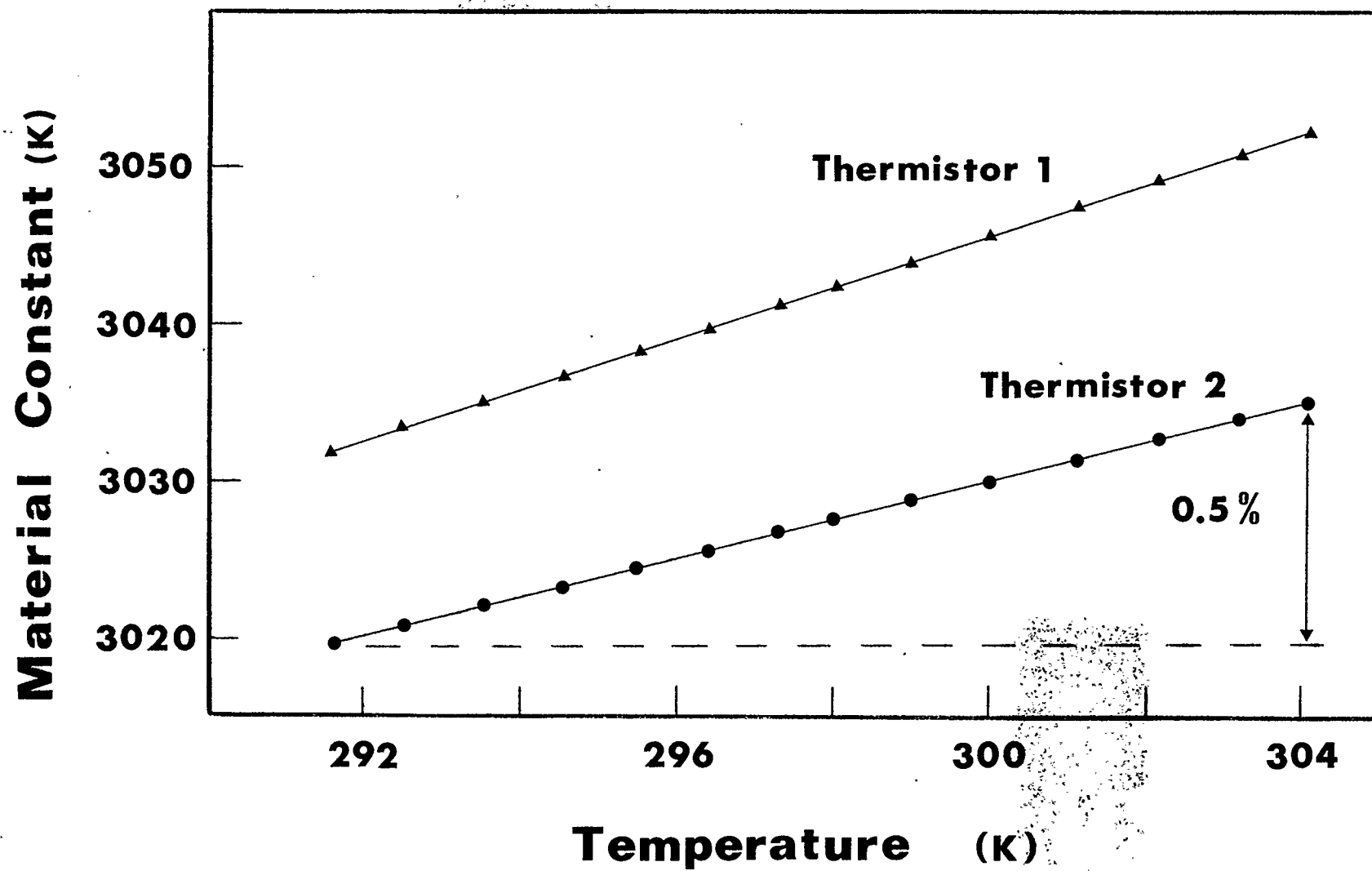
THERMISTOR DETECTOR CALIBRATION DATA

(Polyethylene Film Insulated)

CALIBRATION TEMPERATURE RANGE: 288 - 305 K

Detector	Polyethylene Film Thickness (μm)	Thermistor Diameter (mm)	Thermistor β @ 296 K (K)	% Increase in β per K Increase in Thermistor Temp.	v_{xp}/P (mK/ μW)	% Decrease in v_{xp}/P per K Increase in Water Temp.
A	14.0	0.25	3223	0.09	2.5	1.0
			3195	0.11	2.5	1.0
B	27.9	0.25	3235	0.11	2.8	0.7
			3221	0.10	2.8	0.5
C	41.9	0.25	3126	0.08	3.1	0.5
			3175	0.09	3.3	0.3
D	14.0	0.50	3086	0.08	2.0	1.0
			3085	0.06	1.8	1.2
E	14.0	0.89	3500	0.08	0.69	1.1
			3504	0.07	0.64	1.2
F	41.9	0.89	3515	0.07	0.87	0.9
			3519	0.06	0.89	0.8

Figure 3.2. Variation of Thermistor Material Constant with Temperature



of this experiment was to do a calibration with the same thermistors both in water and in a detector with polyethylene films.

The first calibration was done conventionally with the thermistors mounted in a polyethylene film detector. Immediately afterwards, a 2.5 cm diameter hole was cut out of the films around the thermistors and a second calibration was performed with the thermistors in water. The data from these experiments is shown in Table 3.2 and Figure 3.3. It can be seen from Table 3.2 that the excess temperature per unit power (v_{xp}/P) for the thermistors insulated with 14.0 μ m polyethylene films was two times higher than when immersed directly in water.

The material constant values determined with the thermistors in water were 0.06 % higher than those with the thermistors in polyethylene. This difference is much less than the uncertainty in either determination and was therefore considered insignificant. This was a good indication that the data in Table 3.2 were reliable.

Using equation A.13 (Appendix A) and a thermal conductivity for polyethylene film of $(3.2 \times 10^{-3} \text{ W cm}^{-1} \text{ K}^{-1})$, the calculated increase in the excess thermistor temperature due to 14.0 μ m thick films was 0.5%. In this calculation a thermistor diameter of 0.38

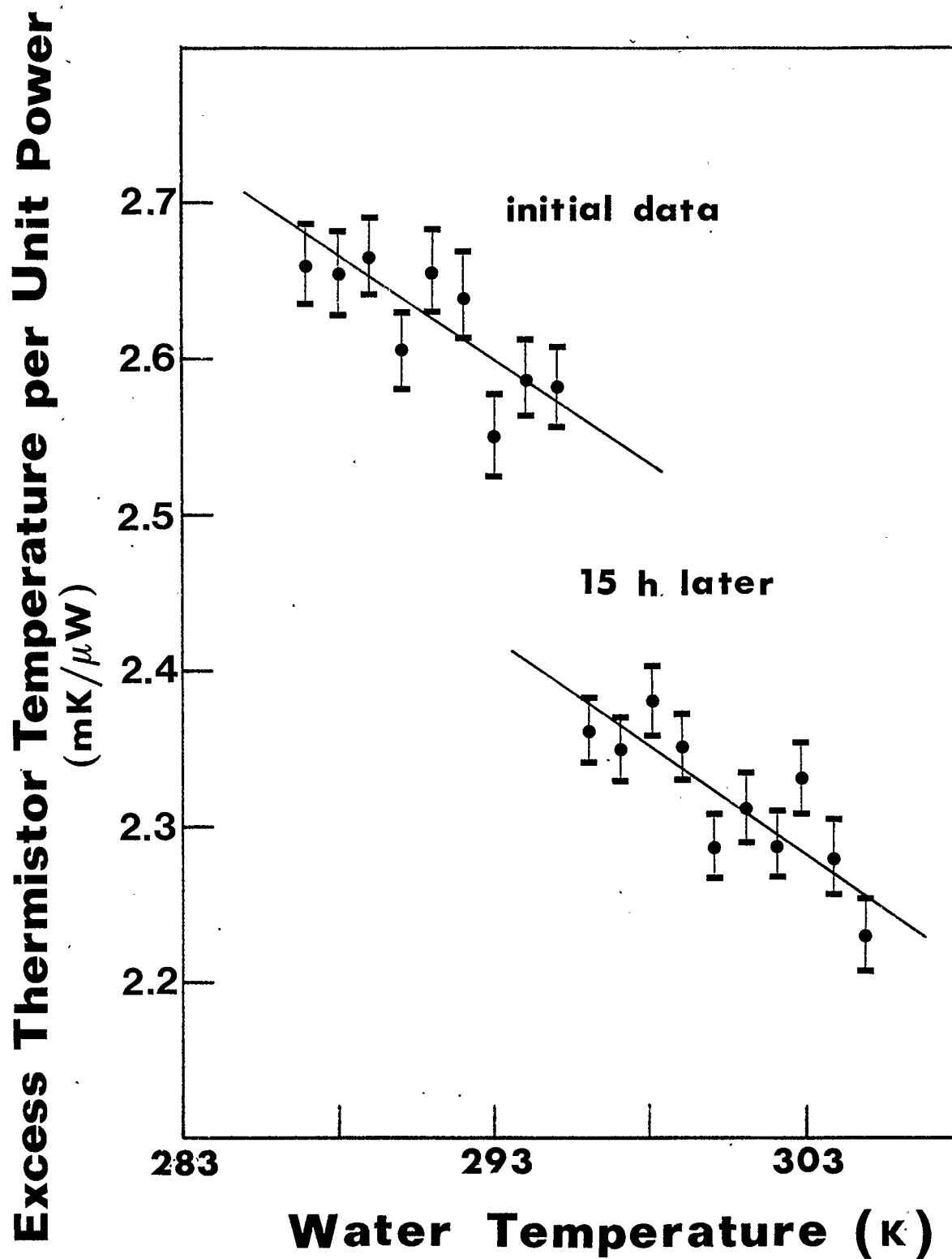
TABLE 3.2

THERMISTOR DETECTOR CALIBRATION DATA
 COMPARISON OF IMMERSIBLE THERMISTOR AND
 POLYETHYLENE FILM INSULATED THERMISTORS
 Calibration Temperature Range: 288 - 305 K

Detector Description	Thermistor β @ 296 K (K)	% Increase in β per K increase in thermistor temp	V_{xp}/P (mK/ μ W)	% Decrease in V_{xp}/P per K increase in water temp
0.33 mm dia immersible thermistors insulated with 14.0 μ m polyethylene film	3146	0.05	2.3	1.2
	3110	0.06	2.4	0.8
0.33 mm dia thermistors immersed directly in water	3148	0.06	1.2	1.3
	3111	0.06	1.2	1.2

Figure 3.3. Variation of Excess Thermistor Temperature Per Unit Power with Water Temperature.

**0.25 mm dia thermistor
in polyethelene films**



mm and a power of 30 microwatts have been used. Even if the thermistor is completely replaced by polyethylene the estimated difference in the excess temperatures is only 10%. These calculations suggest that the factor of two difference observed in Table 3.2 may have been due to the insulating effect of the surrounding air. Large differences in the excess thermistor temperature can be easily demonstrated by using a thermal conductivity for air of $2.54 \times 10^{-4} \text{ W cm}^{-1} \text{ K}^{-1}$ in equation A.13.

The excess thermistor temperature per unit power was found to depend on the amount of time that the thermistor detector had been immersed in water. This was observed by calibrating a detector over a two day period and determining the excess temperatures as described previously. The results of an experiment are shown in Figure 3.4. On the second day (approx 15 h later), the excess temperatures were found to decrease by about 10% presumably due to improved contact (i.e. less air present between the polyethylene films) with the water. While this is only apparent from one point in the graph a similar pattern was obtained from other detectors at different temperatures that were also calibrated over a two day period. On the basis that no further change in the excess thermistor temperature was observed with immersion time, it was concluded that about 15 h was

Figure 3.4. Variation of Excess Thermistor Temperature Per Unit Power with Water Temperature.

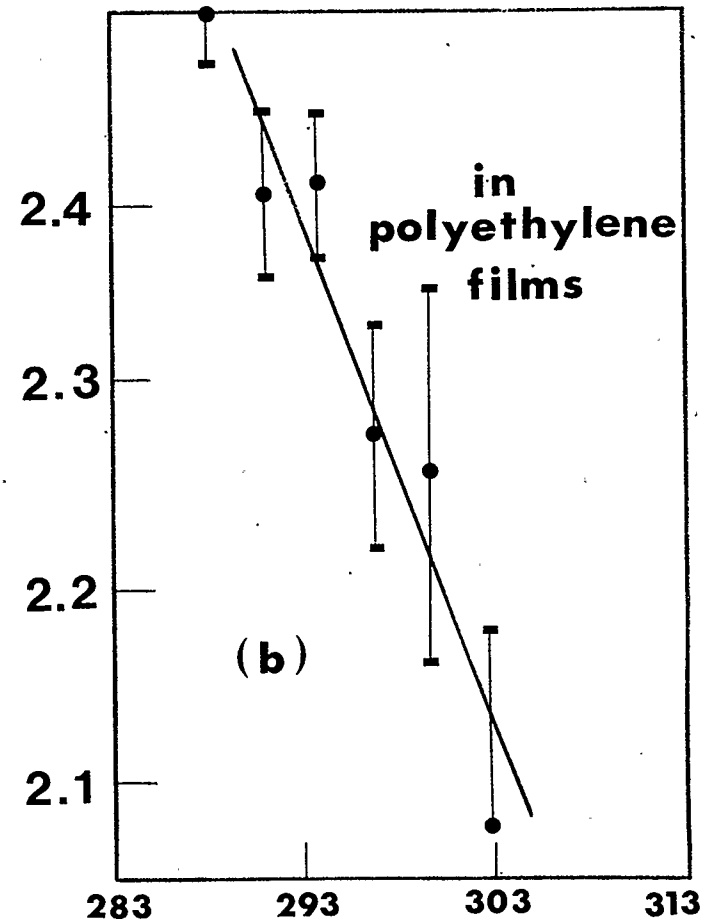
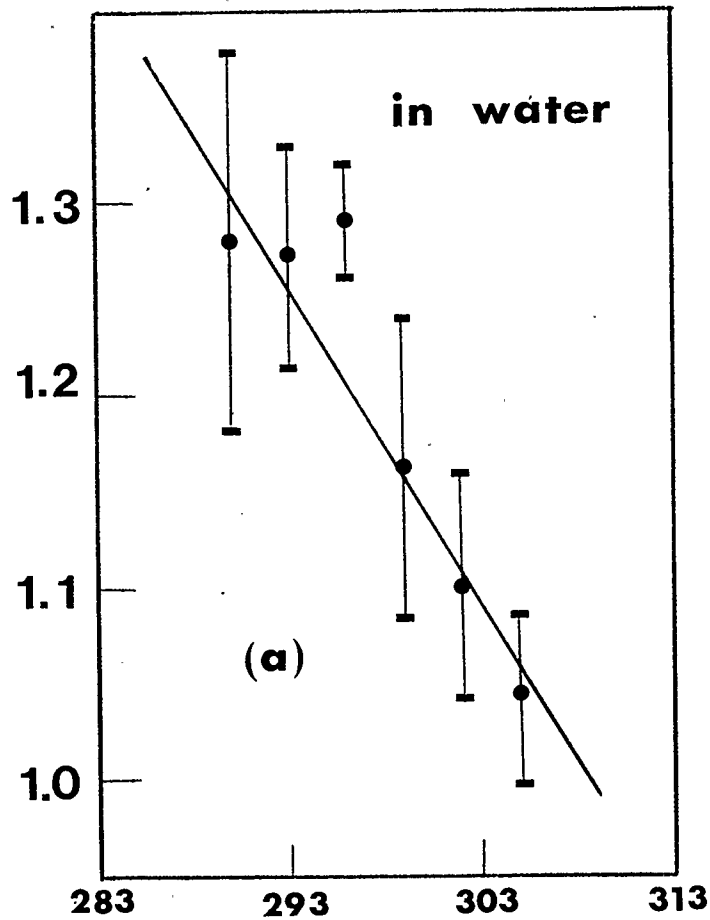
(a) for 0.038 mm diameter immersible thermistors

(b) for the same thermistors but insulated with polyethylene films

Excess Thermistor Temperature

per Unit Power $\left(\frac{\text{mK}}{\mu\text{W}}\right)$

Immersible 0.38mm dia thermistor



Water Temperature (K)

required for any excess air which is initially trapped between the polyethylene films to be forced out of the detector by water pressure (depth = 2.5 cm).

The presence of air in the thermistor detector was also indicated from dose measurements where the excess thermistor temperature produced directly from radiation absorption was several times greater than expected (Figure D.1, Appendix D). It should be pointed out that as long as the air near the thermistors is stagnant (does not circulate) and does not change in volume, then the excess thermistor temperature will not fluctuate. However, because the excess temperature is two orders of magnitude higher than the temperature rise produced from an absorbed dose measurement (100 Gy), short term changes in this quantity can significantly effect dose measurements.

Another observation from Figures 3.3 and 3.4 (also shown in Table 3.1) is that the excess thermistor temperature per unit power decreases with increasing water temperature. Because this trend was observed for thermistors immersed directly in water, it was concluded that this was not due to the polyethylene films and surrounding air mass. It is shown in Appendix B that the thermal conductivity of water increases by about 4% over a temperature range of 288-305 K. According to equation A.13 (Appendix A), the increase in the conductivity of

water would explain some of the observed decrease in the excess thermistor temperature.

3.3.4.3 Thermistor Calibration In A Cobalt-60 Beam -

To investigate the possibility that the material constant changes in a radiation field, a calibration was performed directly in a cobalt-60 beam. The same procedure was followed as for a conventional calibration except that the voltage readings were taken while the beam was irradiating the thermistor detector. The same dose rate was used for the calibration as that for dose measurements. A comparison of the material constants determined in and out of the beam showed a difference of 0.3% which is comparable to the uncertainty in either value. The difference was concluded to be insignificant.

3.4 Nanovoltmeter Calibration

The direct calibration of a nanovoltmeter requires a precision low voltage power supply and is subject to a number of practical difficulties. Noise and thermal emfs can easily perturb sub-microvolt signals.

The Keithley 181 nanovoltmeter has three separate millivolt ranges corresponding to maximum input levels of 2, 20 and 200 millivolts. The accuracy of these ranges

was tested using an EDC (Electronic Devices Corporation Model MV 106G) dc voltage standard. A connecting cable was assembled to go from the Keithley triax format to BNC.

Voltage checks were performed (with both positive and negative polarity) by serially incrementing the voltage from the voltage standard and reading the digital display on the 181. For all three voltage ranges, excellent agreement was observed between the input and measured voltages. Verification for voltages less than 0.1 microvolt was limited by noise.

The accuracy and linearity of the nanovoltmeter was further tested by using equation 2.18. This expression equates a change in bridge voltage to changes in the resistances of a Wheatstone bridge. Simplifying this equation,

$$dV = \frac{1}{4} V_b \frac{dR}{R} \quad (3.5)$$

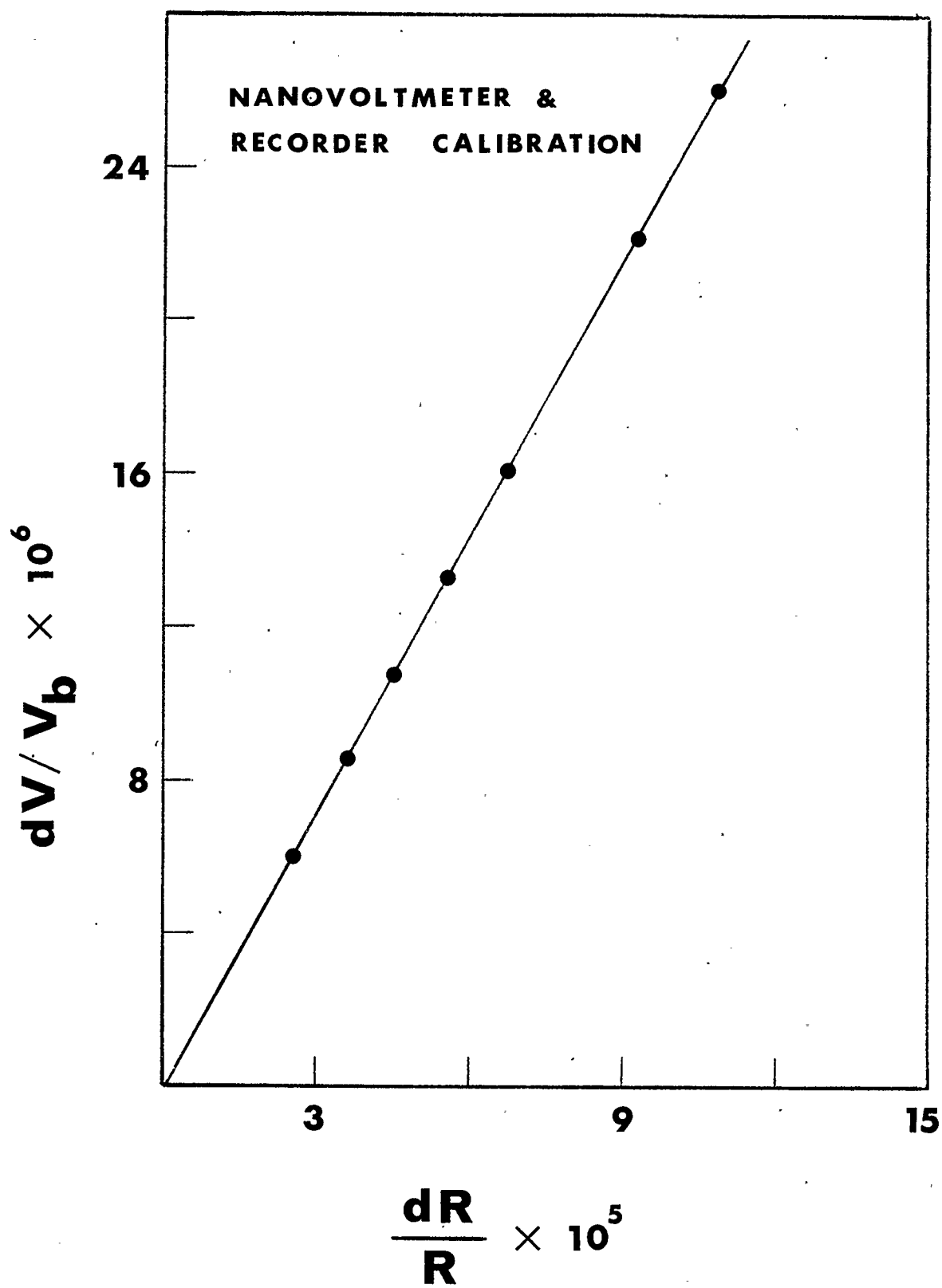
where V_b is the supply voltage, dV is the change in bridge voltage, and dR/R is the fractional change in resistance of one of the arms of the bridge. Because the accuracy of the resistances was better than four significant figures, this method was excellent for determining the meter accuracy down to 10^{-9} V.

The operation of the water calorimeter requires the use of a strip chart recorder to trace out the bridge voltage as a function of time. Thus, it was necessary to calibrate the chart displacement in conjunction with the nanovoltmeter.

The preferred method for the calibration was to use the same circuitry as was used for calorimeter measurements. A detector assembly containing resistors (described in Chapter 2) was installed in the calorimeter in place of a thermistor detector. Calibration data was obtained by varying the bridge supply voltage and determining dV as a function of dR/R . This was done in 0.05 V increments for supply voltages ranging from 0.1-0.5 V. For each data point, the bridge was initially balanced so that the voltage across each arm was equal. Chart deflections were then obtained by adjusting a single decade resistance.

Because the calorimeter measurements were limited to the 20 mV scale of the nanovoltmeter, the calibration procedure was only performed for that range. The accuracy of the 20 mV scale was shown by the slope of a linear graph of dV versus dR/R (Figure 3.5). This was determined to be 3.997 with a 95% confidence interval of $\pm 0.3\%$. This compared very well with the theoretical value of 4.000. The linear correlation coefficient was determined

Figure 3.5. Nanovoltmeter and Recorder Calibration.



to be 0.999997 and this indicated excellent linearity. In practice (to be shown in Chapter 4), equation 3.6 becomes

$$\frac{dR}{R} = 3.997 \frac{dV}{V_b} \quad (3.6)$$

The bridge supply voltage was measured with a 5 1/2 digit voltmeter (Data Precision 3600) and was supplied with a factory calibration traceable to NBS voltage standards. No additional calibration was performed on this meter.

CHAPTER 4

ABSORBED DOSE MEASUREMENTS

4.1 Experimental Procedure

4.1.1 Experimental Parameters For Calorimeter Dose Measurements -

4.1.1.1 Calorimeter Water -

Unless stated otherwise, all calorimeter dose measurements reported in this thesis were made in once distilled water. Resistivity measurements of the water (taken directly in the calorimeter) were between 3 and 5 megaohm-cm.

4.1.1.2 Operating Temperature -

Successful operation of the water calorimeter required several hours of temperature stability. To provide these conditions (Section 2.10.4.2), the initial

water temperature was carefully matched to that of the wall temperature of the calorimeter. Both the water and the calorimeter were stored on the floor of the room for about 16 hours (overnight) prior to setting up. By using the calorimeter wall temperature to establish the initial operating temperature, about 6-8 hours of calorimeter operation were routinely provided with no additional requirement for drift control. An integral part of this technique, however, was the ambient temperature regulation provided by the hospital air conditioning system. Special arrangements were made to leave the air conditioning system on for night and weekend experimentation. A more elaborate technique for controlling ambient temperature has been described by Kubo et al (1985a) and Kubo and Brown (1984).

4.1.1.3 Thermistor Detector Equilibration -

Although the calorimeter can be operated within forty five minutes of adding the water, this procedure was eventually abandoned. On numerous occasions, dose measurements taken within a six hour period from the initial startup were extremely variable. It was assumed that the observed variability was caused by air which was initially trapped between the polyethylene films. The effect of air trapped between the thermistors and the film

is to decrease the conductivity between the thermistor and the surrounding water and therefore increase, for a given power consumption, the difference in temperature between the thermistor and the water. As indicated by the calibration data (Section 3.4), between 10-15 hours are required for the water pressure to push the excess air completely out of the detector. This effect has not been reported by other authors and was assumed to be due to the method described in Chapter 2 for waterproofing the detector. To ensure that the thermistors were in maximum contact with the water, the calorimeter was routinely set up the night before taking dose measurements. In a clinical environment, this procedure limited the available experimental time to nights and weekends.

In Appendix D, an alternate calorimeter detector is described in which the thermistors are immersed directly in water. With this design, data measurements can be taken within 40 minutes of placing the water in the tank. Dose measurements with directly immersible thermistors, however, are limited to beam qualities and geometries in which bulk convection is not observed (Appendix D).

4.1.1.4 Calorimeter Transport And Initial Setup -

To provide adequate mechanical stability and facilitate transportation, a special truck was constructed for the calorimeter. The frame of the truck was made from angle iron and mounted on heavy duty casters. The frame was designed to support two plywood tiers and measured approximately 2 m by 1 m.

The couch assemblies which are provided with most isocentric radiotherapy units are mounted on large turntables which are built into the floor. The turntables are a potential source of unwanted vibration and were not used to support the calorimeter. The 2 m long truck was just sufficient to traverse the largest turntable assembly at our clinic.

In addition to the truck, the calorimeter was supported by a three legged wooden base with an adjustable height from 0 to 25 cm. This was necessary to accomodate different vertical positions of the therapy units. Small levelling adjustments were required each time the calorimeter was positioned under a unit.

The source-to-detector distance was established by inserting a removable stand into the tank and raising the level of the supporting table until the stand made contact with a reference surface on the head of the unit. The

height of the stand was adjustable and was separately calibrated for each unit.

A single water level indicator (Section 2.6, Figure 2.3) was used to attain the desired depth for dose measurement. This was adjusted before adding the water with a tightening screw on the base.

The usual procedure was to slightly overfill the tank and then drain out water until the required depth was reached. This technique ensures that no air was trapped in the drain line which could be displaced during the dose measurements and lower the water level. The estimated uncertainty in establishing the correct source to detector distance and water depth was ± 0.5 mm.

After the water was poured into the tank, styrofoam insulation was added to the external enclosure to minimize the effect of small changes in the air temperature of the room. The signal cable was then attached to the front of the calorimeter along with cable for the temperature probe.

4.1.1.5 Field Size -

For all of the water calorimeter measurements, a rectangular field of 25 x 25 cm was used. These dimensions applied at the depth of measurement and were chosen to cover the water in the tank.

4.1.1.6 Depth Of Measurement -

The selection of a suitable depth of measurement for the calorimeter detector is influenced by conductive heat loss along the central axis of the beam. This problem is discussed in Appendix C where the central axis temperature profiles are shown along with calculations of conductive heat loss as a function of depth and time (Figures C.1 - C.6).

Cobalt-60 measurements were made at depths of either 2.5 or 5 cm. These depths are both well beyond the depth of maximum dose (0.5 cm) where heat loss can be significant. Conductive heat loss corrections were not required at these depths even for measurement times of several minutes.

For calorimeter measurements with the linear accelerator beams, the potential for conductive heat loss is greater. This is mainly due to the axial temperature profiles for the electron beams which are different for

each energy and extremely peaked for nominal energies less than or equal to 10 MeV. Because it was not feasible to change the depth of measurement during a calorimeter experiment a single depth of measurement was chosen for all the beams. An acceptable compromise was 2.5 cm. This is the depth of maximum dose for 10 MeV electrons and is reasonably close to that for the higher energy electrons and x-rays. As shown in Figures C.2 - C.6, conductive heat loss is more significant for the electron beams (for the same decay times) and extremely sensitive to position near the depth of maximum dose. For absorbed dose measurements of 300 monitor units (MU) the measurement time is about one minute and no heat loss corrections were required for any of the beams at a depth of 2.5 cm.

4.1.2 Calorimeter Operation -

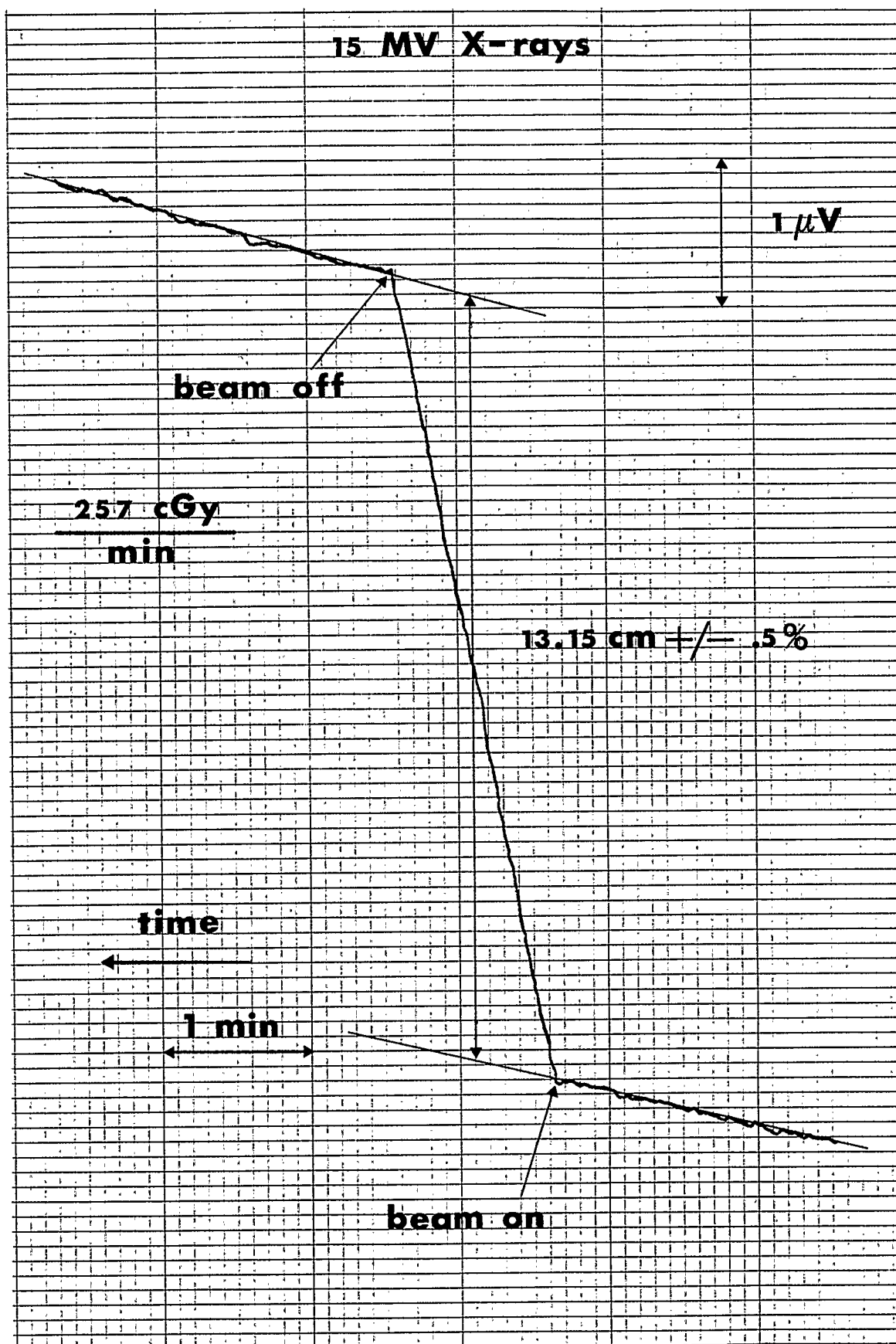
To operate the calorimeter, the bridge voltage was switched on and the Wheatstone bridge was balanced with the decade resistances in two arms of the circuit (R2 and R3 in Figure 2.4). As outlined in Section 2.8 (equation 2.16), the decade resistances were adjusted so that the voltage across each bridge component was equal.

After switching on the bridge voltage, approximately one half hour was required for the thermistors to reach an equilibrium with the water. During this period, the signal voltage increases steadily as the thermistor heats up to its equilibrium temperature. At that point, the thermistor temperature follows that of the environment and the calorimeter is then ready for operation.

The chart recording from a typical calorimeter measurement is shown in Figure 4.1. In order to measure chart deflections to a precision of 1%, the initial and final drifts were recorded for approximately the same duration as the period of dose measurement. After recording the final temperature drift, the bridge was rebalanced and the procedure was repeated for successive measurements.

This method for determining the absorbed dose requires a voltage calibration which is described in Section 3.4. By observing a continuous voltage displacement during an irradiation, the decade resistances remain undisturbed and the entire trace is available for evaluating drift and linearity. Using a well known technique (Keesom and Kok, 1932), the change in bridge voltage was determined by extrapolating the initial and final drifts to mid-run and measuring the chart displacement at that point. As indicated in Figure 4.1,

Figure 4.1. Sample Chart Tracing for a Calorimeter Temperature Measurement in a Beam of 15 MV x-rays.



the uncertainty in the chart displacement for a single dose measurement is approximately $\pm 0.5\%$.

Provided that the bridge voltage does not change significantly no circuit correction is required for the small increase in thermistor power which occurs during the measurements (see Section 2.10.4.3). The bridge and component voltages were frequently checked during an experiment and do not change even for extended dose measurements by more than a few parts in 5000.

4.1.3 Water Calorimeter Data Analysis -

The chart displacement is related to voltage through a calibration constant (Section 3.4). Using the 20 millivolt range on the nanovoltmeter and the 1V range on the recorder, the voltage is related to chart displacement by

$$dV = 0.3937 \times 10^{-6} dx \quad (4.1)$$

where dx is the chart displacement measured in cm. This equation assumes an amplifier gain of 1.0×10^5 and includes a conversion between cm and inches. In a combined calibration of the nanovoltmeter and chart recorder it has been previously (equation 3.6, Chapter 3) shown that

$$\frac{dR}{R} = 3.997 \frac{dV}{V_b}$$

Thus, by combining equations 3.6 and 2.20, the absorbed dose from the water calorimeter is given by

$$D_w = 3.997 c_w \frac{T^2}{(B1 + B2)} \frac{dV}{V_b} \quad (4.2)$$

where c_w is the heat capacity of water, $B1$ and $B2$ are the thermistor material constants, T is the initial thermistor temperature (K), V_b is the bridge voltage, and dV is the signal voltage (bridge output) produced by the absorption of radiation.

The heat capacity (c_w) and the material constants ($B1$, $B2$) are functions of temperature and must be evaluated at the water temperature of the calorimeter. The initial thermistor temperature was determined by calculating the excess temperature for a given thermistor power (see Figure 3.3) and adding it to the measured temperature of the water. As indicated from the calibration data the excess thermistor temperature due to power consumption is also a function of the water

temperature. Due to the tedium of the analysis a computer algorithm was written to implement equation 4.2. As calculated by the computer program, the absorbed dose in water is

$$D = 3.997 \frac{c_w(T)}{w} \frac{(T + v_{xp}(T))^2}{(B1(T) + B2(T))} \frac{3.937 \times 10^{-7} dx}{V_b}$$

(4.3)

where v_{xp} is the excess thermistor temperature due to power consumption, dx is the chart displacement in cm, and T is the water temperature.

Values of the heat capacity of water were obtained from the Handbook of Physics and Chemistry (1971) and fitted to a third order polynomial in temperature. The polynomial coefficients were then stored in a file for future reference.

As indicated in Section 3.3.3, the material constants were derived by fitting the logarithm of the zero power resistance to a polynomial in $1/T$. The appropriate polynomial coefficients were stored in a separate file for each thermistor in the detector.

The excess thermistor temperature was calculated by multiplying the value for the excess temperature per microwatt (obtained from a calibration experiment; see Section 3.3.3) by the thermistor power. These data are also a function of temperature and were derived for each thermistor as a polynomial in T . The thermistor power was calculated from fundamental circuit considerations.

Almost all of the uncertainty in a calorimetric dose determination via equation 4.3 arises from the chart displacement (dx). The temperature variations of the material constants (Table 3.1) and the heat capacity (Table B.1, Appendix B) are very small. The excess thermistor temperature for powers less than 30 microwatts is also quite small (less than 0.1 K) and is only significant for larger thermistor powers.

4.1.4 Ion Chamber Measurements -

One of the objectives of this study was to compare calorimetric dose values with those determined from a calibrated ion chamber. The ion chamber measurements were made with a cylindrical 0.6 cm nylon chamber (NEL model 2505/3B) and a Keithley 616 electrometer. The ion chamber was calibrated against an exposure standard through the dosimetry services of the National Research Council (NRC) in Ottawa. Dose measurements with the ion chamber were

made at a depth of 2.5 cm in water directly in the calorimeter tank. To account for possible scatter from the acrylic ring normally supporting the thermistors, an identical structure was assembled to house the ion chamber.

A set of dose measurements was taken for all beam energies with the calibrated chamber. These were recorded along with ionization measurements from another chamber which was used to monitor the day to day variation in the dosimetry of the accelerator (A procedure for correcting for the variation is discussed in the next section). The uncertainty of the calibrated ion chamber measurements as determined from readings taken on separate days was about $\pm 0.5\%$ for all qualities.

Using the protocol recommended by AAPM TG-21 (1983) the absorbed dose in water for x-ray beams is given by

$$D = M \cdot C_{TP} \cdot N_{\text{gas}} \cdot S \cdot P_{\text{ion}} \cdot P_{\text{repl}} \cdot P_{\text{wall}} \quad (4.4)$$

and the dose in water from electron beams is given by

$$D = M \cdot C_{TP} \cdot S \cdot N_{\text{gas}} \cdot P_{\text{ion}} \cdot P_{\text{repl}} \quad (4.5)$$

where M is the chamber reading, C_{TP} is temperature and

pressure correction, N_{gas} defines the dose to air per electrometer reading, S is the restricted stopping power ratio (water to air), P_{ion} is the reciprocal of the ion collection efficiency, P_{rep1} is a factor which corrects for differences in the electron fluence or dose gradient at the front and back of a cylindrical ion chamber and P_{wall} accounts for differences in the origin of the electrons which cause the ionization in the chamber. The various chamber factors in equations 4.4 and 4.5 are given in Table 4.1 as a function of radiation beam type. N_{gas} for the nylon chamber was determined to be 4.10×10^7 Gy/C which includes an exposure calibration factor of 4.87 R/nC.

4.1.5 Correction Factors For Variation In Machine Dosimetry -

Absorbed dose measurements were taken from two cobalt-60 teletherapy units and an electrom linear accelerator (Siemens Mevatron 77).

The variation in the dose delivered from a cobalt unit is dependent on the accuracy of a mechanical or digital timer and on the consistency of a pneumatic system which moves the source to the "on" position. The latter effect is usually more significant and must be determined by measuring a "shutter correction" to allow for the time

<p>TABLE 4.1</p> <p>PARAMETERS FOR AAPM TG-21</p> <p>ION CHAMBER DOSIMETRY PROTOCOL</p> <p>(As Measured With Cylindrical 0.6 cm³ Nylon Chamber)</p>							
Beam Quality (nominal)	S _{wg}	P _{rep1}	P _{ion}	P _{wall}	E _Z (MeV)	E ₀ (MeV)	d _{meas} (cm)
Cobalt - 60	1.134	0.992	1.000	1.01	n/a	n/a	2.5/5.0
15 MV x-rays	1.109	1.000	1.004	1.003	n/a	n/a	2.5
18 MeV e ⁻	1.003	0.983	1.007	n/a	11.0	15.5	2.5
15 MeV e ⁻	1.016	0.979	1.006	n/a	9.2	13.7	2.5
12 MeV e ⁻	1.038	0.971	1.008	n/a	6.7	11.3	2.5
10 MeV e ⁻	1.053	0.966	1.004	n/a	5.4	10.0	2.5

for the source to engage and disengage. Variation in the shutter correction can be determined with an ion chamber at various times during an experiment. However, no adjustments were required for variation of shutter correction for either of two cobalt units used in this study.

For the linear accelerator however, the internal dosimetry is more complicated. The accelerator is equipped with separate internal monitors for controlling the dosimetry of x-ray and electron beams. Both the electron and x-ray dosimetry are subject to fluctuations (short and long term) in the electronic circuitry which amplifies and integrates the signal from the internal monitor. For electron beams, the internal monitor (ionization chamber) is unsealed and therefore the size of a monitor unit is dependent on the ambient pressure and temperature. The internal monitor for x-rays is sealed.

The variation in the internal monitor of the accelerator was monitored with an external dosimeter. The ion chamber was supported (with buildup) by an acrylic tray and was positioned in the beam directly above the calorimeter. Ionization measurements were recorded for a preset number of monitor units before and after a series of calorimeter measurements. Ionization readings were required separately for 15 MV x-ray and all of the

electron beams. The day to day variation of the accelerator dosimetry was determined by comparing ionization readings from the external chamber.

Since the variation in the dosimetry is relative, one of the ionization readings must be selected as a normalization point. It was convenient, therefore, to determine the absorbed dose in the calorimeter with an exposure calibrated ion chamber and normalize the relative ionization readings to the those measurements. Ion chamber doses were therefore adjusted using

$$D2 = D1 \frac{I2}{I1} \quad (4.6)$$

where I1 and I2 are the ionization readings from the external monitor for days 1 and 2 respectively, D2 is the dose corresponding to I2, and where D1 is the absorbed dose in water as determined from a calibrated ion chamber and taken with I1. Note that these values apply to the same preset number of monitor units.

The same correction factor I2/I1 was used to adjust the calorimeter readings so that the values corresponded to the same quantity of radiation. Typically, the applied corrections were about 1% .

4.1.6 Practical Absorbed Dose Quantities -

From equation 3.1, the calorimetric absorbed dose is equal to the product of the heat capacity of water and the measured temperature rise. For radiation beams produced from the linear accelerator, calorimeter temperature measurements were made for a preset number of monitor units (MU). For cobalt-60 irradiation, calorimeter temperature measurements were made for a preset time.

To provide a practical quantity for discussion and comparison the calorimetric measurements have been reported in this thesis as the dose per monitor unit or the dose per unit time (dose rate). This quantity has been designated D_c/U where U is either monitor units or time. For ion chamber and Fricke measurements the corresponding symbols are D_i/U and D_f/U .

4.2 Effect Of Accumulated Dose On Calorimetric Dose

The initial objective with the water calorimeter was to determine the effect of accumulated dose on the measured absorbed dose. The rationale for this approach is described in Section 1.2 but because of its importance is briefly summarized here.

Ross et al (1984) built a calorimeter to study the heats of reaction produced from the radiolysis of aqueous solutions (containing various dissolved gasses). In their experiments, the temperature rise per unit dose was monitored as a function of accumulated dose. For the radiolysis of aerated water, it was observed that an accumulated dose of about 100 Gy was required to produce a steady state i.e. a condition where the temperature rise per unit dose remained constant with accumulated dose.

Even for highly purified water, the low dose temperature measurements (accumulated doses less than 100 Gy) were typically 2-5% exothermic with respect to the steady state. Ross et al (1984) have suggested that the low dose exothermicity is due to the presence of organic impurities. According to their model, organic contaminants which are initially present can react (during radiolysis) with hydrogen and hydroxyl radicals to produce the observed exothermicity. As the contaminants in the water are consumed (with increasing accumulated dose), the exothermicity decreases until the overall stoichiometry corresponds to the steady state for aerated water.

Two important premises can be drawn from the data of Ross et al (1984);

- o Water should be irradiated to a high accumulated dose to provide an environment in which the measured temperature rise per unit dose is constant.
- o The steady state temperature rise per unit dose is a function of the the composition of the water (i.e may be higher or lower than the steady state temperature rise per unit dose for pure water).

For the water calorimeter measurements in this study, the absorbed dose to the water was not uniform and was dependent on the quality of the beam (depth dose characteristics). This was different from the calorimeter of Ross et al (1984) in which the volume of water was much smaller and was circulated continuously to achieve a uniform dose. To determine the average dose in a non-uniform distribution, the depth dose must be averaged over the entire irradiated volume.

The accumulated dose in these experiments, applies specifically to the position of the thermistor detector (i.e a single point). The average dose for cobalt-60 or 15 MV x-rays is approximately half the accumulated dose. The accumulated dose scale was based on an exposure calibrated ion chamber and a recent protocol recommended by AAPM TG-21 (1983).

The first series of calorimeter measurements were taken in a cobalt-60 beam at a depth in water of 5 cm. From sixteen separate experiments, in which the calorimeter dose was observed as a function of accumulated dose, the observed data were extremely variable and a steady state dose value was never obtained. The maximum accumulated dose for the cobalt-60 measurements was about 175 Gy.

The second series of calorimeter measurements were taken with 15 MV x-rays produced from a Mevatron 77 linear accelerator. For these experiments, the average thermistor power was 30 microwatts. An important difference of the 15 MV x-ray experiments was that the water was added to the calorimeter tank the night before. With this procedure, any trapped air in the detector had sufficient time to be expelled.

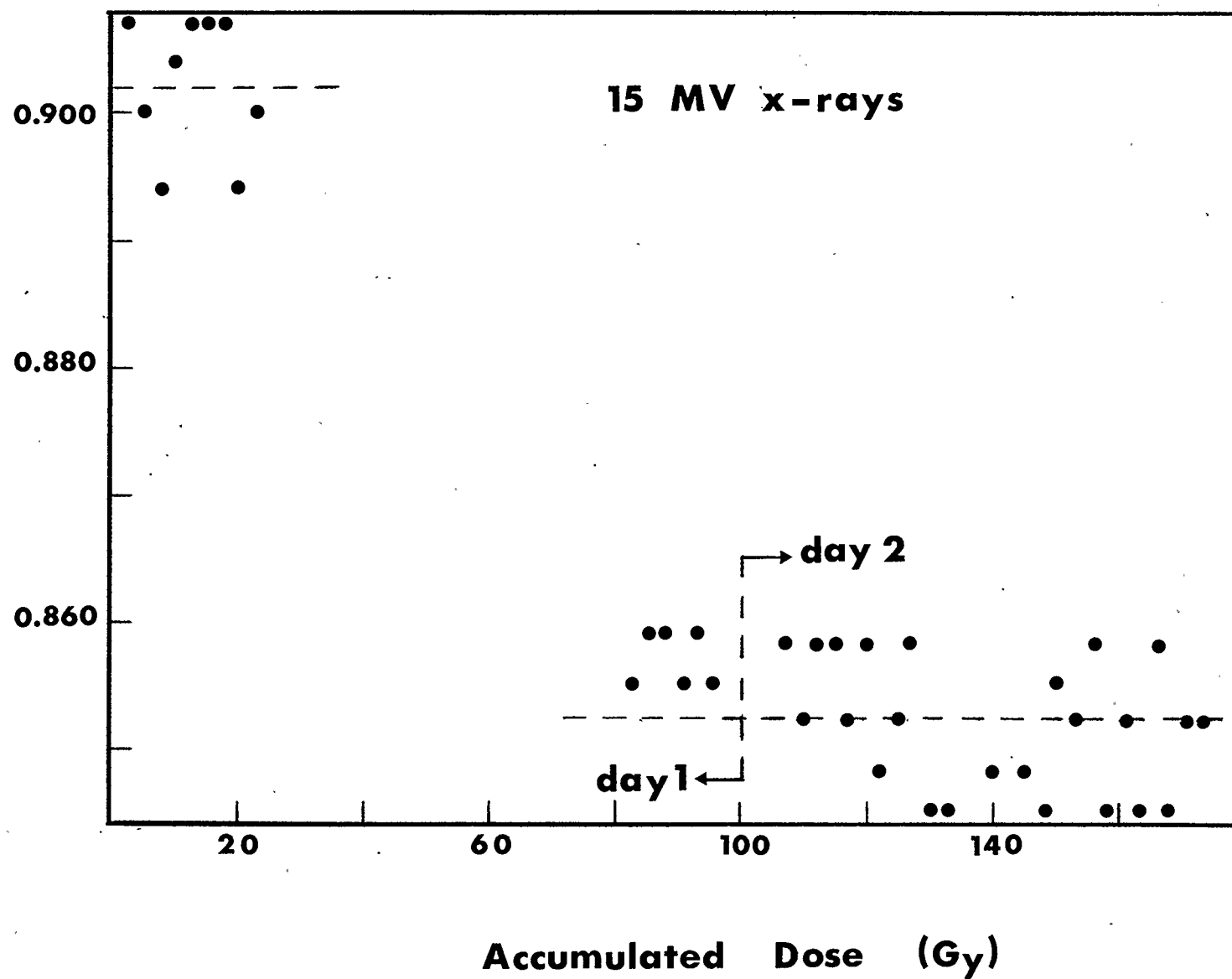
In contrast to the experiments for cobalt-60, a consistent pattern was obtained for irradiation with 15 MV x-rays, and a steady state value of D_c/U was observed for large accumulated doses. The variation of D_c/U with accumulated dose in one experiment is shown in Figure 4.2. A steady state value was observed for accumulated doses above 80 Gy and was defined with an experimental precision of 0.7% (95% confidence) The data shown in Figure 4.2 were obtained over two days of experimentation. The

Figure 4.2. Variation of Calorimeter Absorbed Dose with Accumulated Dose in a Beam of 15 MV-x-rays.

The calorimeter dose was determined from the product of the measured temperature rise per monitor unit (MU) and the heat capacity of water. The accumulated dose applies at the centre of the thermistor detector and was based on an exposure calibrated ion chamber measurement using the protocol recommended by AAPM TG-21 (1983). The average dose to the water is about one half of the accumulated dose.

Calorimeter Dose per Monitor Unit

(cGy/MU)



measurements on the second day were started about 10 h after the first experiment and for a previously accumulated dose of 96 Gy. This is indicated in Table 4.2 for the experiment started August 24. These measurements were consistent with the behavior observed by Ross et al (1984) for the radiolysis of aerated water.

From other experiments using 15 MV x-rays, similar data to that shown in Figure 4.2 were observed. These data are summarized in Table 4.2. The measurements for low accumulated doses (less than 20 Gy) were exothermic and a steady state value of D_c/U was observed for accumulated doses above 100 Gy.

The values of D_c/U for low accumulated doses (less than 20 Gy) in Table 4.3 were between 1-5% exothermic relative to the steady state value. On the basis of the model of Ross et al (1984), the variability could be explained by variable concentrations of organic contaminants.

The essential feature of the 15 MV x-ray data, however, was the day to day consistency of the steady state value of D_c/U . In contrast to the observed variation in D_c/U for low accumulated dose, the steady state value of D_c/U for 15 MV x-rays (from all of the experiments) did not vary by more than $\pm 0.6\%$ (95%

TABLE 4.2			
WATER CALORIMETER ABSORBED DOSE VALUES ¹			
EFFECT OF ACCUMULATED DOSE ²			
15 MV x-rays			
Date of Experiment (1985)	Number of Measurements	Accumulated Dose (Gy)	Calorimeter Dose (cGy/MU)
August 10	8	0 - 20	0.863
	11	59 - 85	0.858
	6	87 - 100	0.855
August 18	11	0 - 30	0.894
	6	90 - 103	0.870
August 24	9	0 - 23	0.902
	6	83 - 96	0.857
August 25 ³	29	107 - 174	0.851
September 1	6	192 - 205	0.859
	7	265 - 280	0.858
November 2	5	201 - 210	0.860
	5	258 - 267	0.857

- 1) The calorimeter dose values in this table have been adjusted for small ($\approx 1\%$) day to day variations in the quantity defined as a monitor unit (MU). The monitor unit has been "normalized" to an absorbed dose value (0.856 cGy/MU) determined with an exposure calibrated ion chamber at the detector position in the water calorimeter.
- 2) The accumulated dose values apply to a single point of measurement located at the centre of a thermistor detector. The detector was positioned at a depth in water of 2.5 cm. The average accumulated doses to the water are about one half of the values shown.
- 3) The data for August 25 was an extension of an experiment started on August 24. The time interval between the experiments was approximately 10 h.

confidence level). Note that this observation includes the uncertainties in source-to-detector distance, and water depth.

The results of Ross et al (1984) indicate that steady state calorimetric dose measurements in aerated water are expected to be endothermic by 2%. This implies that steady state values should be increased by 2% to obtain a true value of absorbed dose. The problem with applying the same adjustment factor to the data in Figure 4.2, however, is determining the equivalence of steady state measurements between the two calorimeters. The data of Ross et al (1984) has been measured in relative terms and does not offer a simple basis for quantitative comparison with other calorimeters. As such, no correction factors have been applied to the calorimeter measurements reported in this thesis.

Following a calorimeter experiment with 15 MV x-rays, in which the water had been added the night before and preirradiated to 250 Gy, the calorimeter was transported to a cobalt-60 unit for a series of dose measurements. These measurements were taken in two segments separated by several hours. The standard error of the mean for the D_c/U values from both segments was $\pm 0.6\%$ (95% confidence). From this data it was concluded that a steady state value for D_c/U had been preserved. D_c/D_i was

determined to be $1.02 \pm 0.7\%$ (D_i/U determined from AAPM TG-21 (1983)).

Additional experiments have been done with a modified thermistor detector (see Appendix D) which indicate that the steady state value of D_c/U for 15 MV x-rays is independent of detector format. The thermistors in this detector are directly immersed in water and are not subject to possible influence by the presence of polyethylene and/or air. Preliminary measurements with this modified detector in the 15 MV x-ray beam were within 1% of the steady state value of D_c/U obtained with the polyethylene film detector (from Table 4.2).

To be considered as a practical radiation dosimeter, the absorbed dose measurements from a water calorimeter must exhibit steady state behavior as is shown in Figure 4.2. In practice, this can only be determined by irradiating the calorimeter to relatively high dose values and observing the dose measurements as a function of accumulated dose.

4.3 Effect Of Thermistor Power On Absorbed Dose

One of the objectives of this study was to investigate the effect of thermistor power on water calorimeter dose measurements. Domen (1982b) had

previously reported that the calorimetrically measured doserate (from a cobalt-60 source) was a function of thermistor power. The doserate with a thermistor power of 10 microwatts was found to be about 4% higher than the doserate with a power of 200 microwatts.

For this study, D_c/U was recorded for thermistor powers between 10 and 60 microwatts. This range is smaller than that used by Domen but encompassed the critical thermistor powers indicated by the data (Domen, 1982b). Five dose measurements were taken at each of four power levels of 8.5, 20, 37, and 63 microwatts. These powers corresponded to thermistor voltages of 0.1304, 0.2005, 0.2725, and 0.3558 V respectively. For this experiment, the water was added to the calorimeter the night before and was preirradiated to an accumulated dose of about 250 Gy. To verify the existence of a steady state value of D_c/U , the 37 microwatt data was taken both at the beginning and end of the experiment. No significant difference (0.4%) in D_c/U was observed. The data from this experiment is shown in Figure 4.3 and Table 4.3.

As derived in Section 2.10.3 (equation 2.30), the signal to noise ratio is directly proportional to the bridge voltage. Thus, in order to compare the dose measurements on an equal basis for different thermistor

Figure 4.3. Variation of Calorimeter Absorbed Dose with Thermistor Power in a Beam of 15 MV x-rays.

The calorimeter dose was determined from the product of the measured temperature rise per monitor unit (MU) and the heat capacity of water. To provide equivalent precision, the dose measurements for lower powers were made for a larger number of monitor units and these are indicated in parentheses. The thermistor power is the average of two thermistors in the detector.

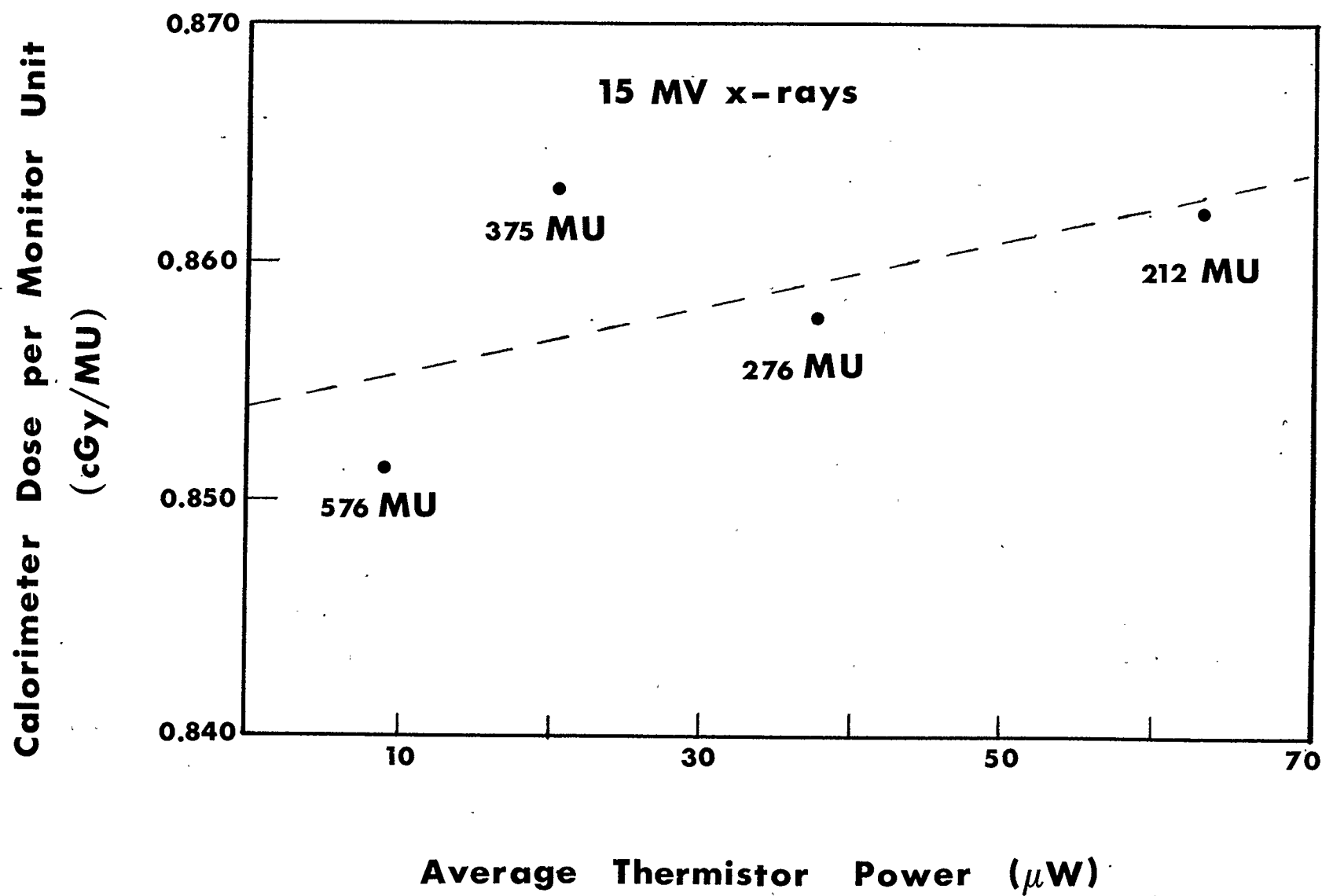


TABLE 4.3 WATER CALORIMETER ABSORBED DOSE VALUES EFFECT OF THERMISTOR POWER 15 MV X-RAYS				
Data Group	Monitor Units	Number Of Measurements	Avg Thermistor ¹ Power (μ W)	Calorimeter Dose (cGy/MU)
1	212	5	63	0.862
2	276	5	37	0.859
3	375	5	20	0.863
4	576	6	8.5	0.851
5	276	6	37	0.856

- 1) The thermistor power is the average of two thermistors in the detector.

power levels, the number of monitor units was increased proportionately at the lower power levels. The number of monitor units is shown for each data point in Figure 4.3.

The dashed line in Figure 4.3 is a linear least squares fit to the data. While a small power dependence of D_c/U is indicated, the data is only weakly correlated (correlation coefficient = 0.590) and the uncertainty in the slope ($\pm 5.65 \times 10^{-4}$ = 95% confidence interval) is about four times larger than the slope itself. On this basis it was concluded that the calorimeter dose was independent of thermistor power between 10 and 60 microwatts.

The low value of D_c/U at the 10 microwatt level may be due to conductive heat loss which occurs for longer measurement times (relative to the higher power levels). This effect is shown in Figure C.2 (Appendix C) for 15 MV x-rays as a function of the measurement depth and the time of measurement (The measurement depth was 2.5 cm and the measurement times can be derived assuming a dose rate of 300 MU/min).

The data shown in Figure 4.3 are significant in consideration of maximum signal to noise ratio. The indication is that the calorimeter is linear in D_c/U for thermistor power levels as high as 60 microwatts. On the

basis of a power dependence reported by Domen (1982b), several investigators (de Marles, 1981; Kubo, 1983; Mattsson, 1984) have reported data using extremely low (less than 10 microwatts) thermistor powers. The problem with such systems is that in order to produce a reasonable signal to noise ratio (i.e. greater than 100:1) a very large number of monitor units must be accumulated. While the dose rates of most linear accelerators are high, a measurement time of a few minutes is still needed to acquire sufficient signal and during this time conductive heat loss may be significant. This is particularly true for electron beams (see Appendix C) where corrections for heat loss can be of the order of a few percent.

The thermistor power dependence of the absorbed dose reported by Domen (1982b) was attributed to a variation in "thermal coupling". It is possible that at higher power levels a loss in signal is encountered because of convection in the vicinity of the thermistors (Section 2.11.2). Because of the potential problem associated with convection it is mandatory to determine the thermistor power range over which the response of the calorimeter is linear.

4.4 Absorbed Dose Comparison

4.4.1 Dosimetry Intercomparison -

An absorbed dose comparison was made between ion chamber, water calorimeter and Fricke dose measurements. Radiation beams of 15 MV x-rays and electrons with nominal energies of 18, 15, 12, and 10 MeV were used in this study. The results of the comparison are shown in Table 4.4.

The ionization measurements (D_i/U) were determined with an exposure calibrated ion chamber and a protocol recommended by AAPM TG-21 (1983) (see Section 4.1.4 for details).

The reported values of D_c/U were determined for accumulated doses that were greater than 100 Gy (Section 4.2). These are referred to as "steady-state" quantities.

Fricke measurements were obtained through a service offered by the National Research Council (NRC) in Ottawa. The dosimeters were prepared in the laboratories of the NRC and shipped to Calgary for placement in the beam. The dosimeters were irradiated with various beams of a Mevatron accelerator and then returned to Ottawa for optical density measurements and dose determinations (K R Shortt, D V Cormack and H R Boese, unpublished data,

TABLE 4.4					
ABSORBED DOSE COMPARISON					
Dosimeter	15MV X-rays cGy/MU	10MeV e ⁻ cGy/MU	12MeV e ⁻ cGy/MU	15MeV e ⁻ cGy/MU	18MeV e ⁻ cGy/MU
Water Calorimeter	0.858	0.819	0.830	0.836	0.865
Exposure Calibrated Ion Chamber AAPM TG-21	0.856	0.813	0.810	0.817	0.835
NRC Fricke	0.869	0.832	0.837	0.844	0.862

1985). The irradiation geometry was not the same as that used in the experiments reported in this thesis. However, ion chamber measurements were made in both cases and it is therefore possible to derive Fricke dose values corresponding to the calorimetric values. The derived Fricke values (D_f/U) are shown in Table 4.4.

4.4.1.1 Experimental Uncertainties -

The largest uncertainty in a water calorimeter temperature measurement is due to the heat produced (or consumed) from chemical reactions which are induced in the water during irradiation. The heat produced (or consumed) per unit absorbed dose has been previously defined as H/U (Section 1.2.3, Chapter 1). Ross et al (1984) have demonstrated that H/U is a function of the composition of the water (dissolved gasses and/or impurities) and the accumulated dose. For irradiation of aerated water and for low accumulated dose, H/U was observed to be positive (relative to $H/U = 0$ for pure water). This was attributed by Ross et al (1984) to exothermic reactions involving organic impurities which were initially present. With continued irradiation (increasing accumulated dose) H/U was observed to decrease as the organic impurities were consumed. Eventually, a steady state was reached in which H/U did not change with increasing accumulated dose.

Due to the design of the water calorimeter in this study, it was not feasible to measure the absorbed dose in pure water (large unsealed water volume). Consequently, a value of H/U for aerated water could not be obtained (H/U would be determined by subtracting the steady state dose values for pure and aerated water). According to the data of Ross et al (1984), the steady state value of H/U for aerated water is 2% endothermic with respect to $H/U=0$ for pure water. However, rather than adapting their value for H/U , it was decided to report the calorimetric values without adjustment. The systematic uncertainty in the calorimeter dose values is obviously unknown and for the discussion to follow has been ignored. To be consistent, the systematic uncertainties for the ion chamber and Fricke measurements have also been ignored (i.e. the uncertainties in quantities such as W , L/ρ , N_x , N_{gas} , ϵ_G etc).

The steady state value of D_c/U for 15 MV x-rays was obtained from the mean of the values in Table 4.2 (for accumulated doses greater than 80 Gy). The experimental uncertainty in this value is $\pm 0.6\%$ (95% confidence).

The steady state values of D_c/U for the electron beams are the averages from two series of measurements taken on non-consecutive days. The experimental uncertainty in the D_c/U for 18, 15, 12, and 10 MeV

electron beams was $\pm 1.1\%$, $\pm 1.5\%$, $\pm 0.9\%$ and $\pm 0.9\%$ respectively (95% confidence). The larger uncertainty in D_c/U for the electron beams is mainly due to the unsealed internal monitor of the accelerator. Although an external monitor was used to correct for variation in the dosimetry of the accelerator, the variable nature of the unsealed monitor was apparent from the applied correction factors. In some cases, the correction factor applied to D_c/U was greater than 2%.

From measurements taken on separate days, the uncertainty in D_i/U was $\pm 0.3\%$ for 15 MV x-rays, $\pm 0.4\%$ for 18 MeV electrons, $\pm 0.4\%$ for 15 MeV electrons, $\pm 0.7\%$ for 12 MeV electrons, and $\pm 0.4\%$ for 10 MeV electrons (95% confidence).

The experimental uncertainty in the Fricke dose values (D_f/U) was not easily determined because of a limited number of vials. The values of D_f/U are inherently dependent on external ion chamber measurements and therefore the experimental uncertainty was assumed to be the same.

The values of D_c/U in Table 4.4 are in good agreement with D_f/U (generally less than 1% difference). For 15 MV x-rays and electron beams with energies of 10, 12, 15, and 18 MeV D_c/D_f was $0.99 \pm 0.7\%$, $0.98 \pm 1.0\%$, $0.99 \pm$

1.1%, 0.99 +/- 1.6% and 1.00 +/- 1.2% respectively (experimental uncertainty for 95% confidence). Slightly larger differences are observed between Dc/U and Di/U. For 15 MV x-rays, and electron beams with nominal energies of 10, 12, 15, and 18 MeV Dc/Di was 1.02 +/- 0.7%, 1.00 +/- 0.7%, 1.01 +/- 1.0%, 1.02 +/- 1.1%, 1.02 +/- 1.6%, and 1.04 +/- 1.2% respectively (experimental uncertainty for 95% confidence).

4.4.2 Comparison With Published Data -

The steady state values of Dc/U obtained in this study are, in general, lower than other published values from water calorimetry studies.

For cobalt-60 irradiation Domen (1982b) reported a Dc/Di value of 1.035 (the NBS cobalt-60 absorbed dose standard is a graphite calorimeter measurement transferred to water with a thick graphite walled ionization chamber). Using copies of Domen's water calorimeter, de Marles (1981), Kubo, (1983) and Mattson (1984) reported Dc/Di values for cobalt-60 of 1.035, 1.038, 1.033 respectively. Dc/Di for this study was found to be 1.02 +/- 0.7% (experimental uncertainty for 95% confidence). This is between 1-2% lower than the published data.

For 6, 18, and 25 MV x-ray beams de Marles (1981) obtained a combined D_c/D_i value of 1.038 (using the NACP (1980) protocol for D_i/U). More recently, Kubo (1983) reported that D_c/D_i for 10 and 25 MV x-ray beams was 1.03 and 1.02 respectively (using the AAPM TG-21 protocol for D_i/U). D_c/D_i from this study for a beam of 15 MV x-rays was 1.00 which is 2-4% lower than published data.

From Table 4.4, D_c/D_i for electron beams with nominal energies of 10, 12, 15, and 18 MeV is $1.01 \pm 1.0\%$, $1.02 \pm 1.1\%$, $1.02 \pm 1.6\%$, $1.04 \pm 1.2\%$ respectively (experimental uncertainty for 95% confidence). These values are different from the electron beam data of Mattsson (1984) which showed no energy dependence for nominal electron energies between 6-20 MeV (D_i/U determined from NACP (1980)). While it was not explicitly stated by Mattsson (1984), it is assumed here that D_c/D_i was 1.035 for all electron dose measurements. Kubo (1983) has reported that D_c/D_i for electron beams with nominal energies of 18 and 25 MeV are 1.034 and 1.036 respectively (D_i/U determined using AAPM TG-21 (1983)). These values are more in agreement with the water calorimeter data of Mattsson. For water calorimeter measurements in electron beams with nominal energies of 13, 17, and 20 MeV, de Marles (1981), however, reported a combined D_c/D_i value of 1.01 (D_i/U determined from NACP (1980)).

For these comparisons, it is important to note that the values of D_c/U in Table 4.4 and in Section 4.2 for cobalt-60 have been experimentally determined as steady state quantities. On the basis of the comparisons discussed above for cobalt-60 and 15 MV x-rays it is possible that previously reported water calorimeter measurements may reflect the absence of the steady state. This is indicated by the observation that published values of D_c/D_i are 2-4% higher than the values determined in this study.

CHAPTER 5

SUMMARY AND CONCLUSIONS

5.1 Calorimeter Design And Calibration

A water calorimeter has been constructed using a design proposed by Domen (1982a). The calorimeter was calibrated and used to measure the absorbed dose in water from various radiation beams used for radiotherapy. These included cobalt-60, 15 MV x-ray, and 10, 12, 15, and 18 MeV electron beams.

The temperature detector of the calorimeter was an assembly containing two metal oxide (0.25 mm diameter) thermistors connected in opposite arms of a Wheatstone bridge. A Keithley 181 nanovoltmeter was used with a chart recorder to monitor the signal voltage from the bridge.

The thermistors in the detector were electrically insulated and supported between two thin polyethylene films. The films were stretched and clamped between two 21.6 cm diameter acrylic plastic (PMMA) rings. A waterproof connector was constructed so that the thermistor detectors could be easily interchanged.

The measurement of absorbed dose, as determined with the water calorimeter, required an independent temperature calibration of the thermistor detector. A material constant was determined for each thermistor by fitting the logarithm of the "zero power" resistance to a polynomial in $1/T$ and calculating the first derivative with respect to $1/T$ (Sapoff, 1982). From calibration data for several thermistor detectors, it was determined that the thermistor material constant increases with increasing temperature by about 1% between 287-304 K.

Assuming semiconductor conductivity (VECO, 1966) the excess thermistor temperature was determined from the calibration data as a function of both thermistor power and surrounding water temperature. An accurate value of the thermistor temperature was required for a dose measurement and was calculated by adding the excess thermistor temperature to the measured water temperature. The excess thermistor temperature was found to increase linearly with increasing thermistor power between 0 and

100 microwatts. In contrast, the excess thermistor temperature was found to decrease with increasing water temperature (approximately 10% decrease between 287-304 K). For a 0.25 mm diameter thermistor sandwiched between thin polyethylene films and immersed in water at 296 K, the excess temperature was about 2.4×10^{-3} K/microwatt.

The excess thermistor temperature was observed to depend on the amount of air which was trapped between the polyethylene films. The air acts to insulate the thermistor and increases the excess temperature for a given power consumption. Because the polyethylene films were held tightly with rubber "o"-rings, the air which was initially between the films required time to escape when the detector was immersed in water. The average time required for the thermistor detector to equilibrate (i.e. for the trapped air to vacate the detector once it has been immersed in water) was observed to be about 15 hours.

The excess temperature of a thermistor is small compared to the temperature of the water and in general has negligible influence on the dose measurements. However, because the excess temperature is approximately two orders of magnitude greater than the temperature increase resulting from dose absorption, small changes in this value can significantly affect the performance of the calorimeter.

To allow the air sufficient time to escape from the detector (under the pressure of the water) the calorimeter was set up several hours prior to taking dose measurements. To alleviate the problem associated with trapping air, small spacers were positioned on the lower "o"-ring during assembly to provide a "channel" for the thermistor leads. A breather hole was also provided in the electrical connector.

To investigate the behavior of thermistors immersed directly in water, (i.e. without polyethylene film insulation) special waterproof thermistors (epoxy coated) were obtained from the manufacturer. These were mounted in the acrylic ring assemblies described previously and were supported in the water with a length of narrow teflon tubing.

Using the immersible thermistor detector, convection was observed in dose measurements in a cobalt-60 beam. These measurements were done at a depth of 5 cm and for a field size of 25 x 25 cm. Convection was characterized by a non linear signal voltage during irradiation and a long recovery period (1-3 min) when the beam was turned off. Convection was strongly enhanced by using smaller field sizes (14 x 14 cm) and reduced for a larger field of 32 x 32 cm. By changing the depth of measurement to 2.5 cm convection was less apparent but a large uncertainty (+/-

4%) was observed in a series of consecutive dose measurements.

In contrast to the cobalt-60 measurements, convection was not observed in dose measurements with a 15 MV x-ray beam (with the immersible thermistor detector). Dose measurements were taken at depths of 2.5 and 5 cm and for field sizes between 10 x 10 and 25 x 25 cm.

From these data it was postulated that the convection observed from cobalt-60 irradiation was critically dependent on both the temperature gradient and the water volume located within the penumbral region.

Having demonstrated convection in a cobalt-60 beam, one of the immersible thermistor detectors was disassembled and the thermistors were transplanted into a detector with polyethylene films. From dose measurements in a cobalt-60 beam at a depth of 5 cm and for a field size of 25 x 25 cm, convection was no longer observed. This experiment showed that the polyethylene films were an essential feature of the detector in providing a barrier to convection.

5.2 Temperature Drift And Operational Control

Environmental temperature drift, which is a significant obstacle for graphite and other solid

calorimeters, was not a problem for the water calorimeter. By premixing the initial temperature of the water to match that of the walls of the calorimeter, approximately six to eight hours of operation were routinely provided. For the dose measurements reported, no additional drift control circuitry was required.

5.3 Experimental Precision

A noise analysis was performed for the water calorimeter circuitry to assess the precision of a temperature measurement. An expression for the signal to noise ratio was derived and found to be directly proportional to the absorbed dose, bridge voltage and the sum of the thermistor material constants.

The noise voltage at the output of the detector was typically 30 nV p-p. For a dose measurement of 100 cGy and a bridge voltage of 0.5V, the observed signal to noise ratio was about 200/1. This represented a maximum attainable precision of $\pm 0.5\%$.

5.4 Absorbed Dose Measurements

Having established the required detector performance for the water calorimeter, a series of dose measurements were undertaken. Radiation beams of cobalt-60, 15 MV

x-rays and electrons with energies of 10, 12, 15, and 18 MeV were used. The 15 MV x-ray and the electron beams were produced from a Mevatron 77 linear accelerator.

For the accelerator beams the temperature rise in water was measured for a preset number of monitor units (MU). The absorbed dose was then determined from the product of the heat capacity of water and the measured temperature rise. To provide a convenient quantity for comparison the calorimeter dose was expressed in terms of cGy/MU.

For cobalt-60 beams the calorimeter dose was measured for a preset time. These measurements were reported in terms of cGy/min; i.e. dose rate.

For clarity in the discussion the calorimeter dose has been symbolized D_c/U where it is understood that the quantity U refers to either monitor units or time. The same symbolism applies to ion chamber (D_i/U) or Fricke dose measurements (D_f/U).

Using the approach of Ross et al (1984), D_c/U was observed as a function of accumulated dose. The main objective was to look for the existence of a steady state dose value; i.e. a value of D_c/U that remained constant with accumulated dose.

For calorimeter measurements with 15 MV x-rays a steady state value of D_c/U was observed. This was generally attained with an accumulated dose of about 100 Gy. In a few of the experiments, the values of D_c/U for low accumulated doses (20-30 Gy) were as much as 5% exothermic relative to the steady state. These observations were compatible to the behavior observed by Ross et al (1984) and the variation in the exothermicity for low accumulated doses could be attributed to variable concentrations of organic impurities.

The day to day consistency of the steady state values of D_c/U was determined from the uncertainty in the overall mean. The standard error of the mean was calculated at $\pm 0.6\%$ (95% confidence). From the observed consistency in the steady state values it was concluded that the water calorimeter was a viable dosimeter.

On the basis of a previously reported power dependence (Domen, 1982b), an investigation of the effect of thermistor power on D_c/U was undertaken. The water was preirradiated with 15 MV x-rays to a large accumulated dose (250 Gy) and the thermistor power was varied between 8.5 and 60 microwatts. To provide equivalent precision, the dose values for the lower powers were measured for larger preset doses. On the basis of a least squares fit to the data, no thermistor power dependence on D_c/U was

observed.

Using beams of cobalt-60, 15 MV x-rays, and electrons with energies of 10, 12, 15, and 18 MeV, a comparison was made between Dc/U and Di/U. For the ion chamber measurements a protocol recommended by AAPM TG-21 (1983) was used.

The values for Dc/U were generally higher than those for Di/U. Dc/Di for cobalt-60, 15 MV x-ray, and 10, 12, 15, and 18 MeV electron beams were $1.02 \pm 0.7\%$, $1.00 \pm 0.7\%$, $1.01 \pm 1.0\%$, $1.02 \pm 1.1\%$, $1.02 \pm 1.6\%$ and $1.04 \pm 1.2\%$ respectively (95% confidence).

A comparison was also made between Dc/U and Df/U (NRC Fricke service). This study was limited to the high energy x-ray and electron beams produced by the linear accelerator. In general, the observed differences in the dose values were about 1% except for 10 MeV electrons where Dc/U was 2% lower than Df/U. The values of Dc/Df for 15 MV x-ray and electron beams of 10, 12, 15, and 18 MeV were $0.99 \pm 0.7\%$, $0.98 \pm 1.0\%$, $0.99 \pm 1.1\%$, $0.99 \pm 1.6\%$, and $1.0 \pm 1.2\%$ respectively.

The value of Dc/Di determined for a cobalt-60 beam was between 1-2% lower than other published values (Domen, 1982b; de Marles, 1981; Kubo, 1983; Mattsson, 1984). For 15 MV x-rays Dc/Di was between 2-4% lower than for beams

of similar quality (de Marles, 1981; Kubo, 1983)

The steady state value of D_c/U for 15 MV x-rays was as much as 5% lower than dose values obtained for accumulated doses less than 20 Gy. On the basis of this evidence and the observation that D_c/D_i for cobalt-60 and 15 MV x-rays were between 1-2% and 2-4% lower respectively than other published values, it was concluded that a steady state value must be determined for the water calorimeter dose values to be reliable.

REFERENCES

- AAPM SCRAD (1971). Protocol for the Dosimetry of X- and Gamma-Ray Beams with Maximum Energies Between 0.6 and 50 MeV. Phys. Med. Biol. 16: 379-396.
- AAPM TG-21 (1984). A Protocol for the Determination of Absorbed Dose from High-Energy Photon and Electron Beams.. Medical Physics 10: 741-771.
- Allen, A.O. (1961). "The Radiation of Water and Aqueous Solutions". Chapters 1 and 6. D. Van Nostrand Company, Princeton, New Jersey.
- Almond, P.R., and Svensson, H. (1977). Ionization Chamber Dosimetry for Photon and Electron Beams. Acta Radiol. Ther. Phys. Biol. 16: 177-186.
- Almond, P.R. (1967). The Physical Measurements of Electron Beams from 6 to 18 MeV: Absorbed Dose and Energy Calibration. Phys. Med. Biol., 12: 13.
- Berger, M.J. and Seltzer S.M. (1982)."Stopping Powers and Ranges of Electrons and Positrons". NBSIR 82-2550. NBS, Washington, DC.
- Bevington, P.R. (1969). "Data Reduction and Analysis for the Physical Sciences". Chapters 6-11. McGraw-Hill, New York.
- Bischel H. (1966)."Charged Particle Interactions", in Radiation Dosimetry Vol. I. Attix, F.H. and Roesch, W.C. eds. Academic Press, New York.
- Boag, J.W. (1966). "Ionization Chambers", in Radiation Dosimetry Vol. II. Attix, F.H. and Roesch, W.C. eds. Academic Press, New York.
- Boyd, A.W., Carver, M.B., and Dixon, R.S. (1980). Computed and Experimental Concentrations in the Radiolysis of Water. Radiat. Phys. Chem. 15: 177-185

- Burch, P.R.J. (1959). A Theoretical Interpretation of the Effect of Radiation Quality on Yield in the Ferrous and Ceric Sulphate Dosimeters. Radiation Research 11: 361
- Burlin T.E. (1966). "Cavity-Chamber Theory", in Radiation Dosimetry Vol. I. Attix, F.H. and Roesch, W.C. eds. Academic Press, New York.
- Carslaw, H.S., and Jaeger, J.C. (1959). "Heat Conduction in Solids". Chapters 1,2,12 and Appendix II. Clarendon Press, Oxford.
- Comite International des Poids et Mesures (1969). Metrologia 5: 35-44.
- Comite International des Poids et Mesures (1976). Metrologia 12: 7.
- Cottens, E., Eggermont, G., Janssens, A., Buysse, J., and Jacobs, R. (1978). "Determination of the G-Value of the Fricke Dosimeter" in Nuclear Physics Laboratory Annual Report, Ghent State University.
- de Marles (1981). Comparison of Measurements of Absorbed Dose to Water Using a Water Calorimeter and Ionization Chambers for Clinical Radiotherapy Photon and Electron Beams. Unpublished thesis, University of Texas Health Science Center, Houston.
- Domen, S.R., and Lamperti, P.J (1974). A Heat-Loss-Compensated Calorimeter: Theory, Design, and Performance. J. Res. Nat. Bur. Stand. (US) 78A: 595-610.
- Domen, S.R. (1980). Absorbed Dose Water Calorimeter. Medical Physics 7: 157-159.
- Domen, S.R. (1982a). Absorbed Dose Water Calorimeter. US Patent No. 4312224.
- Domen, S.R. (1982b). An Absorbed Dose Water Calorimeter: Theory, Design and Performance. J. Res. Nat. Bur. Stand. (US) 87: 211-235.
- Domen, S.R. (1983). A Polystyrene-Water Calorimeter. J. Res. Nat. Bur. Stand. (US) 88: 373-387.

- Evans, R.D., (1966). "X-Ray and Gamma Ray Interactions", in Radiation Dosimetry Vol. I. Attix, F.H. and Roesch, W.C. eds. Academic Press, New York.
- Fletcher, J.W. (1982). "Radiation Chemistry of Water at Low Dose Rates with Emphasis on the Energy Balance: A Computer Study". AECL-7834, Chalk River Nuclear Laboratories, Chalk River, Ontario
- Fricke, H. and Hart, E.J. (1966). "Chemical Dosimetry", in Radiation Dosimetry, Vol. II. Attix, F.H. and Roesch, W.C. eds. Academic Press, New York.
- Goitein, M. (1976). Review of Parameters Characterising Response of Normal Connective Tissue to Radiation. Clin. Radiol. 27: 389-404
- Goldenberg, H. (1951). A problem in Radial Heat Flow. Brit. J. Appl. Phys. 2: 233-237.
- Goldenberg, H., and Tranter, C.J. (1952). Heat Flow in an Infinite Medium Heated by a Sphere. Brit. J. Appl. Phys. 3: 296-298.
- Greene, D. and Massey, J.B. (1966). The Use of Farmer-Baldwin and Victoreen Ionization Chambers for Dosimetry of High Energy X-radiation. Phys. Med. Biol. 12: 257
- Gunn, S.R. (1964). Radiometric Calorimetry: a Review. Nucl. Instr. Meth. 29: 1-24.
- Gunn, S.R. (1970). Radiometric Calorimetry: a Review. Nucl. Instr. Meth. 85: 285-312.
- Gunn, S.R. (1976). Radiometric Calorimetry: a Review. Nucl. Instr. Meth. 135: 251-265.
- Handbook of Chemistry and Physics (1972). 52nd Edition. Chemical Rubber Co., Cleveland Ohio.
- Holt, J.C. and Kessar, N.D. (1977). Discrepancy Between C_λ and Ce. Phys. Med. Biol. 22: 538-540.
- HPA (1969). A Code of Practice for the Dosimetry of 2 to 35 MV X-ray and Caesium-137 and Cobalt-60 Gamma-ray Beams. Phys. Med. Biol. 14: 1-8.

- HPA (1983). Revised Code of Practice for the Dosimetry of 2 to 25 MV X-ray, and of Caesium-137 and Cobalt-60 Gamma-ray Beams. Phys. Med. Biol. 28: 1097-1104.
- HPA (1985). Code of Practice for Electron Beam Dosimetry in Radiotherapy. Phys. Med. Biol. 30: 1169-1194.
- Hubbell, J.H. (1977). Photon Mass Attenuation and Mass Energy Absorption Coefficients for H, C, N, O, Ar and Seven Mixtures from 0.1 keV to 20 MeV. Radiation Research 70: 58-81.
- ICRU Report 14 (1969). "Radiation Dosimetry: X-rays and Gamma Rays with Maximum Energies Between 0.6 and 50 MeV". ICRU Publications, Washington, DC.
- ICRU Report 21 (1972). "Radiation Dosimetry: Electrons with Initial Energies Between 1 and 50 MeV". ICRU Publications, Washington, DC.
- ICRU Report 24 (1976). "Determination of Absorbed Dose in a Patient Irradiated by Beams of X or Gamma Rays in Radiotherapy Procedures". ICRU Publications, Washington, DC.
- ICRU Report 28 (1978). "Basic Aspects of High Energy Particle Interactions and Radiation Dosimetry". ICRU Publications, Washington, DC.
- ICRU Report 31 (1979). "Average Energy Required to Produce an Ion Pair". ICRU Publications, Washington, DC.
- ICRU Report 33 (1980). "Radiation Quantities and Units". ICRU Publications, Washington, DC.
- ICRU Report 34 (1982). "The Dosimetry of Pulsed Radiation". ICRU Publications, Washington, DC.
- ICRU Report 35 (1984a). "Radiation Dosimetry: Electron Beams with Energies Between 1 and 50 MeV". ICRU Publications, Washington, DC.
- ICRU Report 37 (1984b). "Stopping Powers for Electrons and Positrons". ICRU Publications, Washington, DC.

- Johns, H.E., and Rawlinson, J.A. (1976). "Desirable Characteristics of High Energy Photons and Electrons" in High Energy Photons and Electrons. Kramer, S., Suntharalingam, N., and Zininger, G.F. eds., John Wiley and Sons, New York.
- Johns, H.E., and Cunningham, J.R. (1983). "The Physics of Radiology". Chapter 7. Charles C. Thomas, Springfield, Illinois.
- Keithley, J.F. (1972). "Electrometer Measurements". Keithley Instruments, Cleveland, Ohio.
- Keithley, J.F., Yeager, J.R., and Erdman, R.J. (1984). Low Level Measurements. Keithley Instruments, Cleveland, Ohio.
- Keesom, W.H., and Kok, J.A. (1932). On a Method of Correcting for Incomplete Thermal Isolation in Measurements of Small Heat Capacities. Proc. Acad. of Sci. 35: 294, Amsterdam.
- Kubo, H. (1983). Absorbed Dose Determination with a Water Calorimeter in Comparison with an Ionisation Chamber. Phys. Med. Biol. 28: 1391-1399.
- Kubo, H., and Brown, D.E. (1984). On the Steady-State Drift Conditions of a Water Calorimeter in Clinical Megavoltage Photon and Electron Beams. Med. Phys. 11: 317-320.
- Kubo, H., Brown, D.E., and Russell, M.D. (1985a). A Thermoregulated Enclosure for Controlling Thermal Drift in a Radiation Calorimeter. Med. Phys. 12: 344-346.
- Kubo, H. (1985b). Estimate of the Amount of Thermal Diffusion from a Polystyrene-Water Calorimeter Detector to Surrounding Water During Irradiation. Phys. Med. Biol. 30: 785-798.
- Laughlin, J. and Genna, S. (1956). "Calorimetric Methods" in Radiation Dosimetry, Hine, G.J., Brownell, G.L. ed., Academic Press, New York.

- Laughlin, J. and Genna, S. (1966). "Calorimetry", in Radiation Dosimetry Vol. II., Attix, F.H. and Roesch, W.C. eds., Academic Press, New York.
- Law, J., and Naylor, G.P. (1972). A Comparison of Ionization and Ferrous Sulphate Dosimetry for Megavoltage Electrons. Phys. Med. Biol. 17: 400.
- Lempert, G.D., Nath, R., and Schulz, R.J. (1983). Fraction of Ionization from Electrons Arising in the wall of an Ionization Chamber. Medical Physics 10: 1-3.
- Mattsson, O. (1984). Application of the Water Calorimeter, Fricke Dosimeter, and Ionization Chamber in Clinical Dosimetry. PhD. Thesis, Univ. of Goteborg, Sweden.
- McDonald, J.C., Laughlin, J.S., and Freeman, R.E. (1976). Portable Tissue Equivalent Calorimeter. Med. Phys. 3: 80-86.
- McDonald, J.C., Goodman, L.J. (1982). Measurements of the thermal defect for A-150 plastic. Phys. Med. Biol. 27: 229-233.
- McLaughlin, E. (1965). The Thermal Conductivity of Liquids and Dense Gases. Chem. Rev. 64: 389-428.
- NACP (1972). Procedures in Radiation Therapy Dosimetry with 5 to 50 MeV Electrons and Roentgen and Gamma Rays with Maximum Photon Energies Between 1 and 50 MeV. Acta. Radiol. Ther. Phys. Biol. 11: 603-624.
- NACP (1980). Procedures in External Radiation Dosimetry with Electron and Photon Beams with Maximum Energies Between 1 and 50 MeV. Acta. Radiol. Oncol. 19: 55.
- Nahum, A.E. and Greening, J.R. (1976). Inconsistency in Derivation of C_λ and Ce. Phys. Med. Biol. 21: 862-867.
- Nahum, A.E. and Greening J.R. (1978). A Detailed Re-evaluation of C_λ and Ce with Application to Ferrous Sulphate G-values. Phys. Med. Biol., 23: 894-908.

- Nahum, A.E., Svensson, H., Brahme, A. (1981). "The Ferrous Sulphate G-Value for Electron and Photon Beams: A Semi-Empirical Analysis and its Experimental Support" in Proceedings of the Seventh Symposium on Microdosimetry, Vol II. Harwood Academic Publishers GmbH Chur, Switzerland.
- NCRP Report 69 (1981). "Dosimetry of X-ray and Gamma-Ray Beams for Radiation Therapy in the Energy Range 10 keV to 50 MeV". NCRP Publications, Washington, DC.
- Ozisik, M.N. (1980). "Numerical Methods of Solution". Chapter 12 in Heat Conduction. John Wiley and Sons, New York.
- Pruitt, J.S., Domen, S.R., and Loevinger, R. (1981). The Graphite Calorimeter as a Standard of Absorbed Dose for Cobalt-60 Gamma Radiation. J. Res. Nat. Bur. Stand. (US) 68: 495-501.
- Ross, C.K., Klassen, N.V., Smith, G.D. (1984). The Effect of Various Dissolved Gases on the Heat Defect of Water. Med. Phys. 11: 653-658.
- Sapoff M., Siwek R., Johnson H.C., Slepian J., and Weber S. (1982). "The Exactness of fit of Resistance-Temperature Data of Thermistors with Third-Degree Polynomials", in Temperature: Its Measurement and Control in Science and Industry Vol 5 Part 2, Schooley J.F. ed., American Institute of Physics, New York.
- Schmidt, E. (1949). "Thermodynamics". Chapter 16. The Clarendon Press, Oxford.
- Schulz, R.J., and Weinhaus, M.S. (1985). Convection Currents in a Water Calorimeter. Phys. Med. Biol. 30:10 1093-1099.
- Schwartz, H.A. (1962). A Determination of some Rate Constants for the Radical Processes in the Radiation Chemistry of Water. J. Chem. Phys. 66: 255-266.
- Shiragai, A. (1978). A Proposal Concerning the Absorbed Dose Conversion Factor. Phys. Med. Biol. 23: 245-252.

Simpson, R.E. (1974). "Introductory Electronics for Scientists and Engineers. Chapter 11. Allyn and Bacon, Boston.

Sokolnikoff, I.S., and Redheffer, R.M. (1966). "Mathematics of Physics and Modern Engineering." Chapter 5, P336. McGraw-Hill, New York.

Spinks, J.W.T., and Woods, R.J. (1964). "An Introduction to Radiation Chemistry." Chapter 8. John Wiley and Sons, New York.

Svensson, H. and Brahme, A. (1979). Ferrous Sulphate Dosimetry for Electrons Acta. Radiol. Oncol. 18: 326-336.

Thermometrics Inc. (1985). Thermistor part numbers AB0C8-B35KA222M-A2 and AA0C8-B14KA222N-A2.

Thomas, R.F., and MacRoberts, M.D.J. (1965). "RATH Thermal Analysis Program, LA-3264-MS, UC-32". Mathematics and Computers, Los Alamos Scientific Laboratory, Los Alamos, New Mexico.

VECO (1966). Victory Engineering Corporation Technical Bulletin MTD131. Springfield, New Jersey.

Velarde, M.G., and Normand, C. (1980). Convection. Sci. Am. 243:1 93-106, July.

Williams, P.C. (1977). Discrepancy Between C_λ and Ce. Phys. Med. Biol. 22: 535-538.

APPENDIX A

HEAT CONDUCTION AND EXCESS THERMISTOR TEMPERATURE

A.1 Goldenberg Equations

Goldenberg (1951) derived a temperature solution to the Fourier equation (see equation 2.2, Chapter 2) for conductive heat transfer between a solid sphere in which heat is produced at a constant rate and an infinite medium. The equations derived by Goldenberg are directly applicable to thermistor heating (either by radiation absorption or by electrical power) and the determination of the excess thermistor temperature. An analytical solution for the excess thermistor temperature is useful for designing a temperature detector for a calorimeter and for interpreting calibration and temperature measurement data.

The original temperature solution (Goldenberg, 1951) was restricted to the case where the thermal properties of the sphere and the medium were identical. These equations were later extended to describe the more general case where the thermal conductivities and diffusivities were different (Goldenberg and Tranter, 1952).

Using the equations derived by Goldenberg and Tranter (1952), the excess temperature at the centre of a spherical thermistor is given by

$$v_x(r=0,t) = \frac{A \text{ rad}^2}{K_1} \left[\frac{K_1}{3 K_2} + \frac{1}{6} - \frac{2 b}{\pi} \int_0^\infty \frac{e^{-(y^2 t/\gamma)}}{y} \frac{\sin y - y \cos y}{(c \sin y - y \cos y)^2 + (b y \sin y)^2} dy \right]$$

(A.1)

where A is a constant rate of heating (energy per unit volume per unit time), t is the time, rad is the radius of the thermistor, α is the thermal diffusivity and K is the thermal conductivity. The subscripts 1 and 2 refer to the thermistor and medium respectively. The other constants

are defined by

$$b = K_2/K_1 \sqrt{\alpha_1/\alpha_2} \quad (A.2)$$

$$c = 1 - K_2/K_1 \quad (A.3)$$

$$\text{and} \quad \gamma = \frac{\text{rad}^2}{\alpha_1} \quad (A.4)$$

The excess temperature within the thermistor (between the centre and the outer surface) is given by

$$\begin{aligned} v_x(r,t) = & \frac{A \text{ rad}^2}{K_1} \left[\frac{K_1}{3 K_2} + \frac{1}{6} (1 - (r/\text{rad})^2) \right. \\ & - \frac{2 b \text{ rad}}{r \pi} \int_0^\infty \frac{e^{-(y^2 t/\gamma)}}{y^2} \\ & \left. \frac{(\sin y - y \cos y) \sin (ry/\text{rad})}{(c \sin y - y \cos y)^2 + (b y \sin y)^2} dy \right] \end{aligned} \quad (A.5)$$

and the excess temperature outside the thermistor (i.e. in the surrounding medium) is given by

$$v_x(r,t) = \frac{A \text{ rad}^3}{K1 \text{ r}} \left[\frac{K1}{3 K2} - \frac{2}{\pi} \int_0^\infty \frac{e^{-(Y^2 t/\gamma)}}{Y^3} \frac{(siny - ycosy)[bysiny\cos(fy) - (csiny - ycosy)\sin(fy)]}{(csiny - ycosy)^2 + (bysiny)^2} dy \right] \quad (A.6)$$

where f is defined by

$$f = (r/\text{rad} - 1) \sqrt{\alpha_1/\alpha_2} \quad (A.7)$$

In equations A.1, A.5 and A.6, a subscript "x" has been used to indicate that the temperature is in excess of the ambient temperature of the medium. For the derivation of Goldenberg and Tranter (1952), this convention was unnecessary because the temperature of the medium was assumed to be zero. Equations A.1, A.5 and A.6, however, are valid for any temperature of the medium provided that they are interpreted as excess quantities.

A.2 Steady State Thermistor Temperature

The integral terms (transients) in equations A.1, A.5 and A.6 are only required when the heating of the thermistor is of extremely short duration. With reference

to a water calorimeter, the detecting thermistors are continually dissipating electrical power and the radiation times are of the order of minutes. For these conditions, the integral terms are nearly equal to zero, and the remaining terms define the steady state temperatures.

An approximate value for the time required to reach the steady state is given by

$$t_{ss} = \frac{100 \text{ rad}^2}{\alpha^2} \quad (\text{A.8})$$

where α^2 is the thermal diffusivity of the medium. Equation A.8 is not readily obtained from equations A.1, A.5, and A.6 and is more easily derived from the equations in the earlier publication (Goldenberg, 1951). The time required to reach the steady state (according to equation A.8) is independent of the rate of heating and works out to about 11 seconds for a 0.25 mm diameter thermistor placed in water.

The steady state solutions to equations A.1, A.5, and A.6, are given by

$$v_x(r=0) = \frac{A \text{ rad}^2}{K_1} \left[\frac{K_1}{3 K_2} + \frac{1}{6} \right] \quad (\text{A.9})$$

at the centre of the thermistor,

$$v_x(r) = \frac{A \text{ rad}^2}{K1} \left[\frac{K1}{3 K2} + \frac{1}{6} (1 - (r/\text{rad})^2) \right]$$

(A.10)

within the thermistor, and

$$v_x(r) = \frac{A \text{ rad}^3}{3 K2} \frac{1}{r}$$

(A.11)

outside the thermistor. The subscripts 1 and 2 refer to the thermistor and medium respectively.

Integrating equation A.10 over the thermistor volume, the average steady state temperature within the thermistor is given by

$$\bar{v}_x = \frac{A \text{ rad}^2}{K1} \left[\frac{K1}{3 K2} + \frac{1}{15} \right]$$

(A.12)

A.3 Excess Thermistor Temperature From Power Dissipation

In a circuit, a small amount of power is dissipated by a thermistor and the thermistor temperature will be slightly higher than that of the environment. Since the

quantity "A" (equation A.1) is equal to the thermistor power (P) divided by the volume, equation A.12 can be rewritten as

$$\bar{v}_{xp} = \frac{P}{4 \pi \text{ rad}} \left[\frac{1}{K2} + \frac{1}{5 K1} \right]$$

(A.13)

The additional "p" in the subscript indicates that the source of the excess temperature is the electrical power consumed by the thermistor.

Equation A.13 states that the steady state excess thermistor temperature is directly proportional to the electrical power. In practice (Chapter 3), plots of thermistor temperature (or thermistor resistance for powers less than 100 microwatts) versus power were highly linear and were used as the basis for a thermistor calibration (the determination of the material constant).

Equation A.13 also predicts that for a given power dissipation, the steady state thermistor temperature is inversely proportional to its radius. From Table 3.1 (Chapter 3) this dependence can be seen for the thermistors from detectors A and E which correspond to the same polyethylene thickness and thermistor type. The calibration data in Table 3.1, however, apply to different

types of thermistors and detector construction (layers of polyethylene) and therefore a $1/\text{rad}$ dependence of v_{xp}/P is not strictly observed (i.e. the product of v_{xp}/P and rad does not yield the same constant for all entries in the table). Nevertheless, the data in Table 3.1 clearly demonstrates that v_{xp}/P decreases with increasing thermistor size.

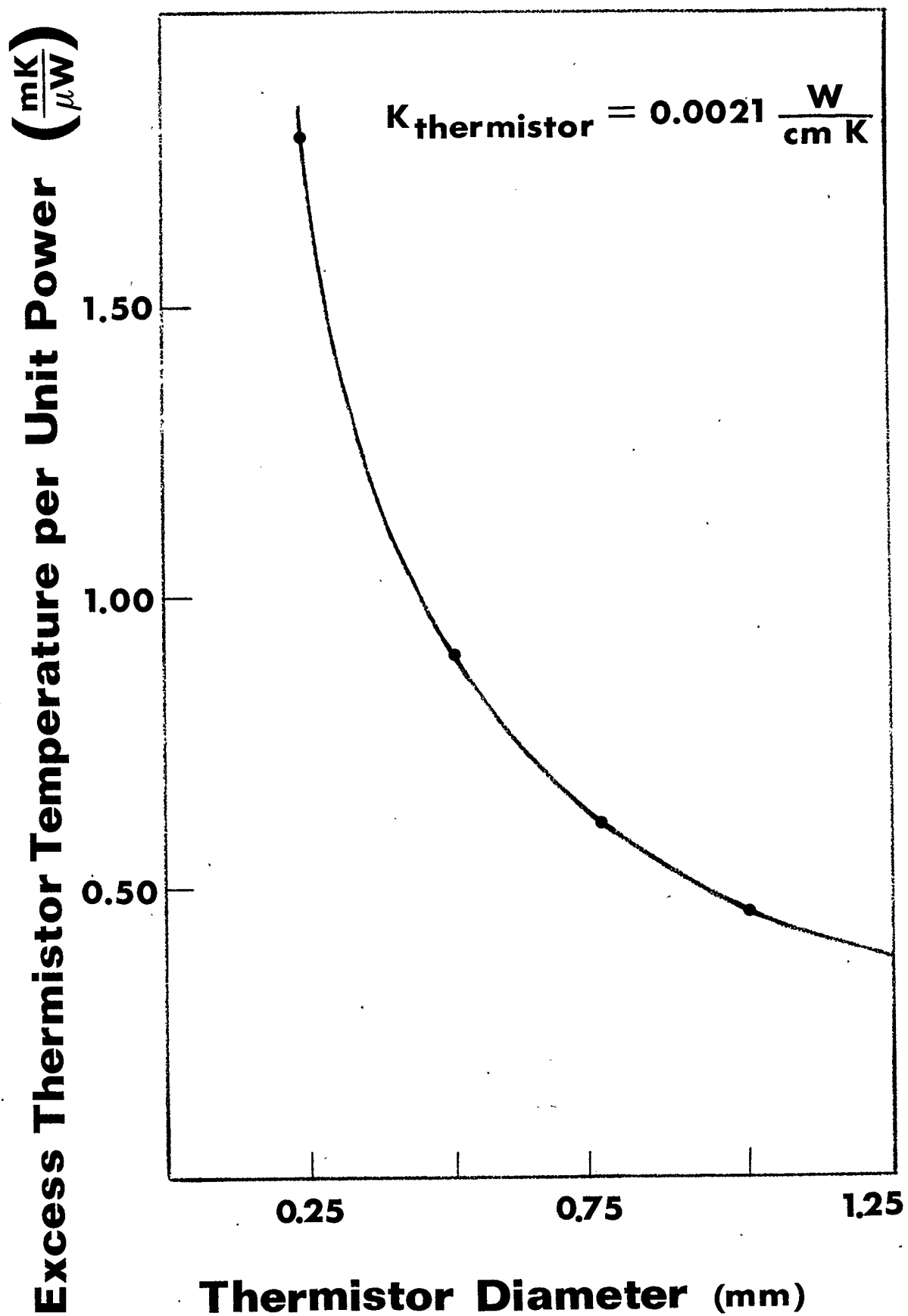
The excess thermistor temperature per unit power (v_{xp}/P) is graphed as a function of thermistor diameter in Figure A.1. For these calculations it has been assumed that the thermistors are immersed directly in water (thermal conductivity 6.0×10^{-3} watts $\text{cm}^{-1}\text{K}^{-1}$ as given in Appendix B) and that the average thermal conductivity of the thermistor material is 2.1×10^{-3} watts $\text{cm}^{-1}\text{K}^{-1}$ (see Section A.6).

A.4 Excess Thermistor Temperature During Irradiation

The excess thermistor temperature resulting from the absorption of radiation can also be determined from equation A.12. In this case, however, it is necessary to calculate an "excess" absorbed dose rate (see Section 2.4.2 in Chapter 2) because the temperature of the surrounding water will also rise from the absorption of radiation (Note that equation A.12 applies to a heat source which is confined to the thermistor and that the

Figure A.1. Variation of Excess Thermistor Temperature with Thermistor Diameter.

For this calculation, the thermal conductivity of the thermistor was assumed to be 0.0021 watt/(cm K).



excess doserate is not the same as the actual doserate). The value of "A" in equation A.12 is the product of the density of the thermistor material and the excess absorbed dose rate (DR_x). Rewriting equation A.12 in terms of these parameters, the average excess temperature in the thermistor resulting from irradiation is given by

$$\bar{v}_{xr} = \frac{DR_x \rho \text{ rad}^2}{3} \left[\frac{1}{K2} + \frac{1}{5 K1} \right] \quad (\text{A.14})$$

where ρ is the density of the thermistor. The "r" in the subscript has been added to indicate that the source of the excess temperature is due to the absorption of radiation. In practice the excess thermistor temperature produced from irradiation appears as an "overshoot" in the chart tracing (see Figure D.1 and D.4, Appendix D) and is more apparent for thermistor diameters greater than 1.0 mm. As predicted by equation A.14, the excess thermistor temperature produced during irradiation is dependent on doserate and not on the dose. Calculations of v_{xr} are graphed in Figure 2.1 (Chapter 2). For the case of a 1.27 mm diameter thermistor immersed directly in water (Figure D.4, Appendix D) the calculated excess temperature (Figure 2.1, Chapter 2) agrees very well with the observed value for irradiation in a beam of 15 MV x-rays. The chart

recordings for these measurements clearly indicate the initial transient effect predicted by equation A.1 and the existence of a steady state thermistor temperature under conditions of irradiation.

A.5 Temperature Gradient In Water Produced By A Thermistor

As discussed in Chapter 2 and Appendix D, convection can occur in water for favorable geometries and when the temperature gradient becomes critically high. Equation A.11 indicates that the temperature outside the thermistor decreases as $1/r$ and that the temperature gradient (for r greater than rad) is described by

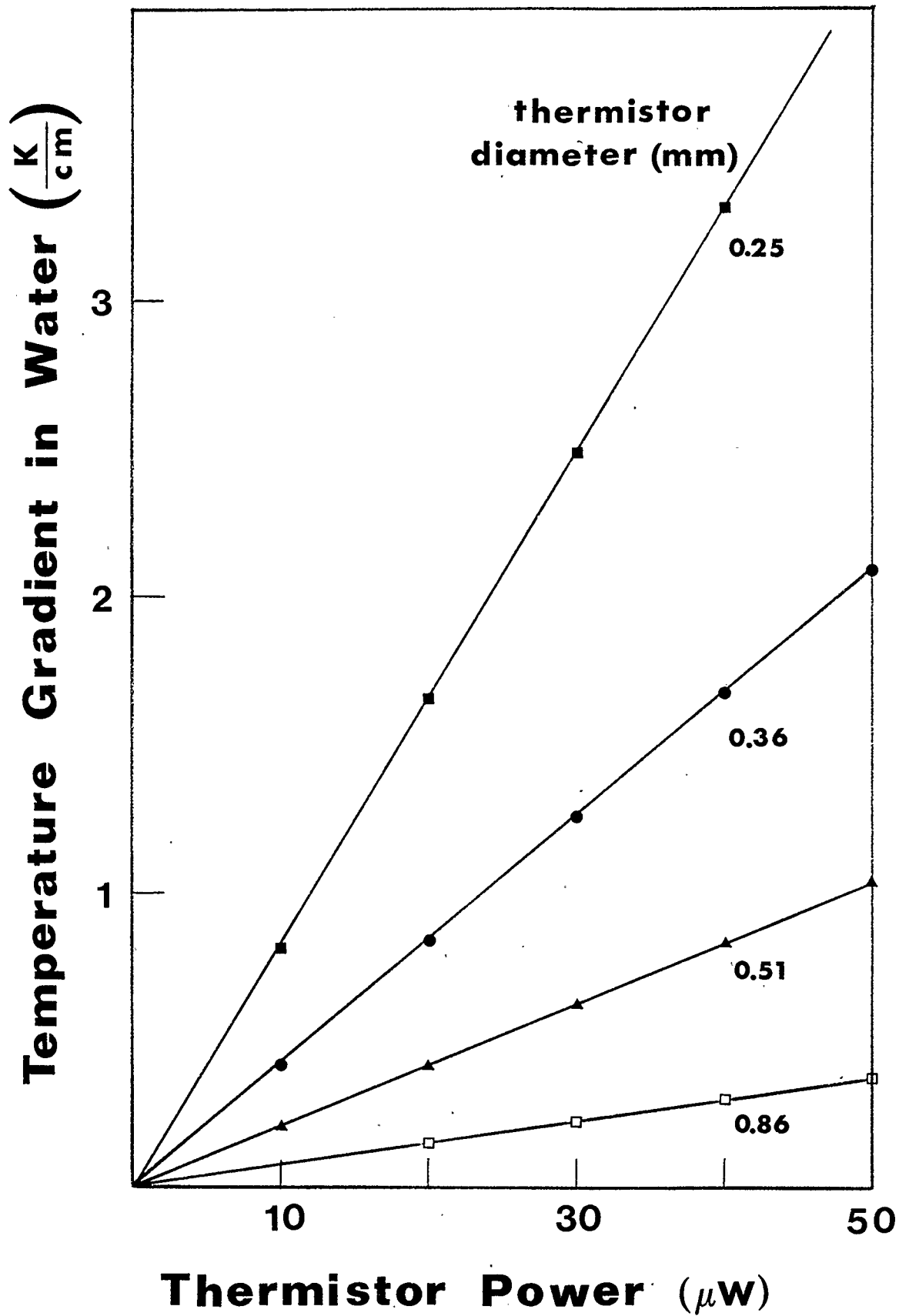
$$\frac{dv}{dr} = - \frac{A \text{ rad}^3}{3 K2} (1/r)^2 \quad (\text{A.15})$$

Rewriting equation A.15 in terms of thermistor power (P), the temperature gradient is given by

$$\frac{dv}{dr} = - \frac{P}{4 \pi K2} (1/r)^2 \quad (\text{A.16})$$

The temperature gradient in water at the outside surface of the thermistor is plotted in Figure A.2 as a function of thermistor power and radius. An interesting feature

Figure A.2. Variation of Temperature Gradient in Water with Thermistor Diameter and Thermistor Power.



predicted by equation A.16, is that the temperature gradient in water is independent of the material in the thermistor and depends only on the physical dimensions and the thermistor power.

Taking the derivative of equation A.16 with respect to r ,

$$\frac{d(dv/dr)}{dv/dr} = -2 \frac{dr}{r} \quad (A.17)$$

For a factor of 2 increase in r , the temperature gradient will decrease by a factor of 4.

Equations A.15, A.16, and A.17 show that the temperature gradient can be reduced by decreasing the electrical power or increasing the thermistor radius.

A.6 Thermal Conductivity Of A Thermistor

An estimate of the thermal conductivity of the thermistor can be obtained from equation A.12. Solving the equation for K_1 , and expressing A in terms of the thermistor power,

$$K1 = \frac{1}{5 (4 \pi \frac{v_{xp}}{P} \text{ rad} - \frac{1}{K2})} \quad (A.18)$$

The quantity v_{xp}/P (excess thermistor temperature/unit power) is determined from the calibration data (see Chapter 3) and the value for the radius is specified by the manufacturer.

The thermal conductivity of the thermistor is needed to estimate the excess temperature produced from the absorption of radiation. For proprietary reasons, this data is not provided by the manufacturer and is not generally available.

Equation A.18 applies to the situation in which the thermistors are located in a homogenous medium of conductivity $K2$. In the thermistor detector, the thermistors are covered with polyethylene films and are partially surrounded with air. The calibration data for thermistors in these detectors was not suitable for a determination of $K1$.

The appropriate calibration data was obtained from thermistors that were directly immersed in water (Chapter 3, Appendix D). A potential difficulty with this approach

is that convective heat transfer in the vicinity of the thermistor may increase the "effective" conductivity of the water and thus lower the excess thermistor temperature for higher powers. For this reason the calibration data was limited to thermistor powers less than 10 microwatts. The excess temperature for a 0.38 mm diameter thermistor was determined to be 1.2×10^{-3} K/microwatt (at a water temperature of 296 K). Using a thermal conductivity for water (K2) of 6.0×10^{-3} watts $\text{cm}^{-1}\text{K}^{-1}$ (McLaughlin, 1965; Appendix B), the conductivity of the thermistor (K1) was calculated to be 2.1×10^{-3} watts $\text{cm}^{-1}\text{K}^{-1}$. This is about the same value as the thermal conductivity of acrylic plastic (PMMA; 2.2×10^{-3} watts $\text{cm}^{-1}\text{K}^{-1}$).

By substituting the appropriate values in equation A.18, it can be seen that the method for determining K1 is very sensitive to the values of v_{xp}/P and rad . The estimated uncertainty in the value of 2.1×10^{-3} watts $\text{cm}^{-1}\text{K}^{-1}$ is $\pm 25\%$.

APPENDIX B

TEMPERATURE DEPENDENCE OF THERMAL PROPERTIES OF WATER

B.1 Thermal Properties Of Water

The thermal conductivity, heat capacity, and physical density of water are all functions of temperature. Tables of these properties can be found in a variety of sources but are included in this appendix for reference.

The thermal diffusivity (α), which is a derived quantity, is calculated from (equation 2.3, Chapter 2)

$$\alpha = \frac{K}{\rho c}$$

where K is the thermal conductivity, ρ is the density, and c is the heat capacity.

The thermal diffusivity, thermal conductivity, heat capacity, and density of water are given in Table B.1 as a function of temperature. The table was generated by

TABLE B.1				
THERMAL PROPERTIES OF WATER				
Temperature K	Thermal Diffusivity cm^2/s $\pm .5\%$	Thermal Conductivity $\text{W cm}^{-1} \text{K}^{-1}$ $\pm .5\%$	Heat Capacity $\text{J g}^{-1} \text{K}^{-1}$	Density g/cm^3
287	0.001407	0.00589	4.187	0.9993
288	0.001412	0.00590	4.186	0.9991
289	0.001417	0.00592	4.185	0.9990
290	0.001421	0.00594	4.184	0.9988
291	0.001426	0.00596	4.183	0.9986
292	0.001431	0.00597	4.183	0.9984
293	0.001435	0.00599	4.182	0.9982
294	0.001440	0.00601	4.181	0.9980
295	0.001444	0.00603	4.181	0.9978
296	0.001449	0.00604	4.180	0.9976
297	0.001453	0.00606	4.180	0.9973
298	0.001458	0.00607	4.180	0.9971
299	0.001462	0.00611	4.179	0.9965
300	0.001466	0.00611	4.179	0.9965
301	0.001470	0.00612	4.170	0.9963

fitting K , α , and c to polynomials in temperature and calculating the thermal diffusivity from equation 2.3. The data for the thermal conductivity of water was taken from McLaughlin (1965). The heat capacity and density of water are tabulated as a function of temperature in the Handbook of Chemistry and Physics (1971).

The thermal conductivity of water is unusual in that it increases with increasing temperature. The increase over the temperature range 287-301 K is about 4%. Because the density and heat capacity decrease marginally (0.3% and 0.2% respectively) over the same temperature range, the thermal diffusivity follows essentially the same temperature dependence as the conductivity.

APPENDIX C

HEAT CONDUCTION IN WATER

C.1 Heat Conduction

The design of the water calorimeter is based on the assumption that conductive heat loss in water is negligible during an absorbed dose measurement.

Heat conduction is described by a well known equation due to Fourier. For heat conduction in one dimension and constant thermal diffusivity (α), the Fourier equation (equation 2.2, Chapter 2) is

$$\alpha \frac{d^2 T(x,t)}{dx^2} + g_0/(\rho c) = \frac{dT(x,t)}{dt}$$

where $T(x,t)$ is the temperature at position x and time t , g_0 is a heat source, and α is the thermal diffusivity (equation 2.3, Chapter 2) defined by

$$\alpha = K/(\rho c)$$

where K is the thermal conductivity, ρ is the density, and c is the heat capacity of water.

C.2 Axial Temperature Profiles

The dose in water produced from the absorption of a beam of radiation is not uniform throughout the irradiated volume. In the direction of the central axis (perpendicular to the surface of the water) the dose increases from a low value at the surface to a maximum at a characteristic depth (d_{\max}). The dose then decreases from the maximum with further depth to zero.

Proceeding away from the central axis and in a radial direction, the dose is relatively constant between the centre and beam edge (penumbral region). Beyond the beam edge, however, the dose decreases sharply to zero and this is potentially a problem area for conductive heat transfer.

If the dimensions of the beam are made sufficiently large, then it is possible to produce a dose distribution in the water calorimeter which varies only along the central axis. For this situation, the consideration of heat loss becomes a one dimensional problem and equation

2.2 is applicable. It is assumed in the analysis to follow that the relative temperature distribution is the same as the dose distribution.

C.3 Conductive Heat Loss In Water

Ideally, the calculation of conductive heat loss should be a solution to equation 2.2 with the source term g_0 present. The problem can be simplified however, by assuming an existing temperature distribution without a heat source (produced from the absorption of a short pulse of radiation) and calculating the decay of the distribution with time.

This procedure has been used by Domen (1982b) who calculated the decay (with respect to time) of various temperature profiles at selected points. The calculation is greatly simplified by using a numerical method due to Schmidt (1949).

A similar analysis was applied in this study to all of the beams used for dose measurements. These included cobalt-60, 15 MV x-ray, electron beams of 18, 15, 12, and 10 MeV. Analytical functions were fitted to the initial temperature profiles to provide accurate and continuous data. In this way, the entire temperature profile was easily determined at later times. The numerical analysis

reduces to a simple averaging technique by using sampling intervals defined by;

$$\frac{dx^2}{dt} = 2 \alpha \quad (C.1)$$

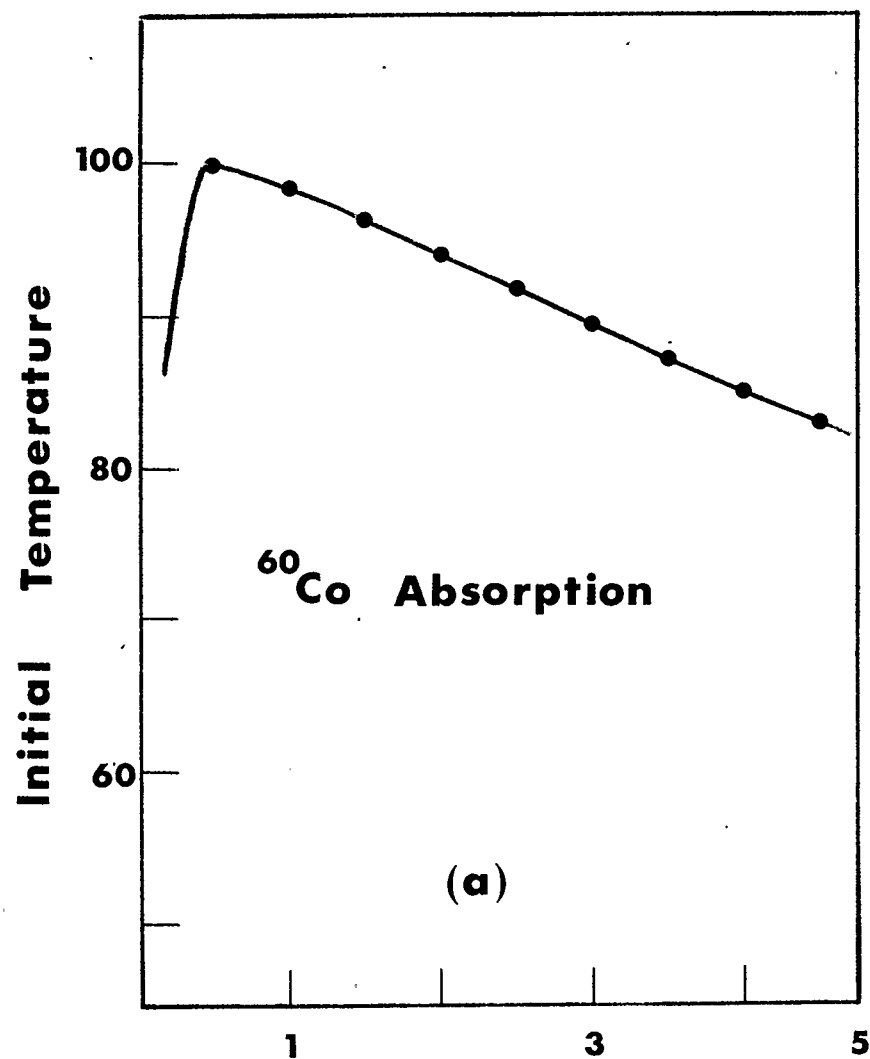
where α is the thermal diffusivity of water ($1.44 \times 10^{-3} \text{ cm}^2/\text{s}$). The results of the analysis are shown in Figures C.1 - C.6. The initial temperature profiles are plotted along with % differences for decay times of 55 and 222 seconds. These curves were produced by sampling the initial temperature profile every 4 and 8mm respectively according to equation C.1. To simplify the analysis, boundary conditions have been ignored and all curves begin at depths slightly below the surface (points near the surface would not be selected for calorimeter measurements).

A discussion of Figures C.1 - C.6 appears in Chapters 2 and 4 and is not repeated in this Appendix. The purpose of this analysis was to provide a reasonable basis for selecting an appropriate depth for water calorimeter measurements and for determining a correction factor for conductive heat loss where required.

Figure C.1. Variation of Conductive Heat Loss in Water with Position and Time for Cobalt-60 Radiation.

(a) Central axis temperature profile in water from the absorption of a short pulse of a cobalt-60 beam.

(b) Percent decrease in temperature as a function of position on the central axis and for times of 55 and 222 seconds after beam turn off.



Depth in Water along Central Axis (cm)

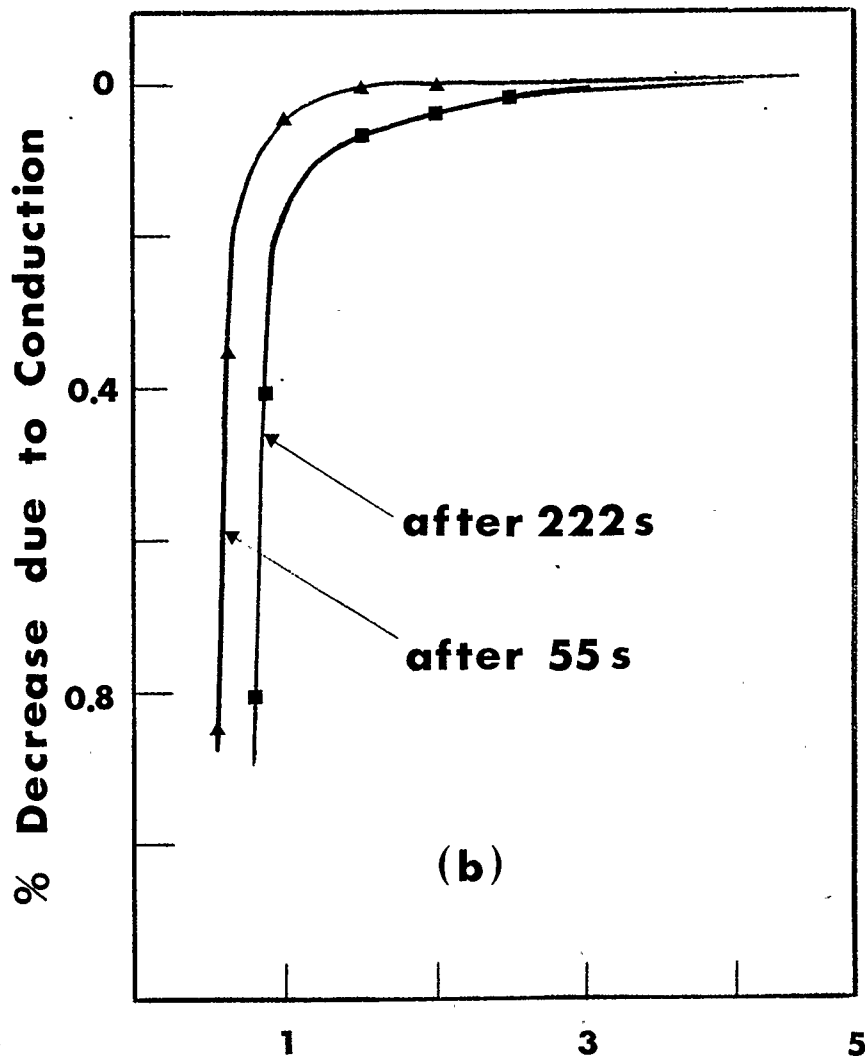
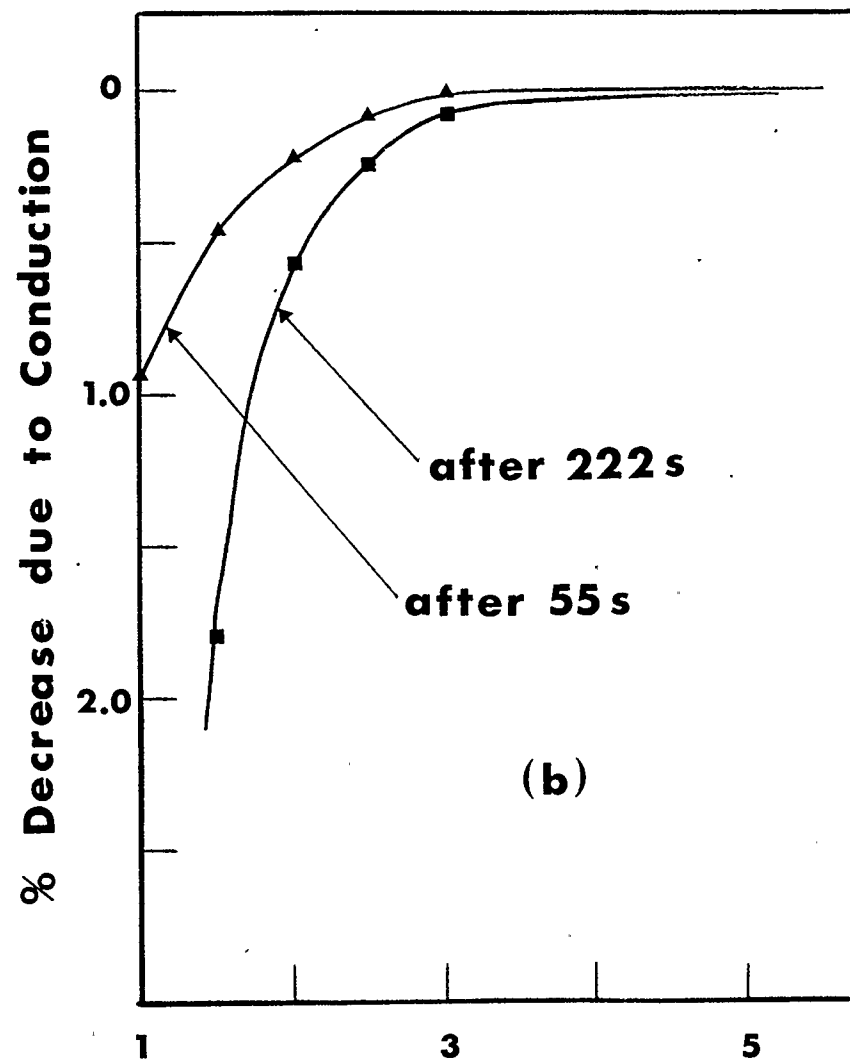
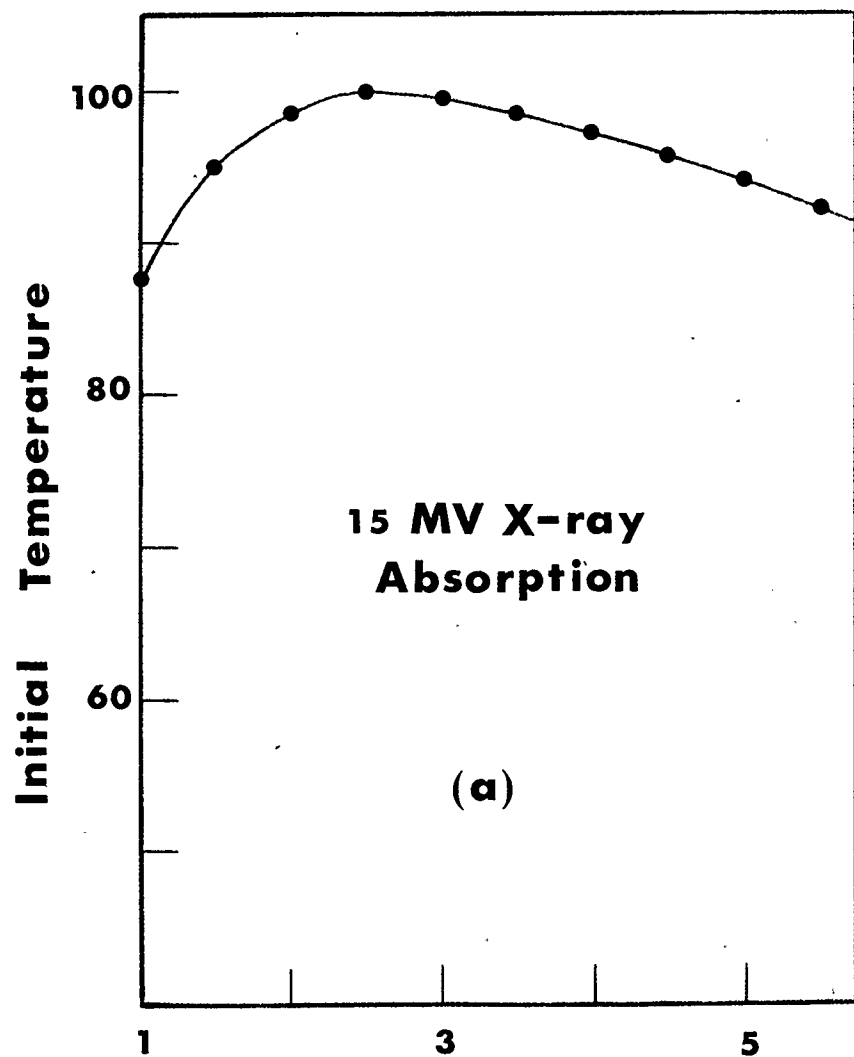


Figure C.2. Variation of Conductive Heat Loss in Water with Position and Time for 15 MV x-rays.

(a) Central axis temperature profile in water from the absorption of a short pulse of a beam of 15 MV x-rays.

(b) Percent decrease in temperature as a function of position on the central axis and for times of 55 and 222 seconds after beam turn off.

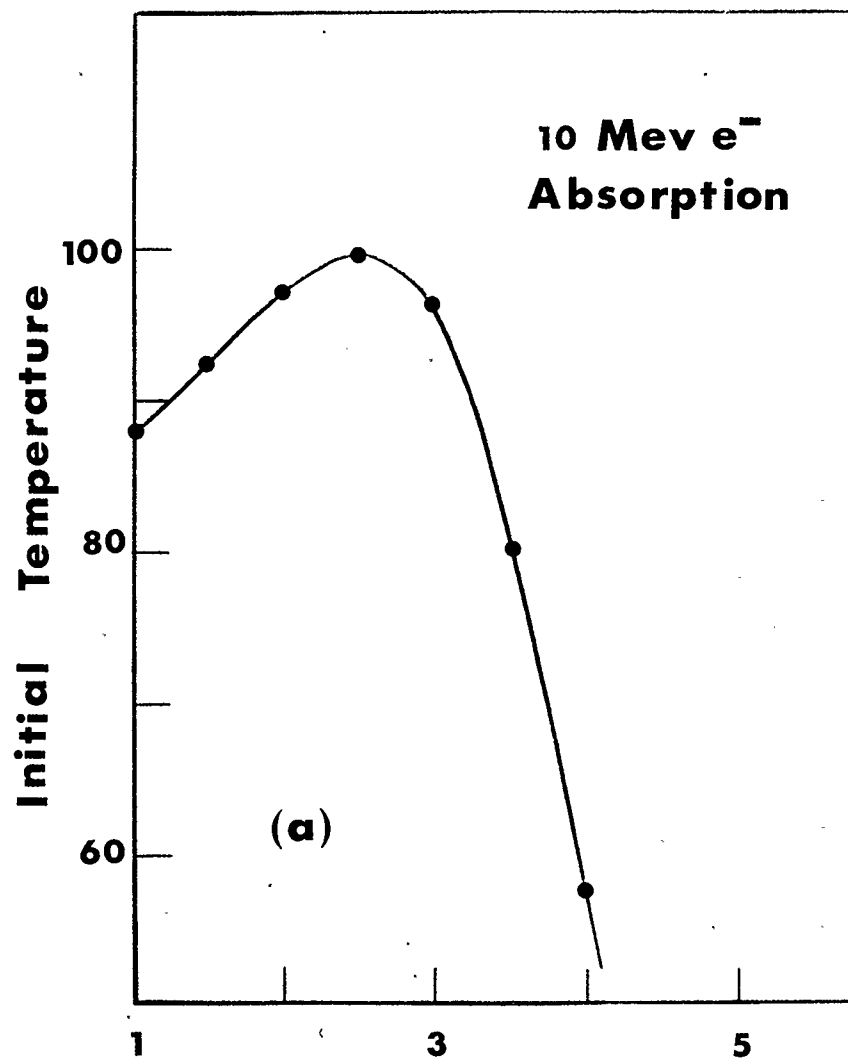


Depth in Water along Central Axis (cm)

Figure C.3. Variation of Conductive Heat Loss in Water with Position and Time for 10 MeV Electrons.

(a) Central axis temperature profile in water from the absorption of a short pulse of a beam of 10 MeV electrons.

(b) Percent decrease in temperature as a function of position on the central axis and for times of 55 and 222 seconds after beam turn off.



Depth in Water along Central Axis (cm)

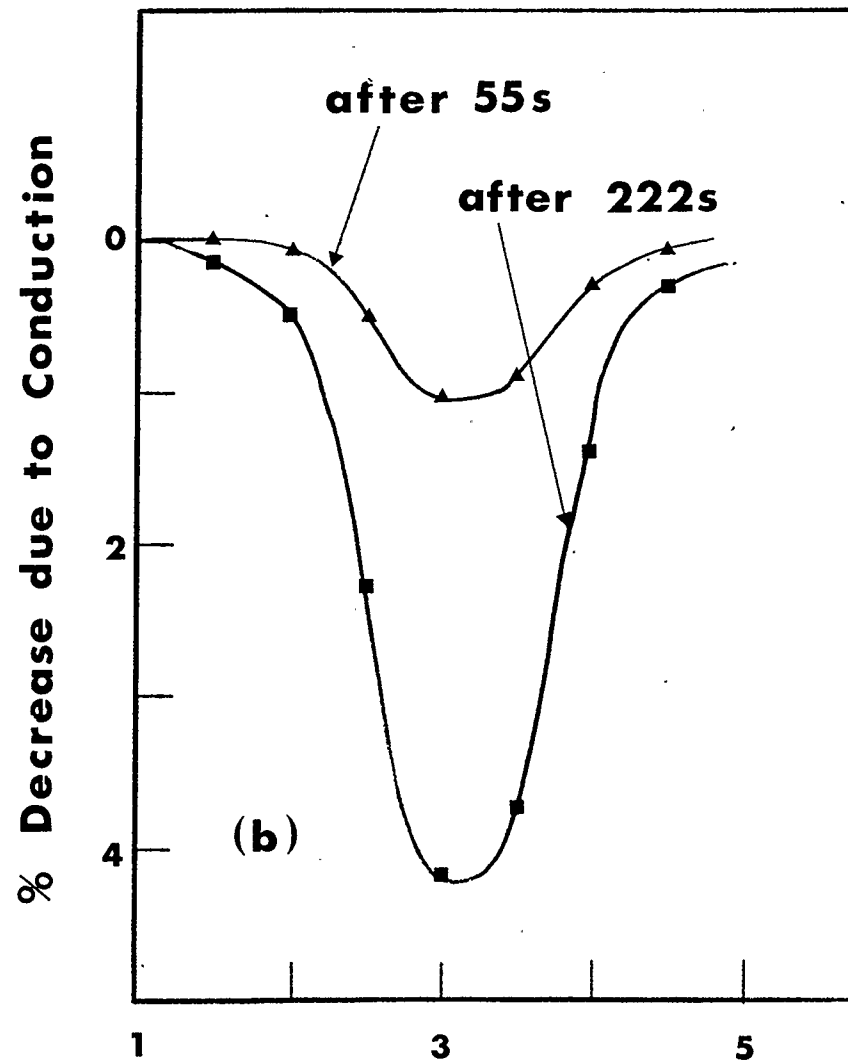
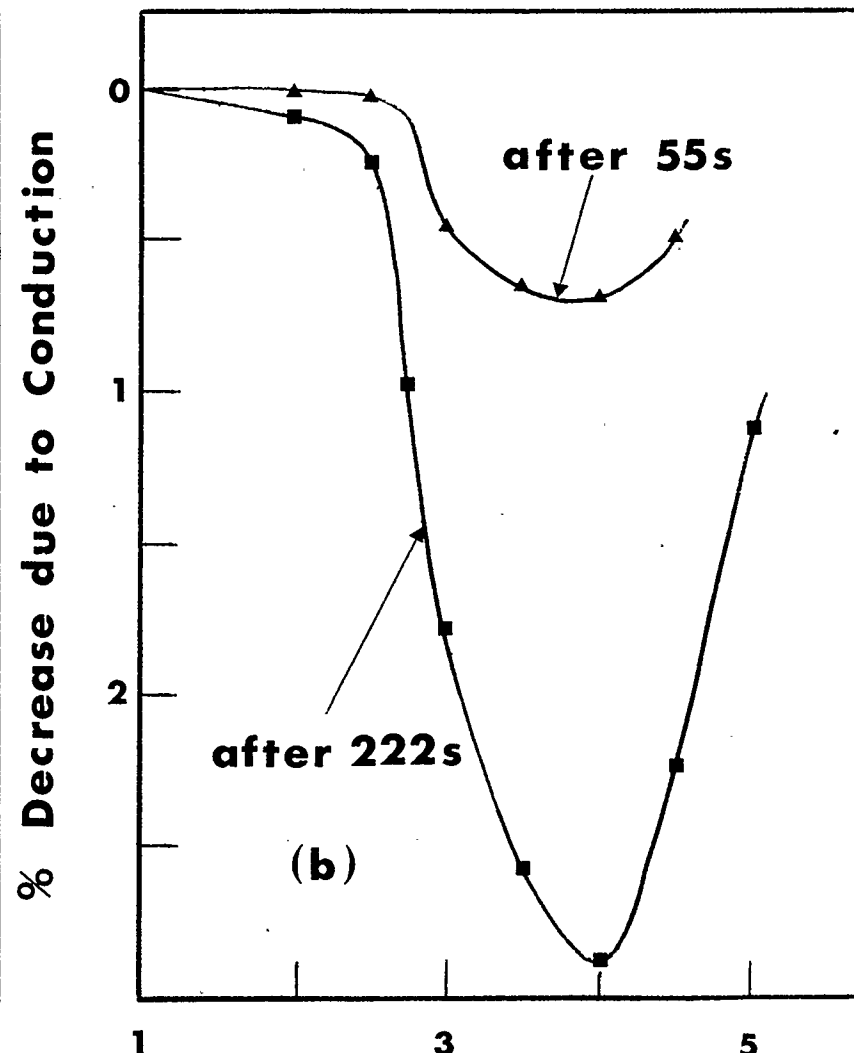
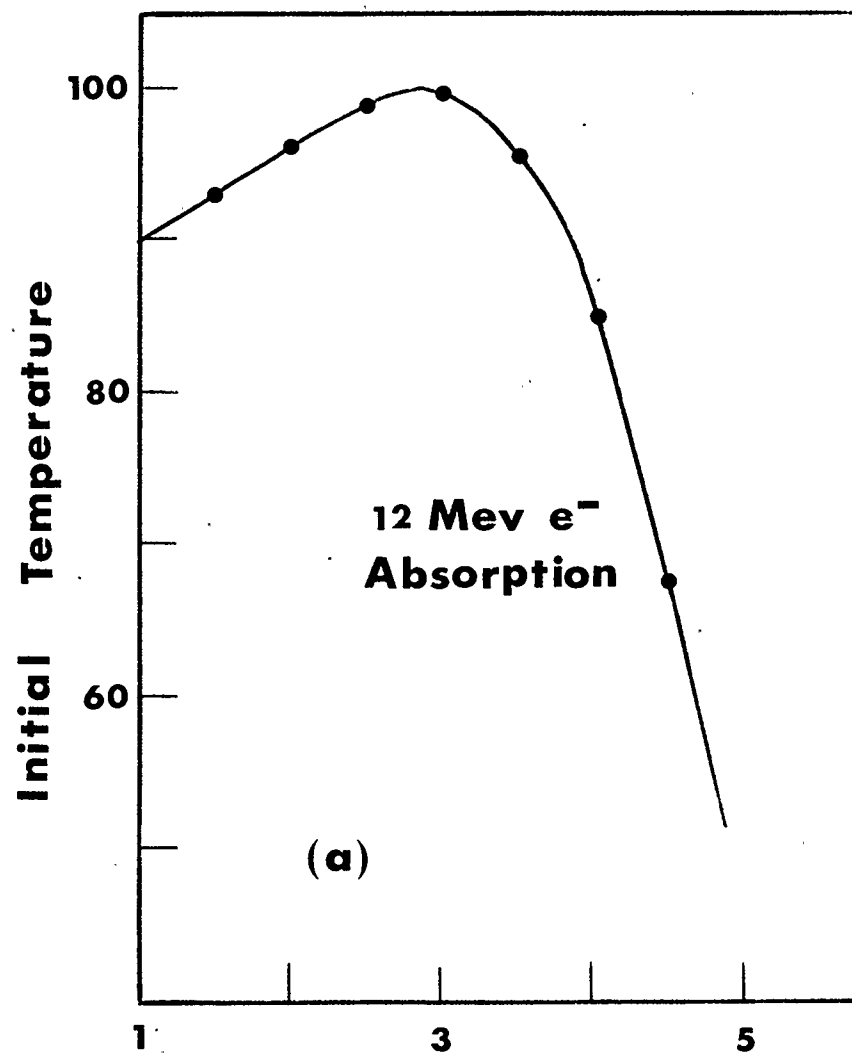


Figure C.4. Variation of Conductive Heat Loss in Water with Position and Time for 12 MeV Electrons.

(a) Central axis temperature profile in water from the absorption of a short pulse of a beam of 12 MeV electrons.

(b) Percent decrease in temperature as a function of position on the central axis and for times of 55 and 222 seconds after beam turn off.

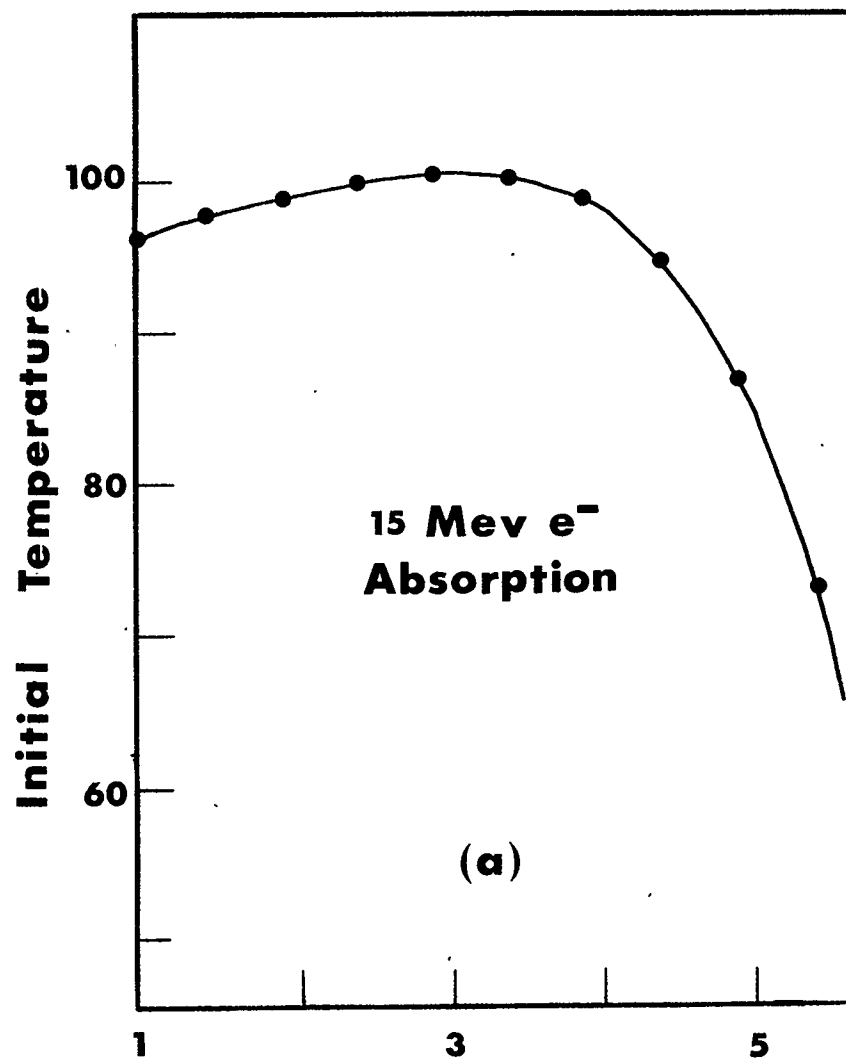


Depth in Water along Central Axis (cm)

Figure C.5. Variation of Conductive Heat Loss in Water with Position and Time for 15 MeV Electrons.

(a) Central axis temperature profile in water from the absorption of a short pulse of a beam of 15 MeV electrons.

(b) Percent decrease in temperature as a function of position on the central axis and for times of 55 and 222 seconds after beam turn off.



Depth in Water along Central Axis (cm)

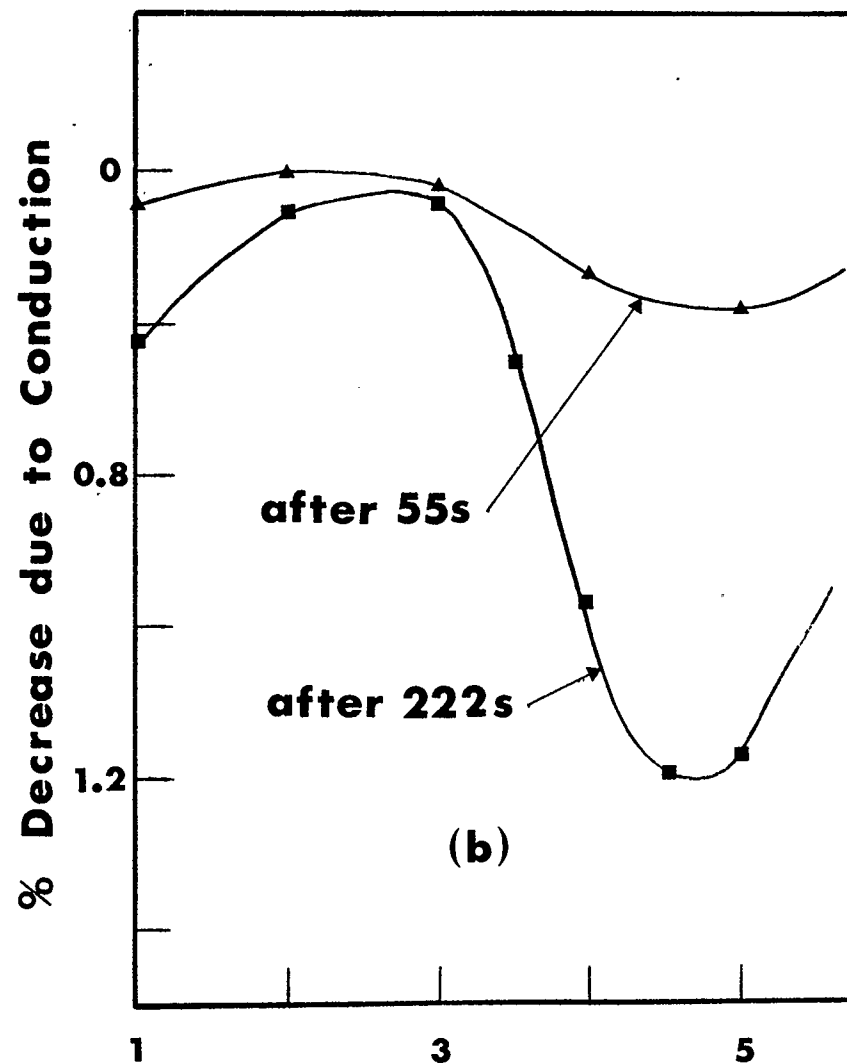
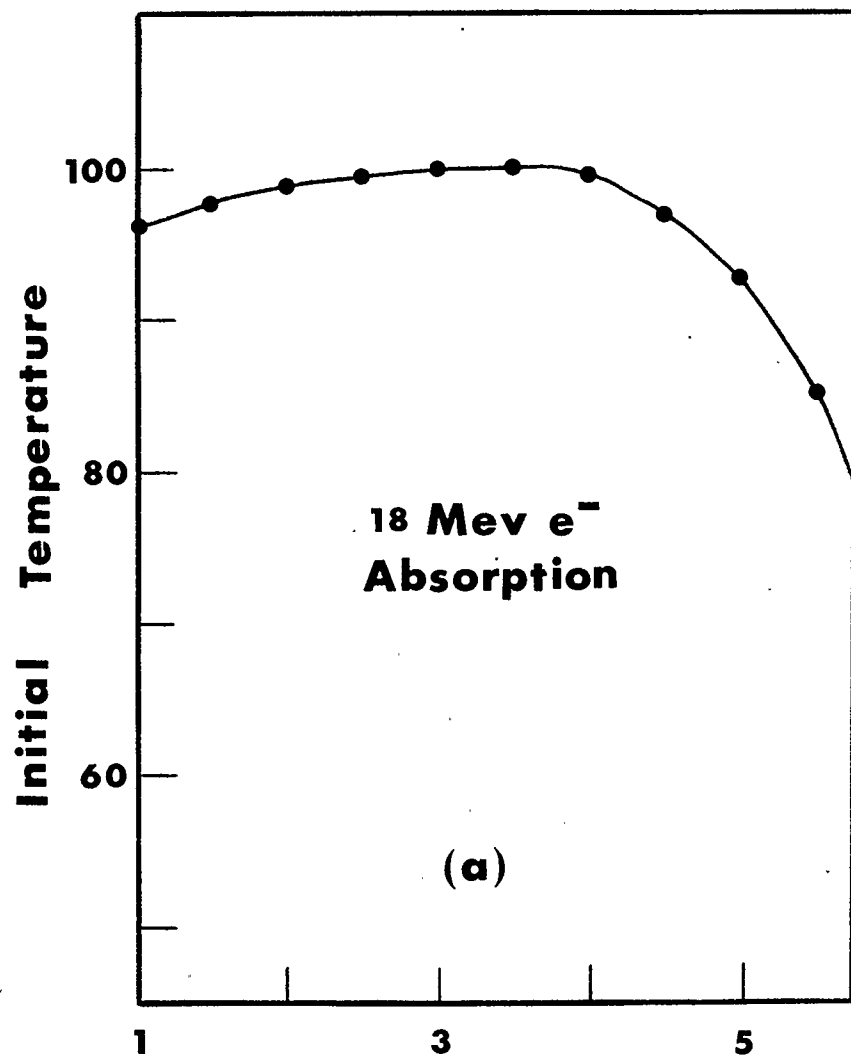


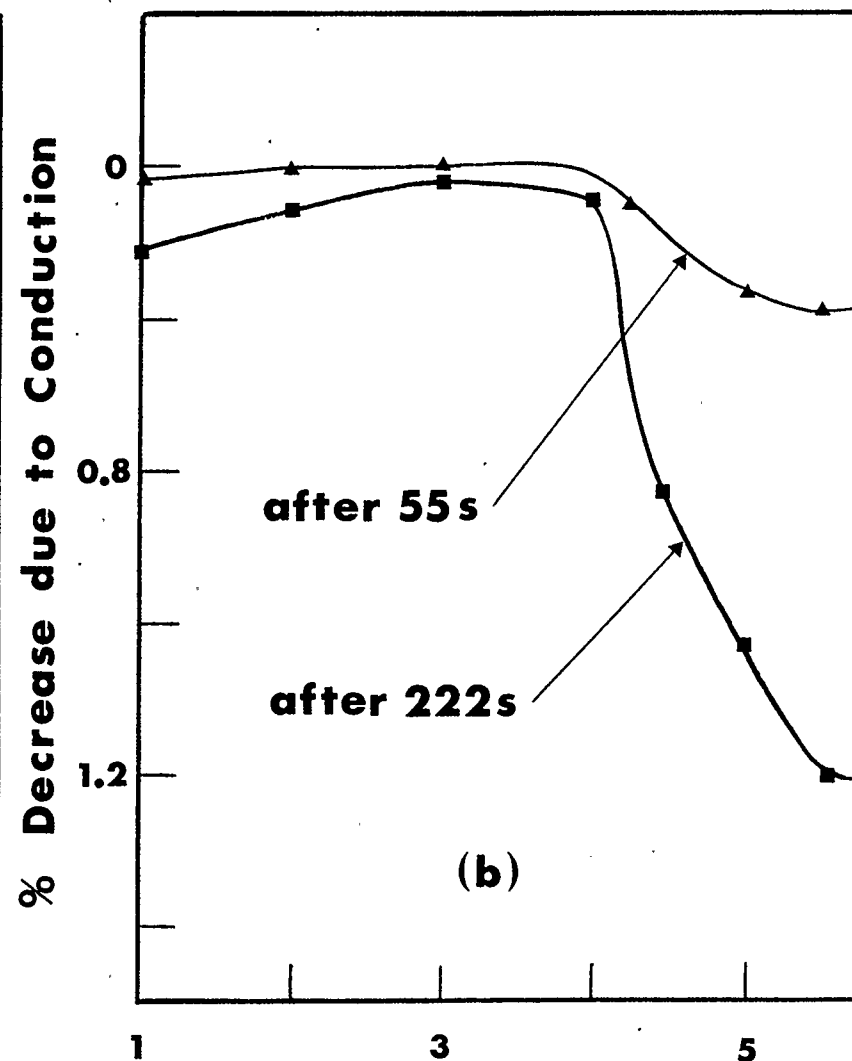
Figure C.6. Variation of Conductive Heat Loss in Water with Position and Time for 18 MeV Electrons.

(a) Central axis temperature profile in water from the absorption of a short pulse of a beam of 18 MeV electrons.

(b) Percent decrease in temperature as a function of position on the central axis and for times of 55 and 222 seconds after beam turn off.



Depth in Water along Central Axis (cm)



APPENDIX D

DOSE MEASUREMENTS WITH IMMERSIBLE THERMISTORS

D.1 Immersible Thermistors

The temperature detector described in Chapter 2 consisted of two thermistors which were supported and electrically insulated with thin polyethylene films. The films were stretched and clamped between acrylic plastic rings to provide a waterproof seal. The necessity for this design arises from the bare Pt-Ir leads which emerge from the thermistor.

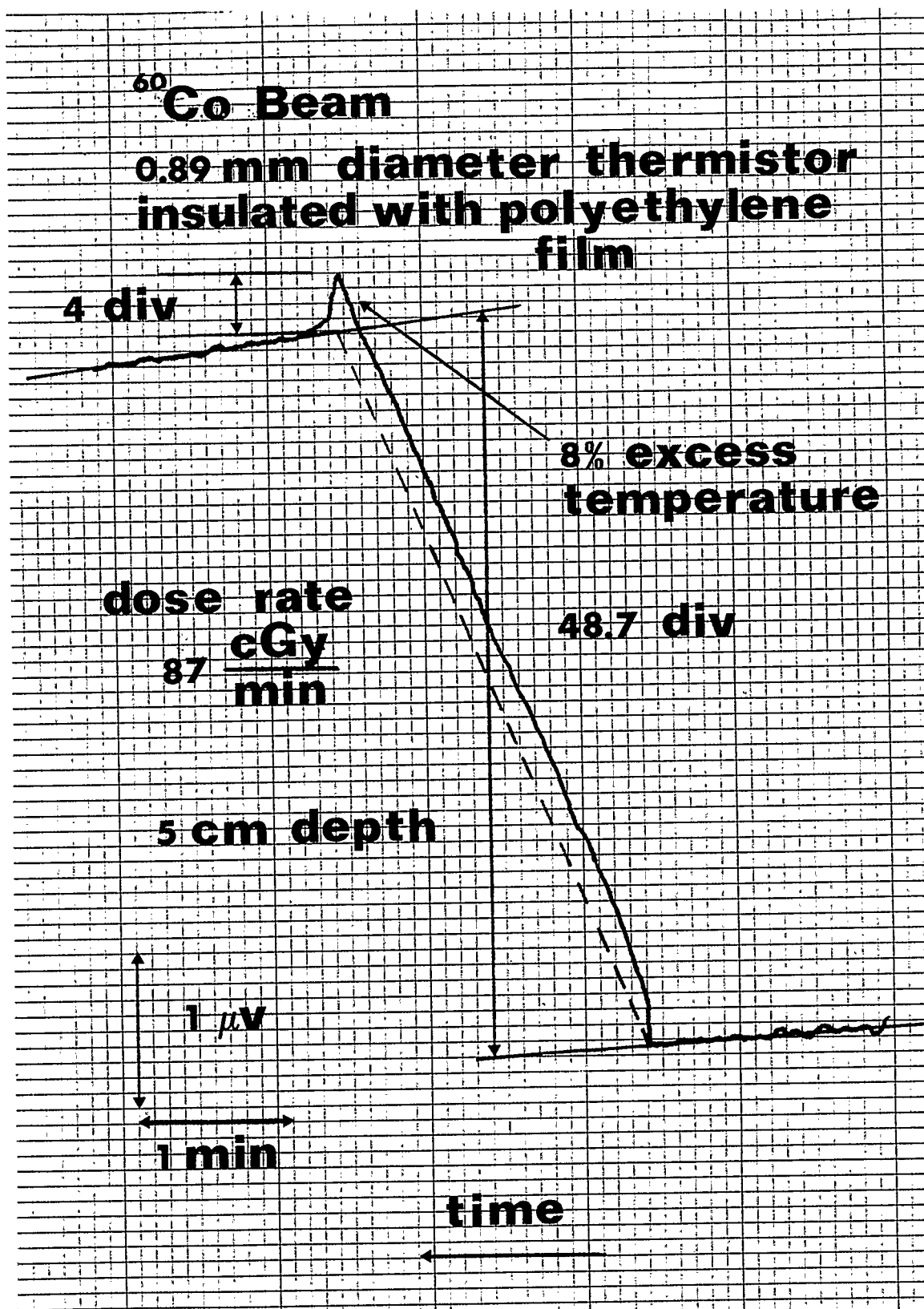
One of the difficulties with this detector format is that air can be trapped between the films and the thermistor when the detector is first immersed in water. The air insulates the thermistor from the water and increases the excess thermistor temperature for a given power consumption. This is not a problem provided that the air mass surrounding the thermistor remains

stationary. However, because the excess temperature of the thermistor is about two orders of magnitude greater than the temperature rise from a typical dose measurement, small changes in the excess temperature can have a significant effect on the measured dose. As demonstrated in Chapter 3, several hours are required for trapped air to be pushed out of the detector after it has been immersed in water.

The insulative effect of air surrounding the thermistor also increases the excess temperature produced by the direct absorption of radiation. This is shown in Figure D.1 in which a thermistor detector has been assembled using polyethylene films and 0.89 mm diameter thermistors. The observed excess temperature of 8% is several times greater than the calculated estimate of 1.5% (Figure 2.1, Chapter 2) assuming that the thermistor is in intimate contact with water. These data are included to draw further attention for the need to allow excess air to escape from the detector prior to taking dose measurements.

Small thermistors (Thermometrics, 1985) can be obtained commercially with insulated leads. This type of thermistor is directly immersible in water and avoids the potential problem associated with polyethylene films. A number of these were purchased from the manufacturer with

Figure D.1. Effect of Thermistor Size and Trapped Air on the Excess Thermistor Temperature During Temperature Measurements in a Cobalt-60 Beam.



diameters between 0.33 and 1.27 mm.

D.2 Modified Detector Construction

The acrylic ring assemblies used for the polyethylene film detectors were easily modified to house the immersible thermistors. To support the thermistors, a length of fine teflon tubing was stretched across the lower acrylic ring. The detector assembly is shown in the bottom of Figure D.2 (The dimensions can be determined from Figure 2.2 in Chapter 2).

D.3 Investigation Of Convection

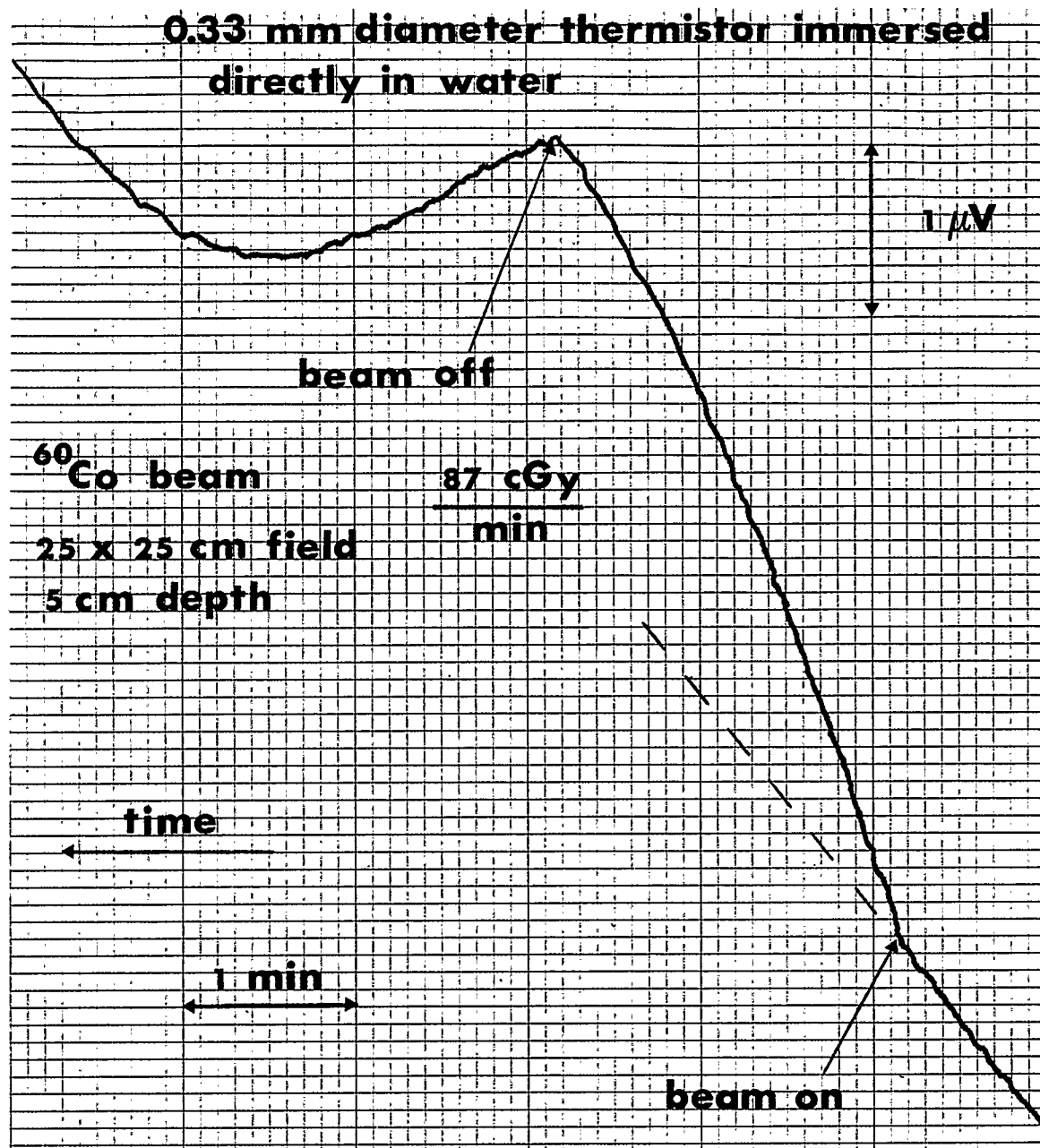
Convection can occur in water as the result of large temperature gradients and a favorable geometry. When this happens, the resulting turbulence makes it impossible to measure small temperature changes in the water near a thermistor.

The potential for convection in a water calorimeter has been considered by Domen (1982b) who made the provision for adding polyethylene baffles at various depths in the water tank. Aside from the polyethylene films in the temperature detector, however, no additional convection baffles were required by Domen for the dose measurements in a cobalt-60 beam.

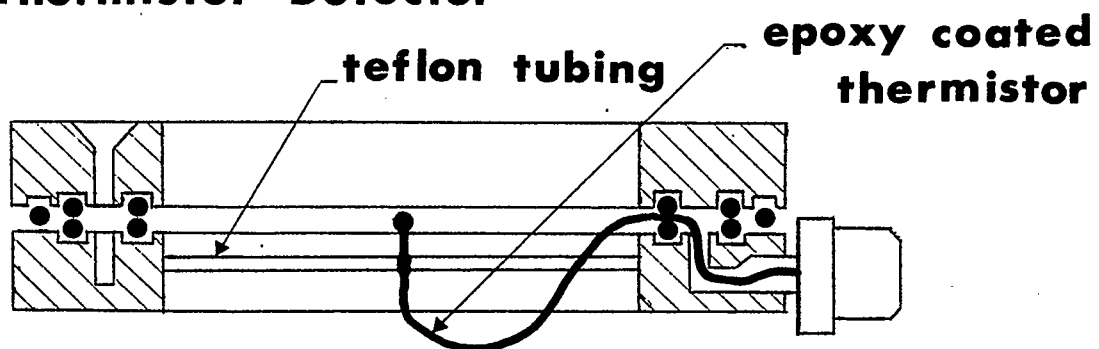
Figure D.2. Convection During Temperature Measurements in a Cobalt-60 Beam.

(a) Chart tracing for a calorimeter temperature measurement using an immersible thermistor detector in a cobalt-60 beam. The measurement was taken at a depth of 5 cm and for a field size of 25 x 25 cm.

(b) Diagram of an immersible thermistor detector. Dimensions can be obtained from the polyethylene film detector shown in Figure 2.2.



**Immersible
Thermistor Detector**



Convection is demonstrated in Figure D.2 which shows a temperature measurement from an immersible thermistor detector for cobalt-60 irradiation. Convection is characterized by a non linear trace during irradiation and a dramatic recovery period immediately after the beam is turned off.

Convection in a water calorimeter has also been reported by Schulz and Weinhaus (1985). The thermistor leads in their detector were insulated with tubing and the thermistors were immersed directly in water. These authors were able to observe convection by irradiating the calorimeter with horizontal beams and monitoring the change in temperature at depths of 6 and 10 cm simultaneously. Radiation beams of 25 MV x-rays and 19 MeV electrons were used. Their measurements indicated a bulk circulation in the water during irradiation; i.e. a large convection current encompassing both thermistors (5 cm apart). On the basis that convection was more severe from measurements with the electron beam these authors have assumed that the effect is largely due to gradients established by the axial temperature profiles of the individual beams. The chart tracing from their data for the "proximal" thermistors is very similar to the tracing in Figure D.2. However, they did not observe convection for vertical beams.

To investigate convection in this study, dose measurements were taken with an immersible thermistor detector in cobalt-60 and 15 MV x-ray beams.

Convection was readily observed for dose measurements in a cobalt-60 beam and found to vary with depth and field size. The measurement in Figure D.2 was taken at a depth of 5 cm and for a field size of 25 x 25 cm. By reducing the field size to 14 x 14 cm, convection was significantly enhanced as indicated by increased curvature of the chart tracing during irradiation and by a longer recovery period when the beam was turned off. By enlarging the field size to 35 x 35 cm convection was reduced but was still discernible. In contrast to the measurements recorded at a depth of 5 cm, convection was not obvious from the chart tracings taken at a depth of 2.5 cm. However, the slopes of the temperature drifts before and after a run were extremely variable and a large uncertainty (4% standard deviation) was determined from a series of eight successive measurements.

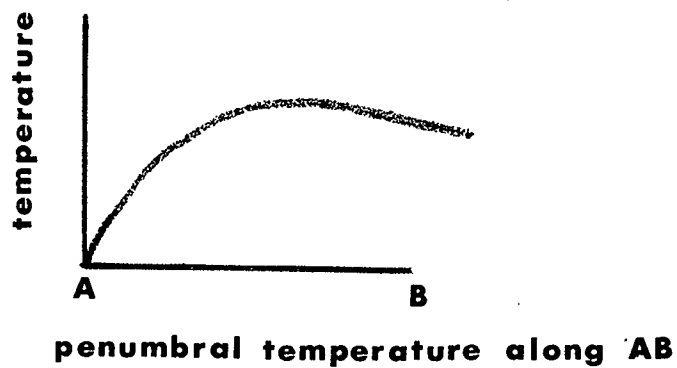
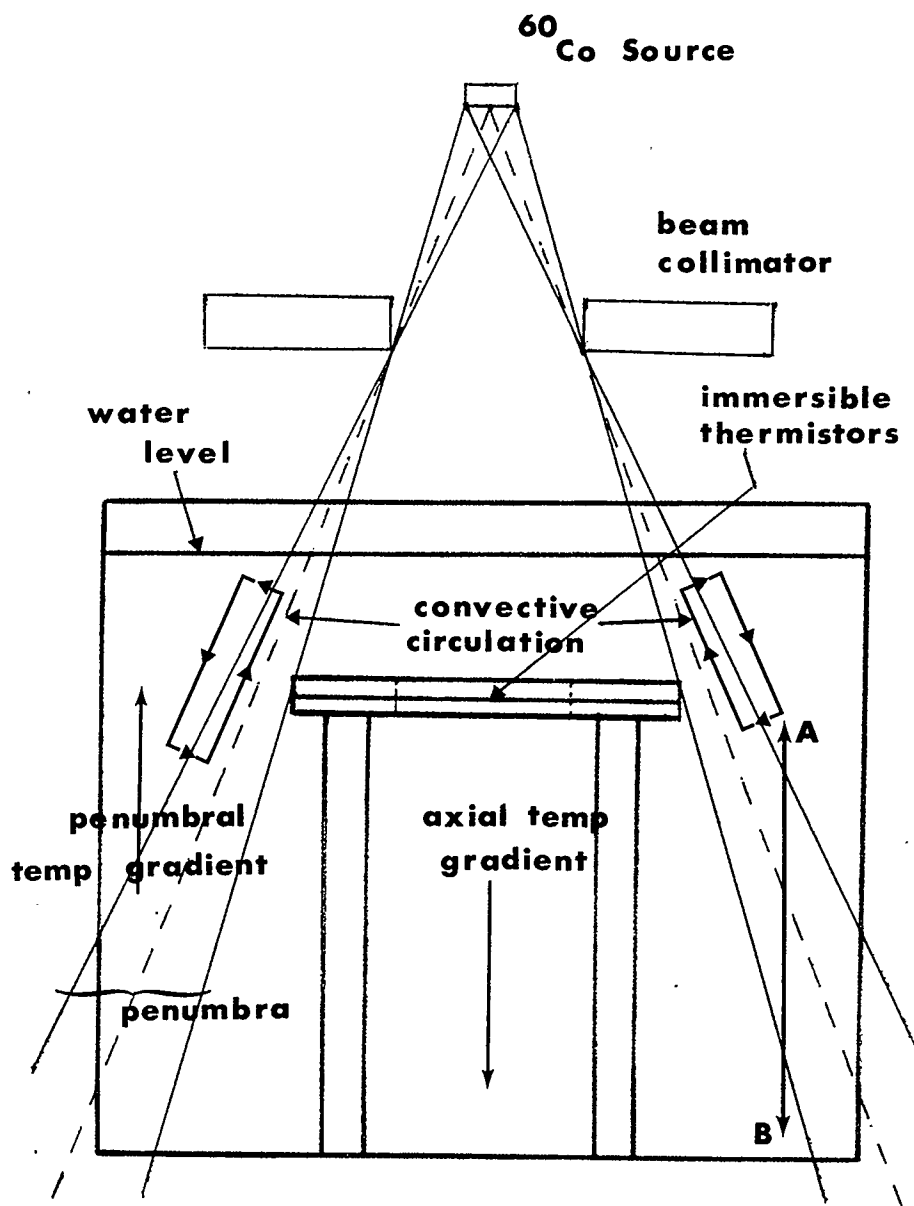
For dose measurements in a beam of 15 MV x-rays convection was not apparent. Chart tracings were recorded at depths of 2.5 and 5 cm for field sizes between 10 x 10 and 25 x 25 cm.

D.4 Explanation Of Convection

For convection to occur, a temperature gradient must be established such that the warmer temperature is at a greater depth. This is obviously not the case for the axial temperature profile of a cobalt-60 beam but applies to the beam penumbra as is shown in Figure D.3.

Along the line AB as shown in Figure D.3, the temperature increases from a low value outside the beam to a maximum at the geometric edge (dashed line). It can be seen that a temperature gradient favoring convection (in a vertical direction) exists at all points along the leading edge of the penumbra. The same reasoning, however, can be applied to a 15 MV x-ray beam (for which no convection was observed) and therefore the penumbral temperature gradient alone is insufficient to drive convection. For cobalt-60 beams, however, the radial absorbed dose profiles are not as flat as for accelerator produced beams and the penumbral region is more extended. The observations suggest, therefore, that both the temperature gradient along the penumbra and a critical water mass (penumbral volume encompassed by a favorable temperature gradient) are essential parameters in driving convection. It should be noted that the penumbral temperature gradient favoring convection is largest near the surface.

Figure D.3. Penumbral Temperature Gradient and Convective Circulation in a Water Calorimeter During Irradiation with Cobalt-60.



The most reasonable path of convective circulation would be one which allows the warmer water inside the penumbra to rise and be displaced by the cooler water outside. This is indicated in Figure D.3 where a large single circulation is illustrated along the edge of the penumbra. For cobalt-60 irradiation and the calorimeter design in this study, the convective circulation was large enough to disrupt the water close to the thermistors (several cm away). Convection is driven continuously while the beam remains on. As water flows past the thermistors the existing temperature equilibrium is temporarily destroyed. When the beam is turned off a new equilibrium will be established and the required time will depend on how severely the equilibrium was disturbed (i.e. the strength of the convection current).

By using different size thermistors with the same power consumption it was observed that the recovery period (i.e. the period immediately after beam turn off as in Figure D.2) was longer for smaller thermistors. The recovery time for a 0.33 mm diameter thermistor was about twice as long as for a 1.27 mm diameter thermistor. Assuming that small temperature gradients (10^{-3} K/cm) can cause bulk convection in water then it is likely that large temperature gradients produced by thermistors can cause convection currents (circulation) near the

thermistor. From equation A.15, it can be shown that temperature gradient in water for a constant power consumption is about an order of magnitude greater for a 0.33 mm diameter thermistor than for a 1.27 mm in diameter. It is therefore possible that the circulation in the vicinity of the smaller thermistors is more extended and requires more time to establish an equilibrium.

The immersible thermistors were sufficiently durable that they could be interchanged without damage. It was therefore possible to compare dose measurements for the two detector formats (with and without polyethylene films) using the same thermistors. When 0.33 mm diameter immersible thermistors were put into a polyethylene film detector convection was no longer observed for dose measurements in a cobalt-60 beam. These measurements were done at a depth of 5 cm and for a field size of 25 x 25 cm as used previously. It was therefore concluded that the polyethylene film detector was a mandatory format for dose measurements in a cobalt-60 beam.

D.5 Dose Measurements With 15 MV X-rays

In a series of dose measurements taken with a 1.27 mm diameter thermistor detector, the steady state dose value (i.e. for an accumulated dose of about 250 Gy at the

point of measurement) for a 15 MV x-ray beam was within 1% of the mean steady state value obtained from the polyethylene film detector.

For this detector the excess heating from direct absorption of radiation was about 3% of the total chart displacement. As shown in Figure D.4, this adds to the uncertainty in extrapolating the final temperature data and hence to the determination of the dose. These data agree well with the calculated estimates for the excess temperature shown in Figure 2.1 (Chapter 2).

Figure D.4. Sample Chart Tracing for a Temperature Measurement in a Beam of 15 MV x-rays Using an Immersible Thermistor Detector.

15 MV X-ray Beam

**1.27 mm diameter thermistor
in water**

